HOMOGENEOUS CHARGE COMPRESSION IGNITION STEADY STATE OPERATION AND MODE SWITCH WITH TWO-STEP CAM AND PHASING SYSTEM IN METAL AND OPTICAL ENGINE

By

Andrew M. Huisjen

A DISSERTATION

Submitted to
Michigan State University
in partial fulfillment of the requirements
for the degree of

Mechanical Engineering – Doctor of Philosophy

2013

ABSTRACT

HOMOGENEOUS CHARGE COMPRESSION IGNITION STEADY STATE OPERATION AND MODE SWITCH WITH TWO-STEP CAM AND PHASING SYSTEM IN METAL AND OPTICAL ENGINE

By

Andrew M. Huisjen

Homogeneous Charge Compression Ignition (HCCI) is a concept that has for years held potential for increasing gasoline engine efficiency while lowering emissions. HCCI allows efficient part load operation by inducing fast combustion despite high levels of exhaust gas dilution and lean air fuel mixtures, which generally result in slow combustion speeds in spark ignition (SI) engines. By trapping large amounts of exhaust gas, heat from the previous engine cycle is reused in order to help the air-fuel mixture to autoignite in multiple locations throughout the cylinder. Proper control of the mixture conditions is vital for controlling ignition timing and avoiding knock and misfires. HCCI is a viable operating mode only at low to moderate engine loads and speeds. Thus, for practical implementation, an engine must be able to switch in and out of HCCI operation seamlessly.

This work studies HCCI operation and mode transition using a production-style valvetrain with 2-step cam profile switching and electric cam phasers mounted on a 4-cylinder engine which has been converted to run as a 1-cylinder engine. Combining this valvetrain with direct injection strategies allows steady state HCCI operation, which displays vastly reduced pumping losses as well as increased load compared to an SI condition run with the same fueling rate. A control strategy has been designed to reliably transition the engine from SI operation into this steady HCCI operation quickly in eight to ten engine cycles without a significant fluctuation in engine output. Cycle-by-cycle analysis of this mode transition shows a distinct

hybrid combustion mode which combines traditional spark-induced flame propagation with the fast autoignition present in HCCI. The initial cycles of the transition show a large percentage of SI flame propagation which gives way to a small amount of fast autoignition at the tail end of combustion; on successive cycles during the transition, the onset of autoignition advances, decreasing the percentage of SI flame propagation until full autoignition is present at the end of the transition.

The HCCI autoignition process has also been captured via high-speed digital imaging in a single-cylinder optical version of the metal engine. This engine, which uses the same valvetrain as the metal engine, was equipped with a sapphire window in the Bowditch-style piston which allows visible light images of the combustion process to be recorded at 10000 frames per second. The images clearly show multiple ignition points which expand rapidly and result in very fast heat release.

ACKNOWLEDGEMENTS

I would like to recognize the many people who have been involved in making this work possible. Thank you to Dr. Harold Schock for the financial support that gave me the opportunity to spend my years of graduate school studying and learning about engines. Thank you to Dr. George Zhu for the countless advice and guidance that made this work a success. Thank you to Dr. Giles Brereton and Dr. Dennis Miller for serving on my committee and for providing good perspectives on the project.

This project also would not have been possible without the work done by staff at the lab. Thanks to Tom Stuecken for the hard work and creativity in building the engines used for all of the testing, and thanks to Jeff Higel and Brian Rowley for talents in the machine shop. Thanks to Xuefei Chen and Shupeng Zhang for their assistance in running and setting up the controls systems, and to Kevin Moran for his expertise and willingness to help when we ran into electronics problems that we could not solve on our own. Thanks to both my current officemates Chao Cheng and James Holly Jr., and my past officemates Cody Squibb and Mulyanto Poort for making the years spent here enjoyable and interesting.

Finally, thank you to my family for all the support over the many years I've been in school, and a special thank you to Melody for the encouragement you've provided and the happiness you've given me over the last four years.

TABLE OF CONTENTS

LIST OF TABLES

LIST OF FIGURES

KEY TO SYMBOLS AND ABBREVIATIONS

ATDC: After Top Dead Center

BDC: Bottom Dead Center

BTDC: Before Top Dead Center

BTDC F: Before Top Dead Center Firing

BTDC GE: Before Top Dead Center Gas Exchange

COV: Coefficient of Variation

CR: Compression Ratio

DI: Direct Injection

ECL: Exhaust Cam Center Line

EVC: Exhaust Valve Closing

EVO: Exhaust Valve Opening

FFVT: Fully Flexible Valve Train

HCCI: Homogeneous Charge Compression Ignition

IMEP: Indicated Mean Effective Pressure

ICL: Intake Center Line

IVC: Intake Valve Closing

IVO: Intake Valve Opening

MAF: Mass Air Flow

MAP: Manifold Absolute Pressure

NMEP: Net Mean Effective Pressure

NVO: Negative Valve Overlap

PMEP: Pumping Mean Effective Pressure

TDC: Top Dead Center

WOT: Wide Open Throttle

Chapter 1: INTRODUCTION AND BACKGROUND

As demand for fuel rises throughout the world and regulations on fuel economy and emissions demand cleaner and more efficient vehicles, innovations to the way automobile engines are designed to operate become increasingly important. An area with much potential for improvement is the efficiency of an engine run at part-load. Large percentages of a normal vehicle trip are spent with the engine operating in a throttled part-load condition, and traditional spark-ignition gasoline engines still suffer from significant pumping losses during this sort of operation. Finding ways to significantly reduce these losses allows more of the work produced during combustion to be converted into forward motion of the vehicle. Doing so without also losing some combustion efficiency improves this work conversion process even more. Homogeneous charge compression ignition (HCCI) is a concept that can allow for both this important pumping loss reduction and high combustion efficiency.

HCCI was first demonstrated as a means of improving engine efficiency in the late 1970s and early 1980s. The general idea of the concept is to induce autoignition of a gasoline-air mixture by utilizing the leftover heat from the exhaust gases of the previous engine cycle. While originally demonstrated for 2-stroke engines [1], the ideas were soon applied to 4-stroke engines as well [2]. With rapidly changing capabilities in areas of valvetrain control and advancements in injection techniques that allow higher compression ratios in standard gasoline engines, much further research has been done in an attempt to fine-tune the HCCI process to make it more viable for a production vehicle.

HCCI Operation Overview

HCCI operation has been described by some as running a gasoline engine like a Diesel engine. This is partially an accurate statement. In a Diesel engine, fuel is ignited by compression, part-load operation can be achieved without throttling the intake air, and air-fuel mixtures tend to be lean; these characteristics are also true of HCCI operation. However, typical HCCI operation utilizes early injection timings to create a homogeneous air-fuel mixture, whereas Diesel operation involves late fuel injections that begin to ignite immediately upon injection. Thus, HCCI is more accurately described as a mix of the two.

The main efficiency benefits from HCCI come from the ability to run unthrottled, highly diluted with exhaust gas, and lean (though HCCI can also be run stoichiometric). Through various breathing techniques discussed below, unthrottled operation can greatly reduce the pumping work that usually results in lost work at low-load highly-throttled conditions in normal SI operation. The high level of trapped exhaust gas and excess air also leads to low peak combustion temperatures in the cylinder, which can result in low NOx formation. Combustion durations tend to be quite short in HCCI operation when compared to SI operation, and this short duration more closely approximates the ideal Otto cycle constant volume heat release, also adding to the increased efficiency; by minimizing the amount of fuel that is burned before the piston reaches top dead center (TDC), the work needed to compress the fuel-air mixture is reduced, and the fast combustion time increases the work done during the expansion stroke.

While in a standard SI gasoline engine, combustion timing is easily controlled by the specified spark timing, in HCCI there exists no simple trigger that can be used to induce combustion at the correct time. Instead, the necessary conditions for proper combustion must exist already at the start of the compression stroke once the valves are shut and all fuel has been injected. Many studies have found a relatively limited operating window in which the process can work. At higher loads, HCCI is limited by knock and extreme pressure rise rates as the combustion becomes stronger and faster; at low loads, the amount of heat that can be captured from the previous cycle can become too small to continue to induce autoignition, resulting in misfires. Engine speed can also factor into the limited operating window, as at higher speeds, the gas exchange process can limit the control of trapped residual gas levels [3].

With a limited operating window, it is apparent that for production vehicle use of HCCI, the engine would need flexibility to easily switch back and forth between SI and HCCI combustion. Such a setup would allow the engine to run in standard SI mode during times of high-load operation like acceleration or hill climbing, and then transition into an HCCI mode by automatically adjusting valve timing and other necessary parameters once the load on the engine reduces to that demanded by cruising at a steady speed. While both the SI and HCCI processes can be achieved at a given load in that operating window, the transition between them can cause problems with either a surge or a drop in output for a few cycles [4,5,6].

Four common methods for achieving HCCI operation as summarized by Zhao et al. [3] are:

-Heating the intake charge

-Increasing compression ratio

-Using a more volatile fuel

-Trapping exhaust heat to aid in auto-ignition.

Intake charge heating is somewhat impractical for a vehicle that will experience frequent load and speed changes which drastically change air flow demands; the transient nature of air delivery through the intake system makes delivering a steady amount of heat to that air difficult to manage as thermal inertia becomes a problem. However, small scale charge heating may be practical in some vehicle applications, and very high temperature charge heating may still have some uses in certain experimental research engines run at steady state. An increased compression ratio can be utilized to an extent, though it must remain in a range that is suitable for standard SI operation as well. Mainstream modern direct injection gasoline engines have reached compression ratios up to and over 12:1, which can also be a suitable range for HCCI operation. A dual fuel setup in which an extra tank of HCCI-only fuel would be utilized is not a desirable solution for a market in which standard gasoline is by far the dominant fuel.

The most important of these strategies for a production vehicle is the fourth, exhaust gas trapping, which can be done through the use of variable valve lift and timing. The most common strategy to use is called Negative Valve Overlap (NVO), in which short duration valve profiles are used to create a period during the pumping strokes in which no valves are open. An example of the valve timing for this strategy is shown below along with sample standard valve profiles, labeled “Base” (Figure 1). The early exhaust valve closing (EVC) position works with a

late intake valve opening (IVO) position to create a recompression period between the exhaust and intake strokes during which a large amount of exhaust gas is trapped in the cylinder as the cylinder nears TDC [7] (Figure 2).

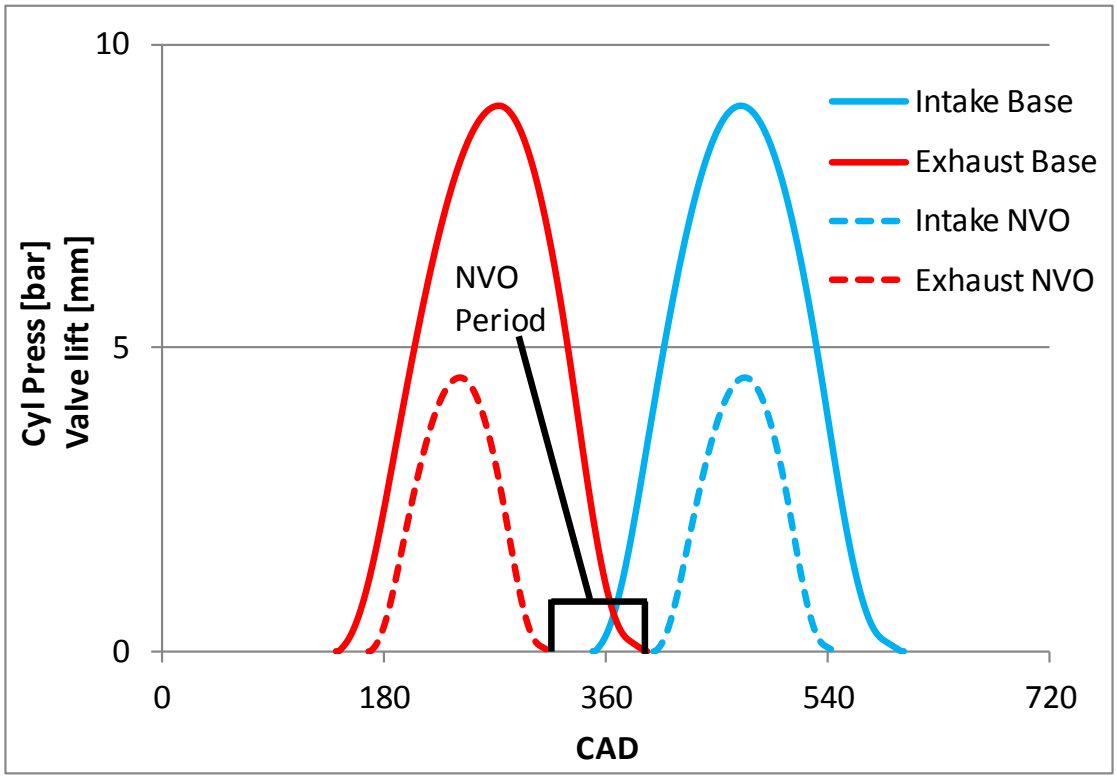

Figure 1: Traditional and NVO Valve Timing Comparison. For interpretation of the references to color in this and all other figures, the reader is referred to the electronic version of this dissertation.

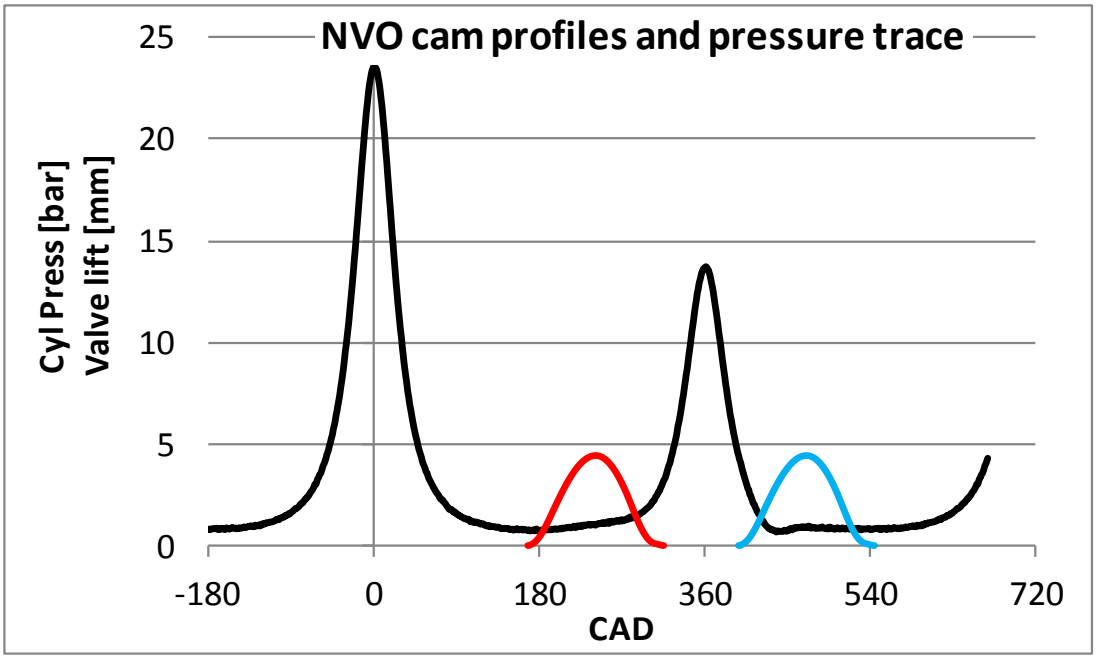

Figure 2: NVO Valve Timing with Recompression in Pressure Trace

Another strategy that can be used for exhaust gas trapping is exhaust rebreathing, where the exhaust valve is actually re-opened during the intake stroke to ingest recently exhausted gas back into the cylinder from the exhaust port [7, 8]. This method requires a complicated valve actuation system than would either have a special cam with multiple lobes or a Fully Flexible Valvetraing (FFVT) such as a camless system that can be controlled by hydraulics or pneumatics. NVO, on the other hand, can be achieved through a fairly straightforward use of two-step cams and cam phasing, both of which are already common in production engines today.

The timing of the valve actuation is the key driver in how combustion proceeds, as combustion timing and duration are dependent on the heat and the dilution of the final mixture in the cylinder. This mixture is very much determined by EVC timing. Earlier EVC timing traps more residual exhaust gas, which means more heat is re-used, and recompression temperature and

pressure are higher. This strategy often can be used to create in-cylinder mixture diluted with as much as 50% exhaust gas or more [9]. NVO durations all the way up to and beyond 200° have been used [8,10], though more common durations are in the 120° to 180° range. Residual gas level has a dual effect on combustion; more heat from exhaust and higher recompression helps to advance or even initiate combustion, but at a certain point the higher dilution overcomes heating effects and helps to slow the burn rate once combustion has started due to the heat capacity effects [9,11]. Balancing these two effects with a suitable fueling level is key to controlling burn characteristics of HCCI.

With EVC used to determine trapped gas levels, IVO must also be considered. A typically used technique is to set IVO symmetrical with EVC about TDC [7]. This helps to reduce the pumping loss that could otherwise occur from IVO occurring too early and not allowing a full expansion of the recompressed gas, and stops the gas from backflowing into the intake port, where heat loss could occur, before it is re-ingested into the cylinder during the intake stroke. However, backflow from using non-symmetrical IVO timings has been suggested as a way to slow combustion if early ignition and fast burn rates are troublesome at certain operating conditions [3]. Also worth considering are the effects of extreme EVC and IVO timings on EVO and IVC, respectively. In a FFVT system each of these four parameters can be controlled independently of the others; valve opening durations are fully variable, so an extremely early EVC can be combined with a standard EVO to allow for a full expansion stroke and a high level of trapped exhaust gas. However, in a simpler 2-step cam setup, the fixed profiles do not allow for this level of flexibility. An extreme EVC timing can potentially force an earlier EVO timing than is

desired if the valve opening duration is too long. The tradeoffs must be considered in the design of system that is to be implemented for HCCI operation.

Further tuning of the combustion characteristics can be done by introducing multiple injection strategies and spark assist strategies. Using a short injection during or just before the recompression period can allow a small amount of fuel reformation to occur during recompression, and this can help to initiate autoignition during the following compression stroke and extend the low-load capabilities of HCCI [12]. Splitting up the remaining fuel into short and spaced-out injection pulses and using properly timed spark assist can help turn HCCI operation into something of a hybrid of stratified spark ignition and HCCI in which the spark initiates a flame kernel in one region before the remaining mixture in the cylinder autoignites. This strategy has even been demonstrated at idle-load conditions [13], and can also be exploited during mode transitions between SI and HCCI.

These increasingly complex multiple-injection and spark assist schemes have led some to move away from the name HCCI due to the increasingly non-homogeneous nature of the fuel-air mixture and the use of a spark to initiate some amount of the combustion. Some simple refer to the concept as Controlled Autoignition (CAI), which can encompass everything from pure homogeneous autoigntion to highly stratified spark assisted autoignition. The terms Reactivity Controlled Compression Ignition (RCCI), Partially Pre-mixed Charge Compression Ignition (PPCI) and Premixed Charge Compression Ignition (PCCI) have been introduced to refer to HCCI-style

operation that utilizes multiple injection timings to produce particular fuel stratification regions that help to further control the auto-ignition process.

Chapter 2: PROJECT OVERVIEW AND SETUP

This research has involved two engines to investigate HCCI combustion. The first stage of work involved attempts to capture the HCCI autoignition process with high-speed digital imaging in a single-cylinder optical engine equipped with a production-worthy 2-step cam lift system and electric cam phasers. The second stage utilized a 1-cylinder gasoline SI metal engine with the same modified valvetrain that was used to perform steady state SI and HCCI tests as well as the mode-switching process between each of those modes. This engine was adapted from a standard 4-cylinder engine by firing only one cylinder and isolating its intake and exhaust ports from those of the other cylinders. This is similar to what Borgqvist et al. have done in previous HCCI-related research with a 1-cylinder engine adapted from an inline-five design [7]. Numerous tests were performed with this engine to explore the flexibility and efficiency improvements allowed by the modified valvetrain setup while running in typical SI operation; these test points served as a baseline for comparison with the steady-state HCCI test points that were explored later. With steady HCCI conditions mapped out, a mode-switch scheme was designed that could reliably transition the engine from SI to HCCI with minimal disruption in engine output.

The design and tuning of a mode-switch involves coordinating cam lift, cam phasing, throttle position, spark timing, injection timing, and fueling amount in order to smooth the engine output between the steady SI condition and the steady HCCI condition. A 5-cycle transition window (Figure 3) was initially proposed as an ideal concept for the mode transition. Through

testing, this plan was adjusted as necessary due to the physical limitations of the actuators (throttle, cam phasers, and cam lift mechanism) and tuned based on results found during the initial transition tests.

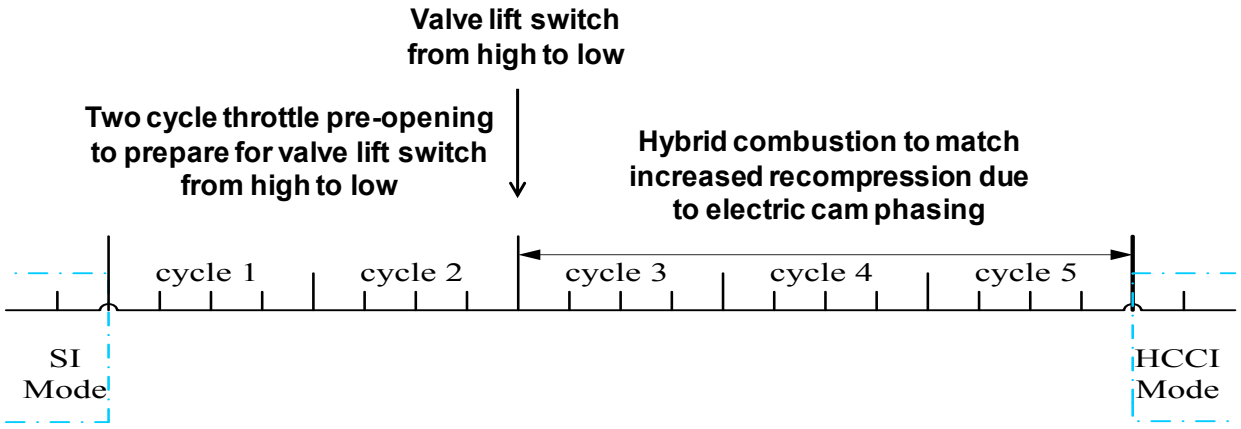

Figure 3: Proposed 5-cycle HCCI-to-SI Mode Transition

Engine and Valvetrain Specifications

Both the optical and metal engines are based off of the same 2.0L 4-cylinder architecture provided by Chrysler. This engine has an 86mm x 86 mm bore and stroke, a 4-valve per cylinder head design, and centrally mounted direct injection (DI) gasoline injector that injects fuel at 10 MPa. This fuel pressure is supplied by a small bladder fuel tank which is pressurized with a nitrogen cylinder. The major modification to the engine was the addition of a 2-step variable cam lift system developed by Delphi [13] dual independent electric cam phasers by Denso.

The two-step system utilizes a tri-lobe cam design with a 2-step rocker arm that controls which cam profile is transferred to the valve. This rocker arm (Figure 4) consists of two roller

followers which contact the outer low-lift cam profiles and a slider follower which contacts the middle high-lift cam profile. The rocker is controlled by a solenoid that provides oil pressure to a pin in the rocker mechanism. With the solenoid off, only the motion from the low-lift profile is transferred to the valve through the outer roller followers, while the middle slider rocker deflects on a spring but does not transfer motion to the valve. With the solenoid on, the oil pressure pushes a pin that locks the two parts of the rocker arm together, and the motion of the high-lift profile is transferred to the valve.

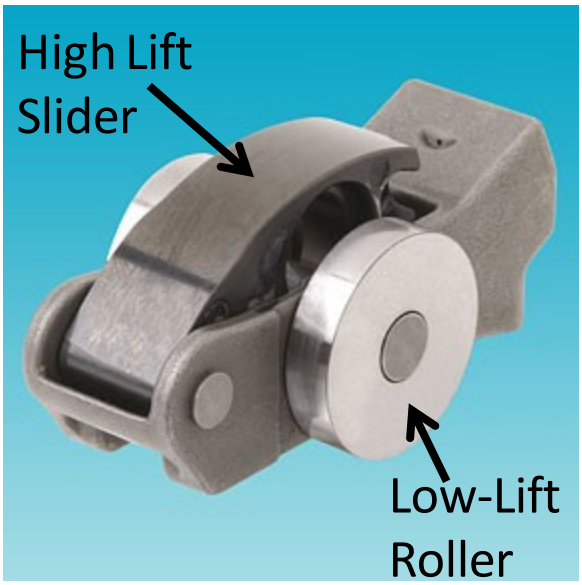

Figure 4: Delphi Multi-lobe 2-step Cam Lift Rocker Arm

In standard SI application, this type of system would be implemented on only the intake side so that the low-lift profile could be used to reduce throttling losses during the pumping loop. An early intake valve closing (EIVC) strategy can be used to control airflow into the cylinder at low and medium loads while the throttle can be left more open to produce a higher manifold

pressure than is standard with high-lift valve profiles. This can reduce part-load pumping losses significantly.

For HCCI operation, the 2-step system is also implemented on the exhaust side, allowing the engine to operate with low lift exhaust and intake profiles. This is the key to running with the NVO valve timing scheme that traps the exhaust gas and makes HCCI possible. Since the intake and exhaust lifts are controlled by separate solenoids, the engine also maintains the capability to run in the SI EIVC strategy mentioned above.

The other key head modification that helps enable HCCI operation is the dual independent cam phasing system. This system, made by Denso, allows 80 CAD of phasing independently on each cam through electric motors. These motors give fast and accurate response that can phase the cams on command in just a few cycles. The default position of the cams with these phasers is in their fully retarded position. During SI operation, the exhaust cam is left close to this position while the intake cam is advanced significantly; during HCCI, the opposite is true, with the exhaust cam being advanced fully and the intake cam moving to the default fully-retarded position. This setup with the low-lift valves provides the NVO period necessary to trap exhaust gases. Figure 5 below shows the default position (solid lines) and the fully advanced (dotted lines) position of both the high and low lift cam profiles. The cam profiles are designed such that EVC and IVO are unchanged regardless of whether the high-lift or low-lift cam is being used.

For all cam timings mentioned, since the default position is fully retarded, this will be referred to as 0° (meaning not advanced at all); the fully advanced position will be referred to as 80°. An advance of 40° will be referred to as the 40° position. An overview of the opening, closing, and center line timings at fully retarded and fully advanced positions is found in Table 1.

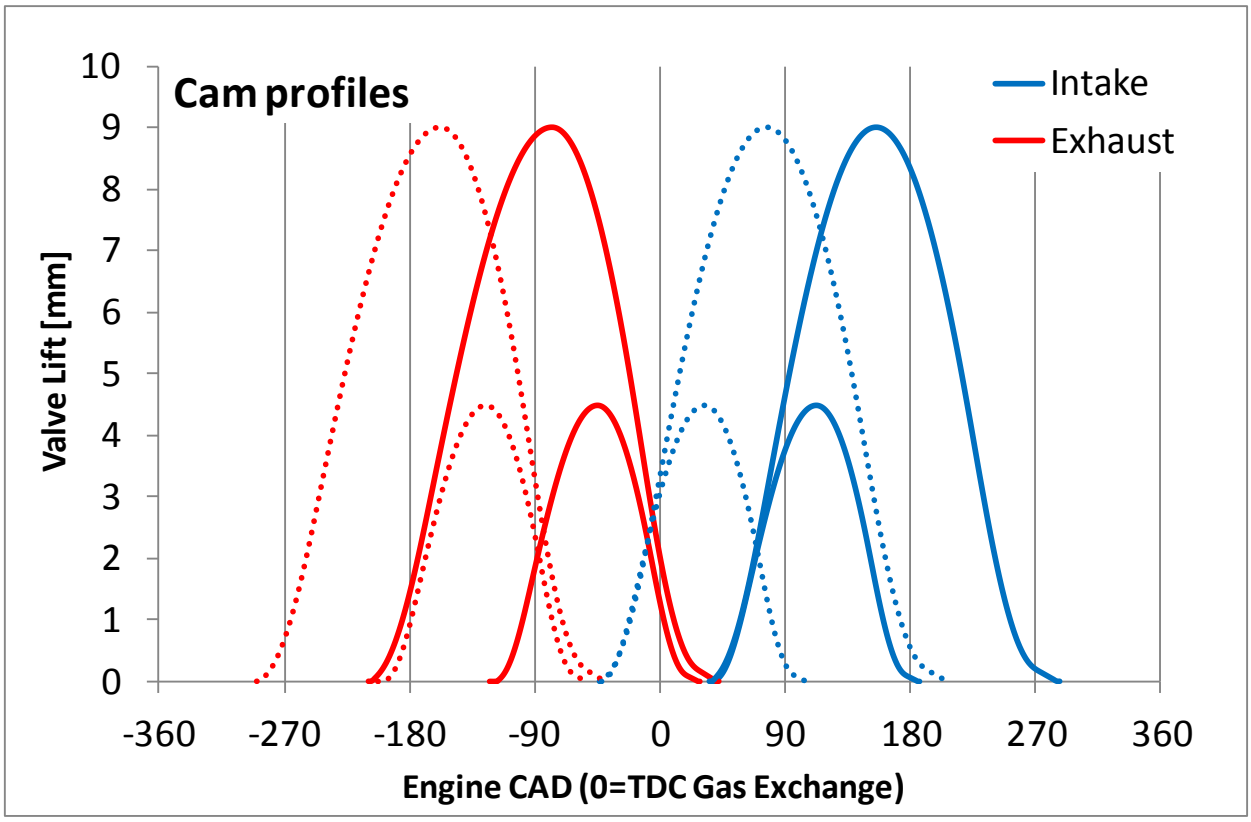

Figure 5: Original Fully Retarded and Fully Advanced Cam Profiles

Table 1: Valve Timing Specifications Relative to TDC GE

		Open Spec	Open effective	Center line	Close effective	Close Spec
Fully Retarded 0° Position	Intake High	36	46	156	278	288
	Intake Low	38	53	112	171	186
	Exhaust High	-210	200	-78	32	42
	Exhaust Low	-119	-104	-45	14	29
Fully Advanced 0° Position	Intake High	-44	-34	76	198	208
	Intake Low	-42	-27	32	91	106
	Exhaust High	-290	-280	-158	-48	-38
	Exhaust Low	-199	-184	-125	-66	-51

With the exhaust cam fully advanced and the intake cam fully retarded, the maximum effective low-lift NVO duration is approximately 119° (NVO by EVC and IVO spec is just 89°). This is relatively short compared to the NVO used in many other studies. Also of note is that the max NVO is asymmetrical; EVC to TDC with the exhaust cam fully advanced is 66°, while TDC to IVO with the intake cam fully retarded is only 53°. From an efficiency standpoint, a symmetrical NVO would be best, since the full expansion of the recompressed gases and effectively make the recompression period act as an air spring on the piston where the energy used for compression is regained as the piston moves down. With the asymmetry of this setup, some of the trapped exhaust can escape into the intake ports upon IVO, causing it to lose some heat. However, as mentioned above, Zhao et al. utilized a similar setup and mentioned that this was an effective way to trap large amounts of exhaust gas for dilution while also lowering the amount of heat held in that exhaust that could lead to premature autoignition [3]. Successful

HCCI operation did eventually require adjustment to these initial cam positions to increase NVO; these changes will are discussed in Chapter 4.

Optical Engine Setup

The optical engine, shown in Figure 6, features a flat-faced Bowditch-style piston with a sapphire window for optical access to the combustion chamber. The compression ratio with this piston is approximately 9.5:1. In order to compensate for this low compression ratio compared to the normal HCCI range of about 10:1 to 13:1 [3,4,7,8,9,10,15,16], a simple compressed air boost system was added to the intake system in order to increase the peak motoring pressure that could be achieved.

In addition to boost, an intake air heating system was added to aid in the autoignition process (Figure 7). Though the cylinder is pre-heated with a coolant jacket running 190°F heated coolant though it before tests are run, the limited number of cycles for which the engine can be run at one time limits the operating temperature of the engine—the engine does not reach the high temperature of steadily running metal engine. Thus, electric ceramic heaters with the ability to heat the air over 200°C were built in to the intake system to compensate for the lower levels of heat. These heaters also can help to compensate for a lack of exhaust gas heat during the initial cycles of HCCI operation before stable combustion has been achieved.

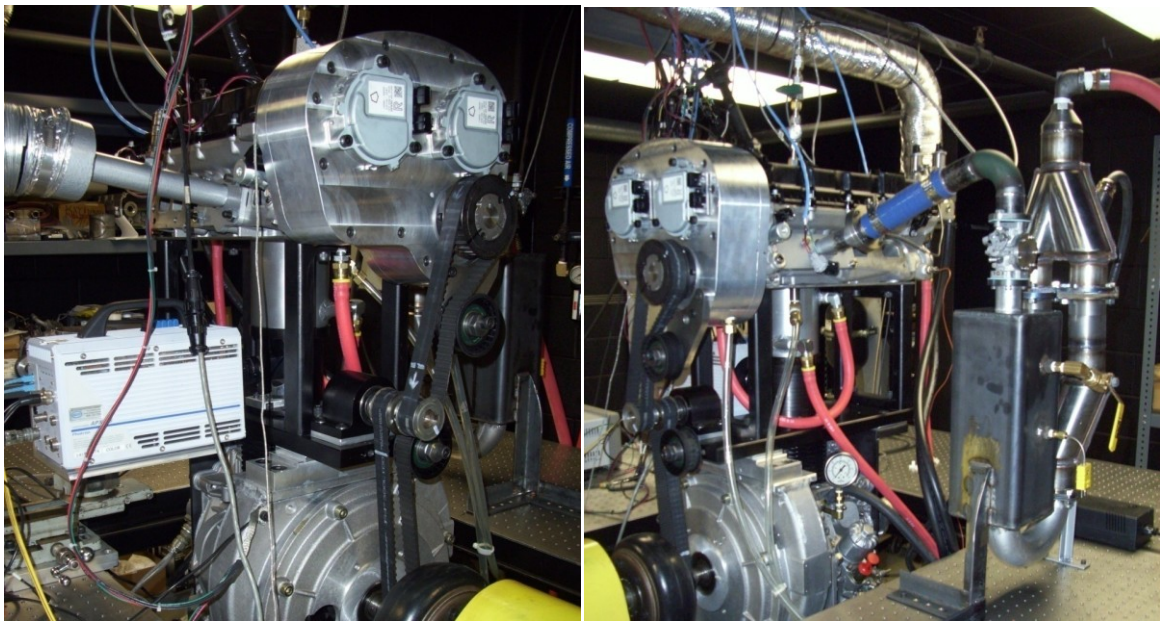

Figure 6: Optical Engine

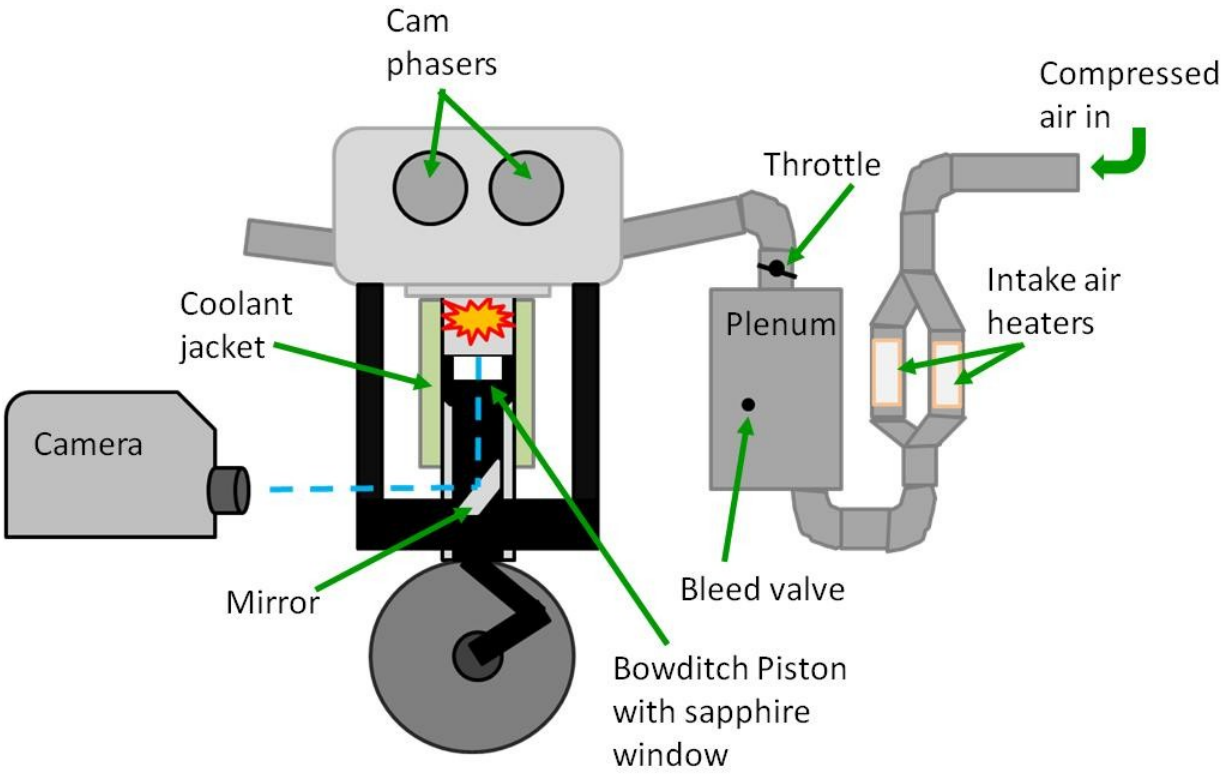

Figure 7: Optical Engine Setup Schematic

Metal 4-Cylinder Engine Setup

The naturally-aspirated metal 4-cylinder engine (Figure 8, Figure 9) was fabricated for steady-state testing and mode transition testing. It has the same head modifications with the 2-step cam and electric phasers as the optical engine. It has a slightly different piston design with a small central bowl that catches the spray from the centrally mounted DI injector. Two sets of pistons have been used in this engine. The original pistons had a compression ratio of 9.8:1. For HCCI studies, a higher compression ratio is desired, so new pistons with a roughly 12.5:1 compression ratio were machined with a design very similar to the originals only with a shallower center bowl (Figure 10). In place of the large electric intake heating system used in the optical engine, a coolant-fed heat exchanger is mounted in the intake manifold. This setup allows intake air temperatures to reach approximately 170°F by take heat from the hot engine coolant. This heat exchanger was removed during testing when heated intake air was not desired.

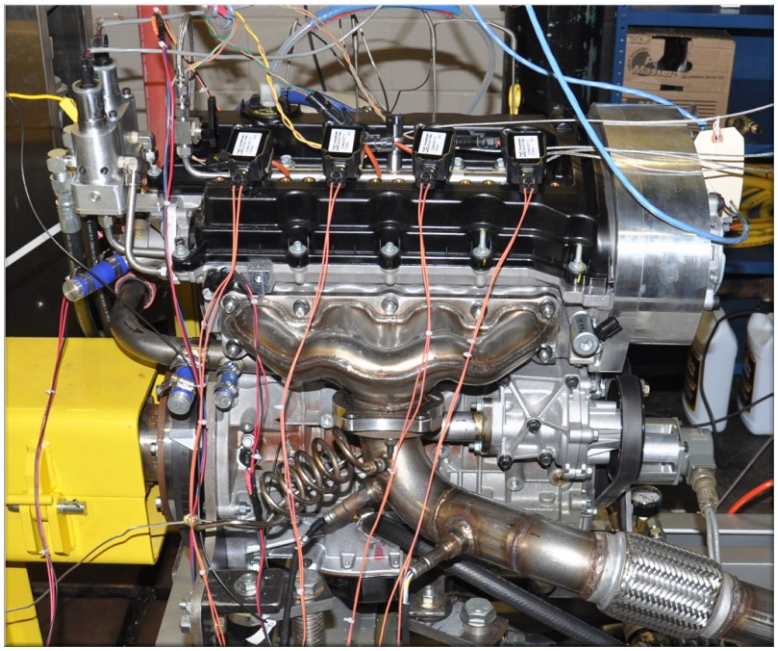

Figure 8: Metal 4-Cylinder Engine

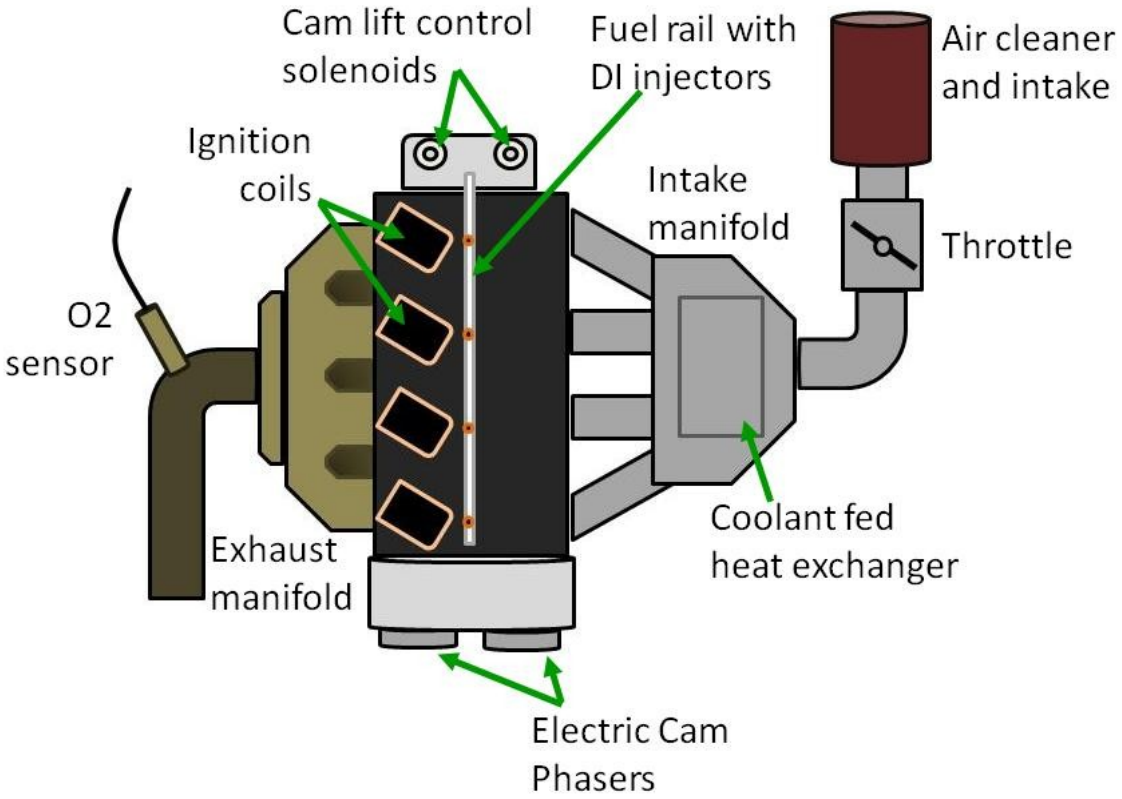

Figure 9: Metal 4-Cylinder Engine Schematic

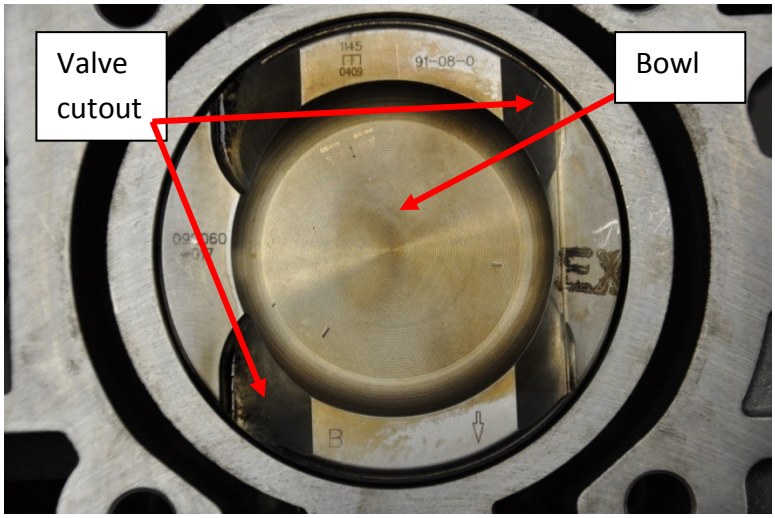

Figure 10: Piston Face Design

The 4-cylinder engine was also run in a 1-cylinder mode for many tests (Figure 11). Reasons for this modification are discussed in Chapter 4. To make this modification, the runners for cylinders 1, 3, and 4 were welded shut with metal plates at the end of the intake manifold to prevent air from entering the cylinder during the intake stroke. Similarly, a metal plate was used to block the exhaust ports on these same cylinders, and a new exhaust system was fabricated that only connected to the port from cylinder 2. To allow for improved throttle control, a modified narrow-diameter throttle body was fabricated to compensate for reduced intake air flow rate; deactivating 3 of the cylinders cuts air flow by 75%. All pistons and valvetrain components of the unused cylinders were left in place, and the pistons in those cylinders were allowed to motor for balance while cylinder 2 was fired.

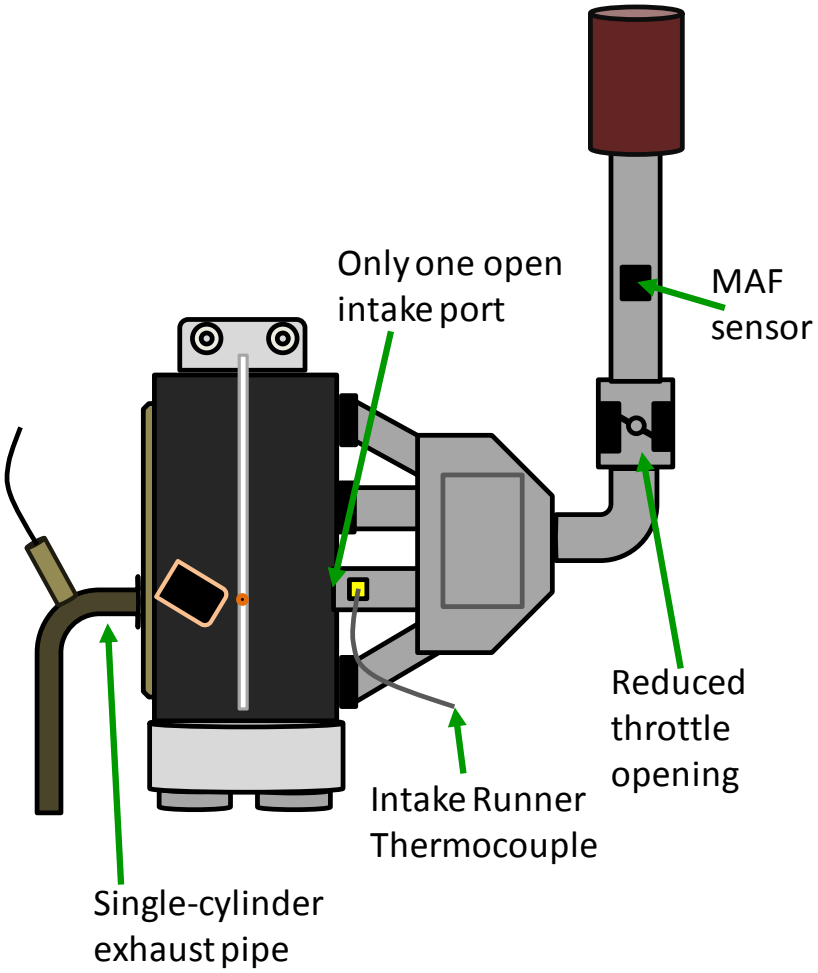

Figure 11: Metal Engine 1-Cylinder Modification Schematic

Chapter 3: OPTICAL ENGINE

Optical engine fabrication was completed ahead of metal engine fabrication. Because of this, it was used to learn about the operation of the valvetrain and injection controls before HCCI testing was begun.

Valvetrain Validation Tests

It was necessary to test the capabilities of the 2-step cam lift and electric cam phasers under both motoring and firing conditions to be sure they would be capable of performing in the way necessary for the proposed mode transition tests. Any lag in response between a commanded event and the actual actuation would be necessary to design the transition control strategy to mimic the ideal 5-cycle transition proposed previously as closely as possible; phaser response speed was necessary to know since it was potentially a limiting factor in the overall length of the transition.

During these motoring tests, it was found that cam phaser response varied slightly depending on whether the engine was hot or cold. At 1500 RPM, a 70° advancement took 11 cycles when cold and 9 cycles when hot. Firing the engine while performing this same phasing operation had very little effect on the response. Retarding the cam timing back to the default position was quicker, at 7 and 6 cycles for cold and hot 70° retarding, respectively (Table 2).

Table 2: Cam Phaser Response Times, Optical Engine

	CAD	Cycles	Combustion/motoring	Heated/cold
Advance	70	11 cycles	motoring	cold
Advance	70	9 cycles	motoring	heated
Advance	70	9 cycles	combustion	heated
Advance	35	7 cycles	motoring	cold
Advance	35	6 cycles	motoring	heated
Advance	35	6 cycles	combustion	heated
Retard	70	7 cycles	motoring	cold
Retard	70	6 cycles	motoring	heated
Retard	35	5 cycles	motoring	cold
Retard	35	4 cycles	motoring	heated

Part of the response time is from the lag between when the signal is sent and when the cam begins to respond. As shown in the figures below, from heated 70° phasing experiments, there is a 2-cycle lag before the cam begins to move after the signal is sent. Thus, when a 70° advancement is commanded, it takes approximately 2 cycles to initially respond, and then another 7 cycles to actually complete the phasing (Figure 12). A similar lag is seen when commanding the cam to retard (Figure 13).

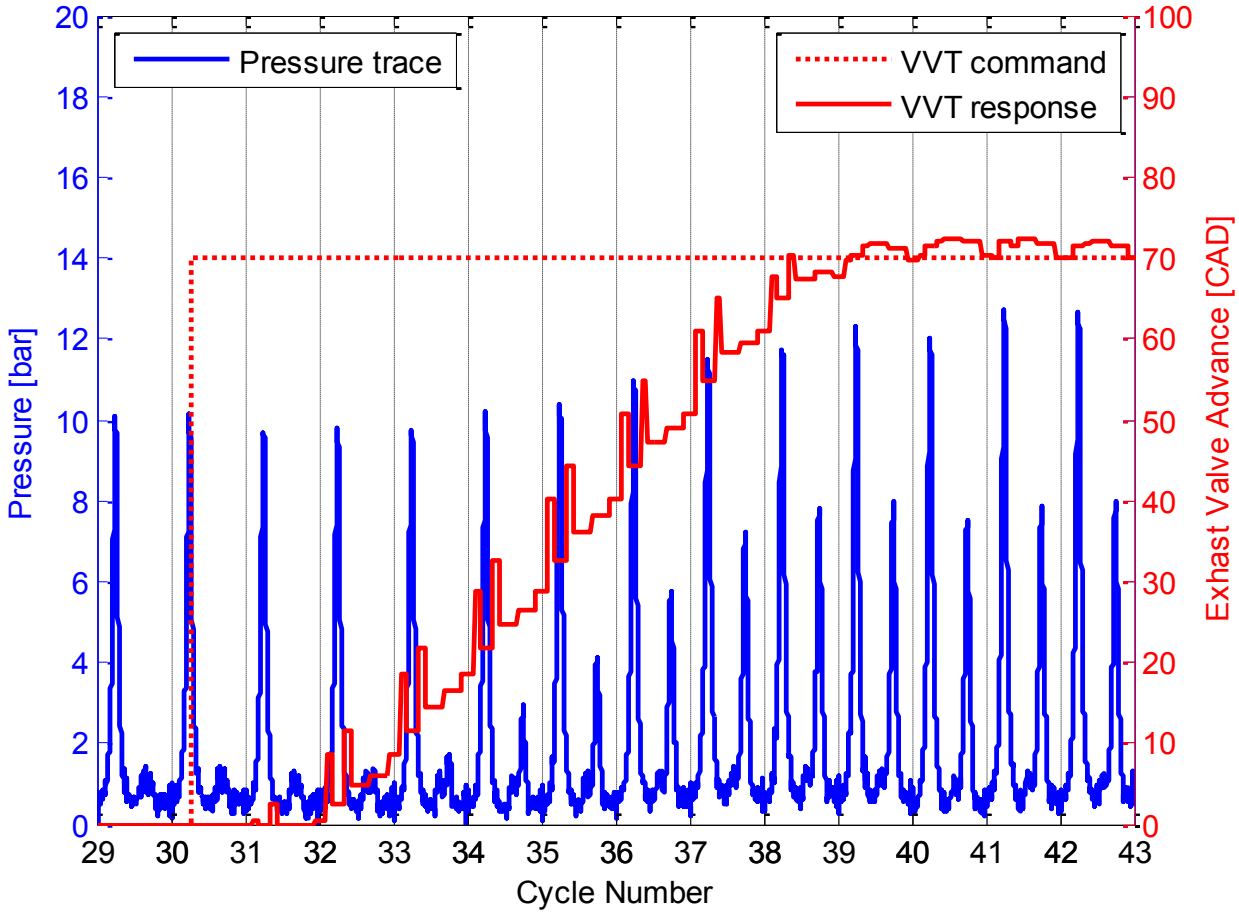

Figure 12: Cam Phaser Response, 70 CAD Advance

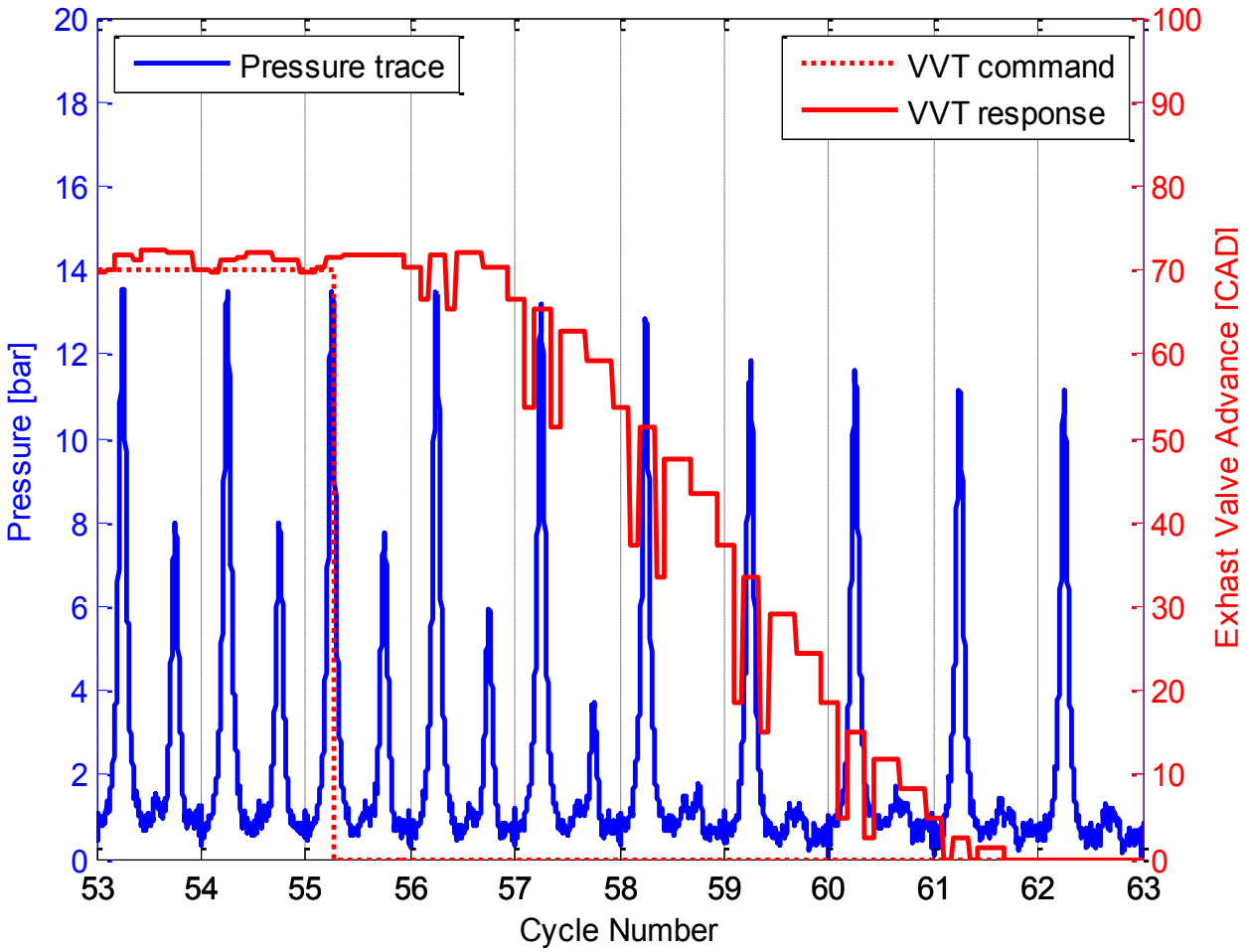

Figure 13: Cam Phaser Response, 70 CAD Retard

An overlay of cam phaser response while motoring and firing shows that the response is approximate half of a cycle longer when firing (Figure 14). This may be due to the increased friction force from opening the valves against higher in-cylinder pressure.

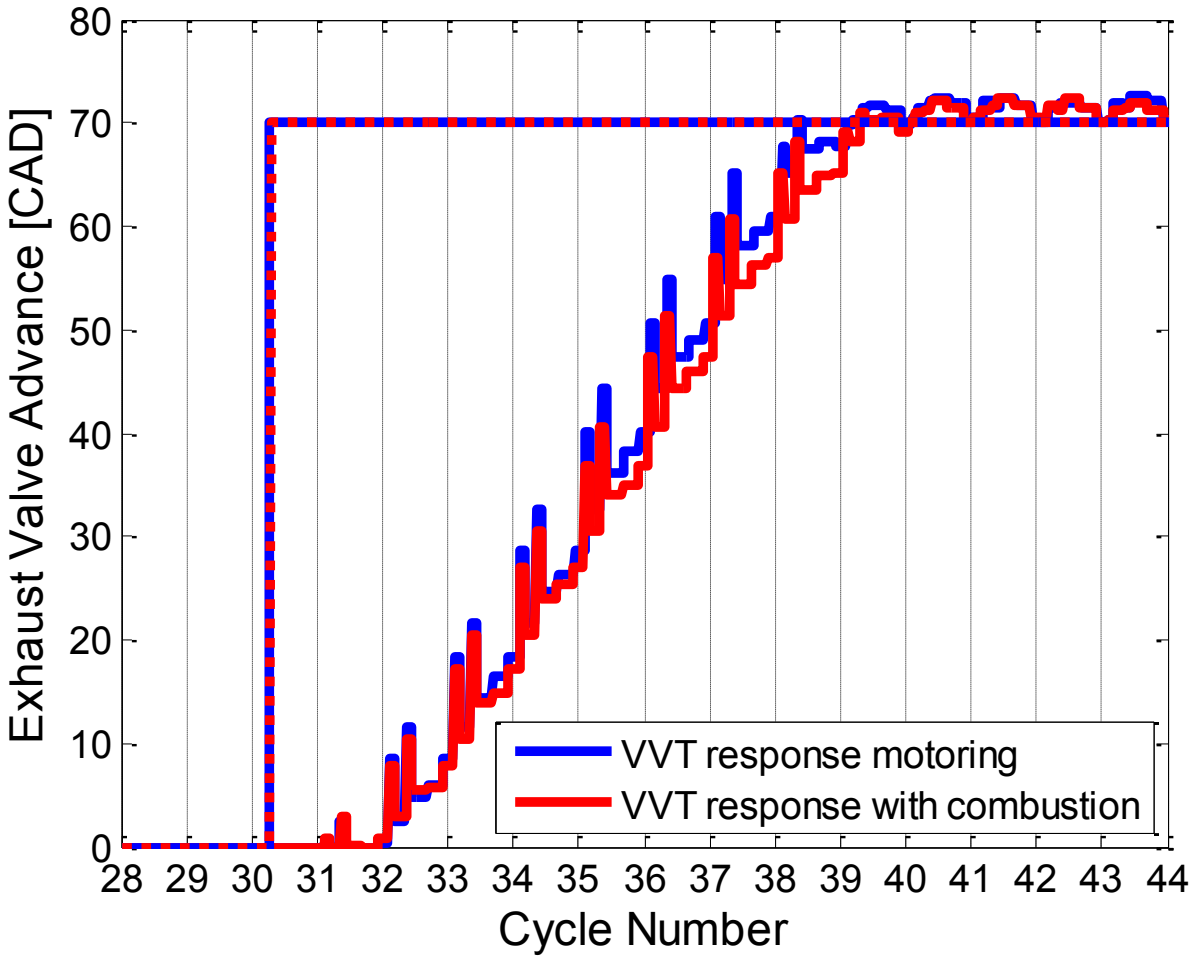

Figure 14: Cam Phaser Response Comparison, Firing vs. Motoring

The actuation of the 2-step cam lift mechanism can be seen by the change in the motoring pressure trace behavior; the low lift cam allows less air to enter the cylinder, resulting in lower peak cylinder pressures. It was found that when actuating just one cam, the cam lift system responded with a 1-cycle lag for both high-to-low (Figure 15) and low-to-high (Figure 16) lift tests. However, when both cams were commanded to change simultaneously, the lag on the high-to-low switch lasted 2 cycles (Figure 17), while it remained at just 1 cycle on the low-to-high switch (Figure 18). Since the switch from high lift to low lift on the exhaust cam can be

used as the trigger that supplies recompression for HCCI, this 1-cycle lag is important to know when designing the mode switch control strategy.

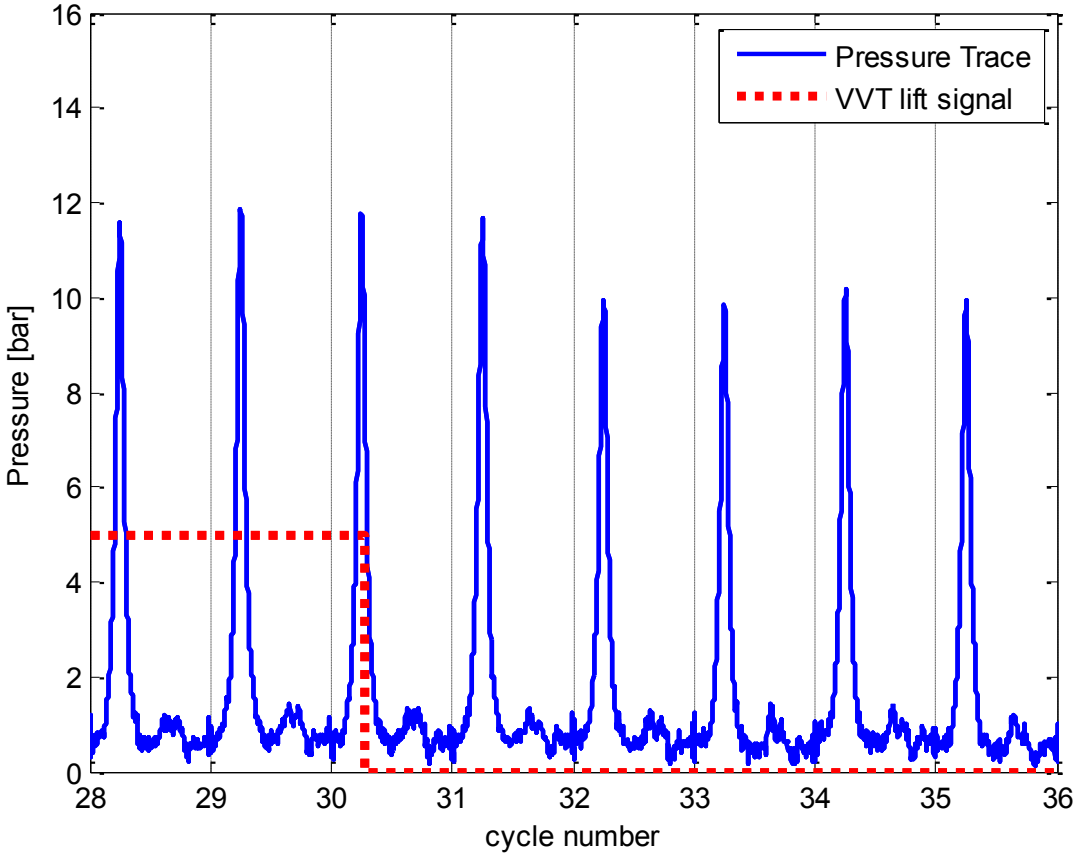

Figure 15: Single Cam Lift Response, High to Low Lift

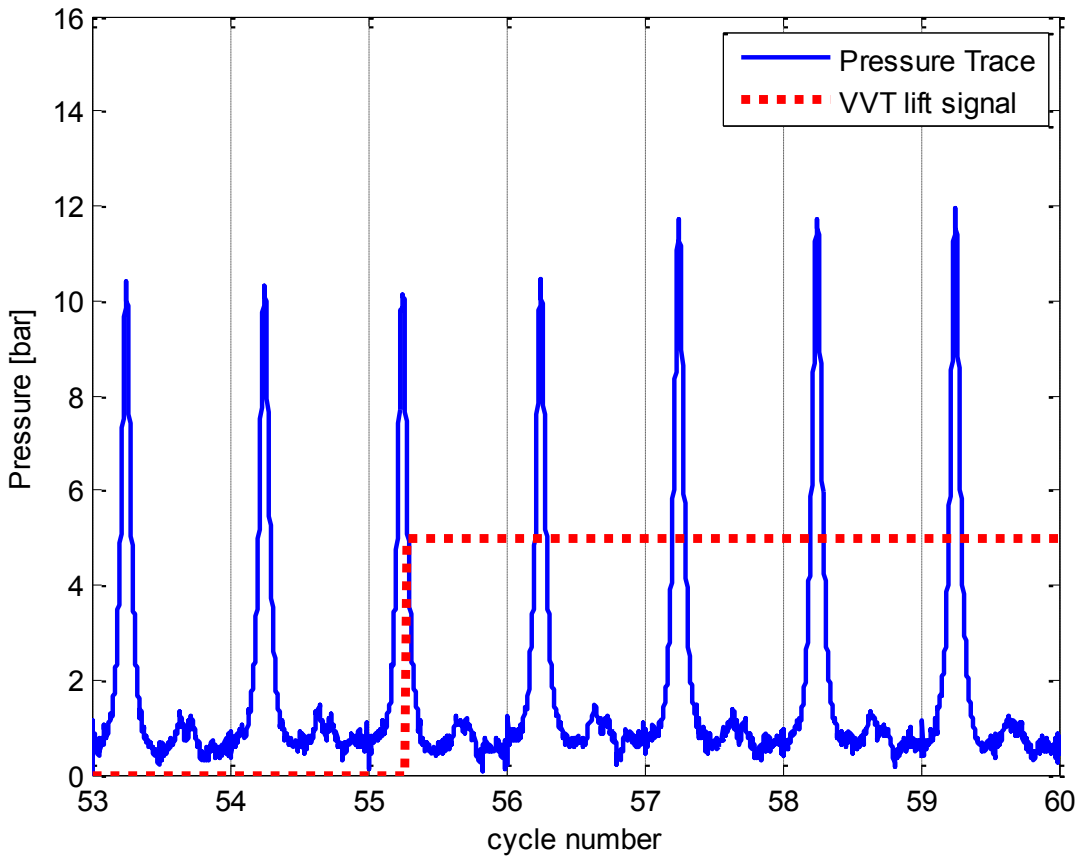

Figure 16: Single Cam Lift Response, Low to High Lift

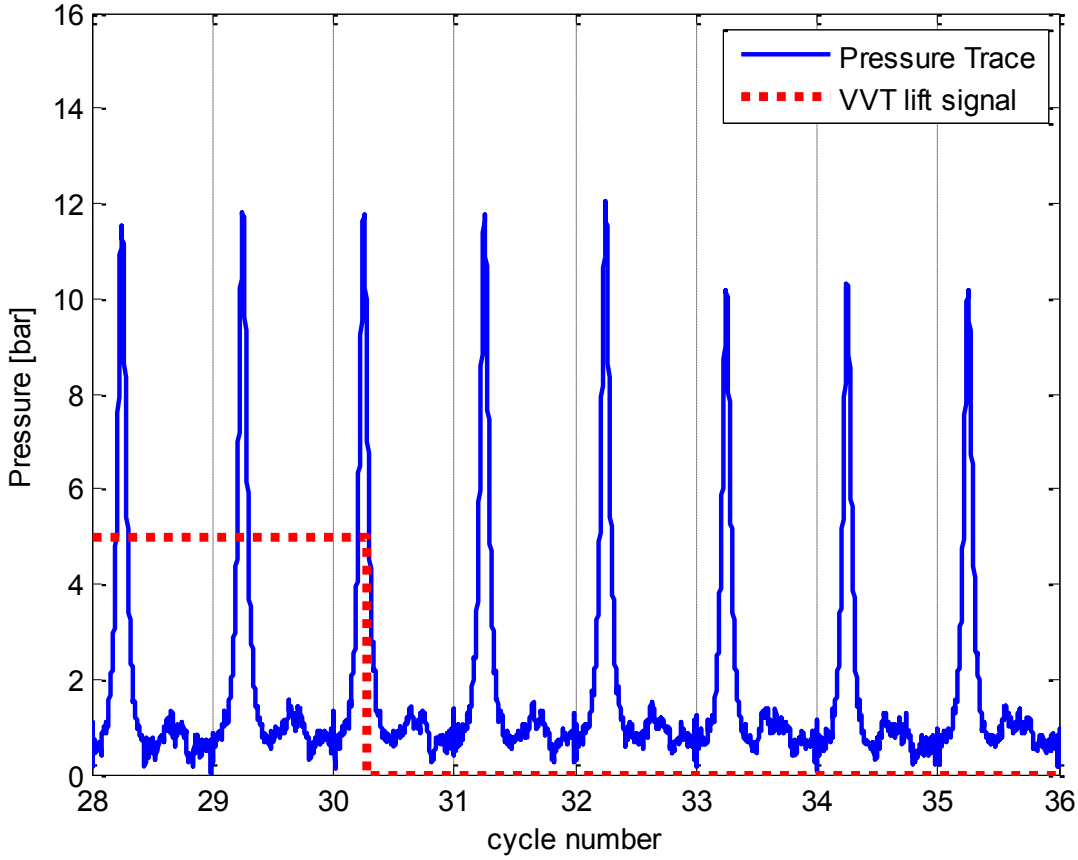

Figure 17: Cam Lift Response, Both Cams High to Low

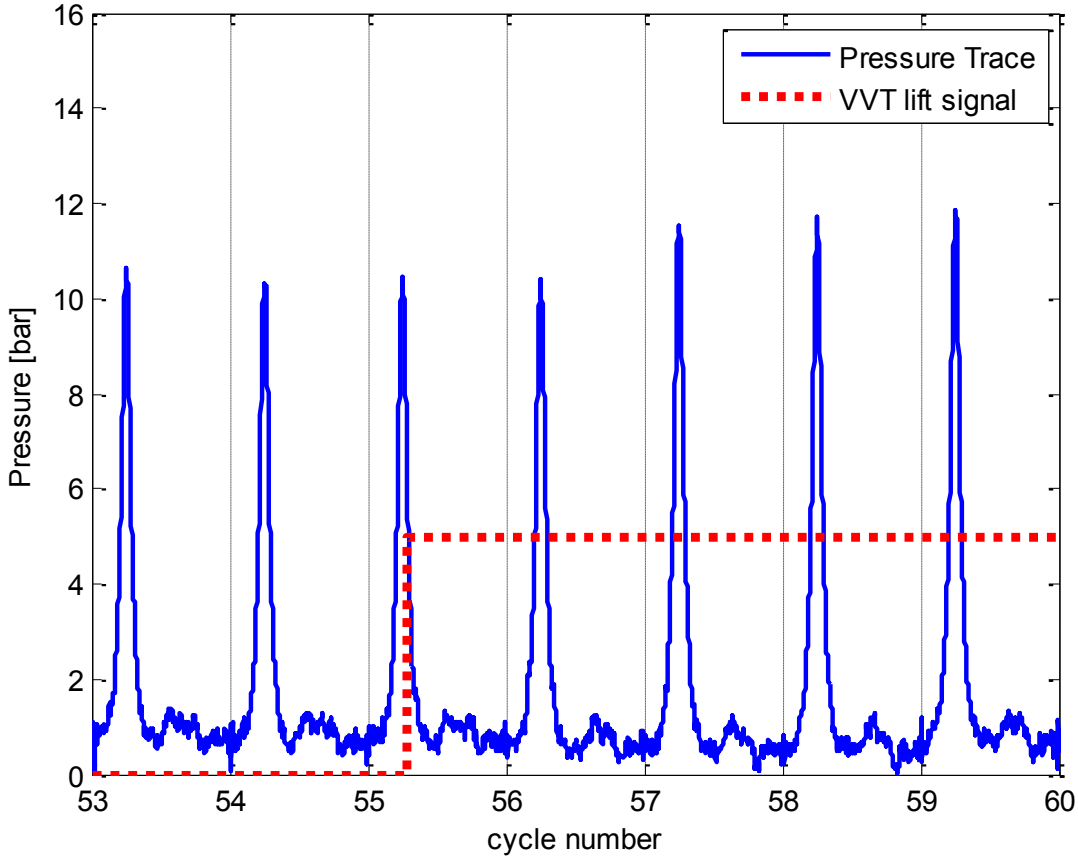

Figure 18: Cam Lift Response, Both Cams Low to High

With these completed valvetrain validation tests, it became evident that the proposed 5-cycle transition strategy would actually be closer to an 8 to 10 cycle transition because of the cam phaser limitations under a large advancement.

Injection Control Validation Tests

An important detail for running SI-to-HCCI transitions is the control of the fuel delivery on a cycle-by-cycle basis. The controller needs to be able to change the fuel pulse width for

individual cycles as the engine moves from a stoichiometric SI condition to a series of hybrid SI-HCCI cycles and finally to lean HCCI cycles over a short specified window and throttle position and valve timings change. A simple way to demonstrate the necessary transient fuel delivery capability was to design a test on the optical engine with a sweep of fuel injection pulse widths that would alter the air-fuel ratio over the 50 cycles.

For these tests, run at 1500 RPM, the first 25 firing cycles use a constant injection pulse that allows the engine to run steadily at a rich condition; the last 25 cycles run with a steadily decreasing injection pulse that gradually leans the mixture slightly with each cycle.

Visible light images were taken with the high-speed camera to see differences in flame propagation and intensity as the mixture leaned out. This work successfully demonstrated that a fast air-fuel ratio switch is possible in a short 50-cycle operation window on the optical engine, and the images clearly show the operating differences as the engine transitions from rich to lean combustion.

An example of the commanded fuel pulse, lambda response (Figure 19), and resulting cycle-by-cycle IMEP (Figure 20) are shown in the figures below. For this test, the injection pulse was held at 2.3 ms for the first 25 cycles, and then swept steadily from 2.3 to 1.8 ms over the next 25 cycles. Spark timing was held constant at 30°BTDC. IMEP was close to 4 bar.

Fuel injection began at cycle 12, but there is a lag in the response of the O2 sensor shows that the lambda doesn't level off until about 15 cycles have been run. This is believed to be a combined mixing and warm-up effect; it takes a few cycles for the exhaust to fully displace the air in the exhaust port, and it also takes a number of cycles before the cylinder is up to operating temperature that allows for full fuel evaporation. At cycle 37, the fuel pulse width starts to decrease, and lambda responds according, getting progressively leaner until the end of the test. Once fueling has stopped, the O2 sensor still registers a reading as the remaining exhaust is displaced by fresh air again. The lambda response to the varying fuel pulse was found to be repeatable on multiple runs of this setup.

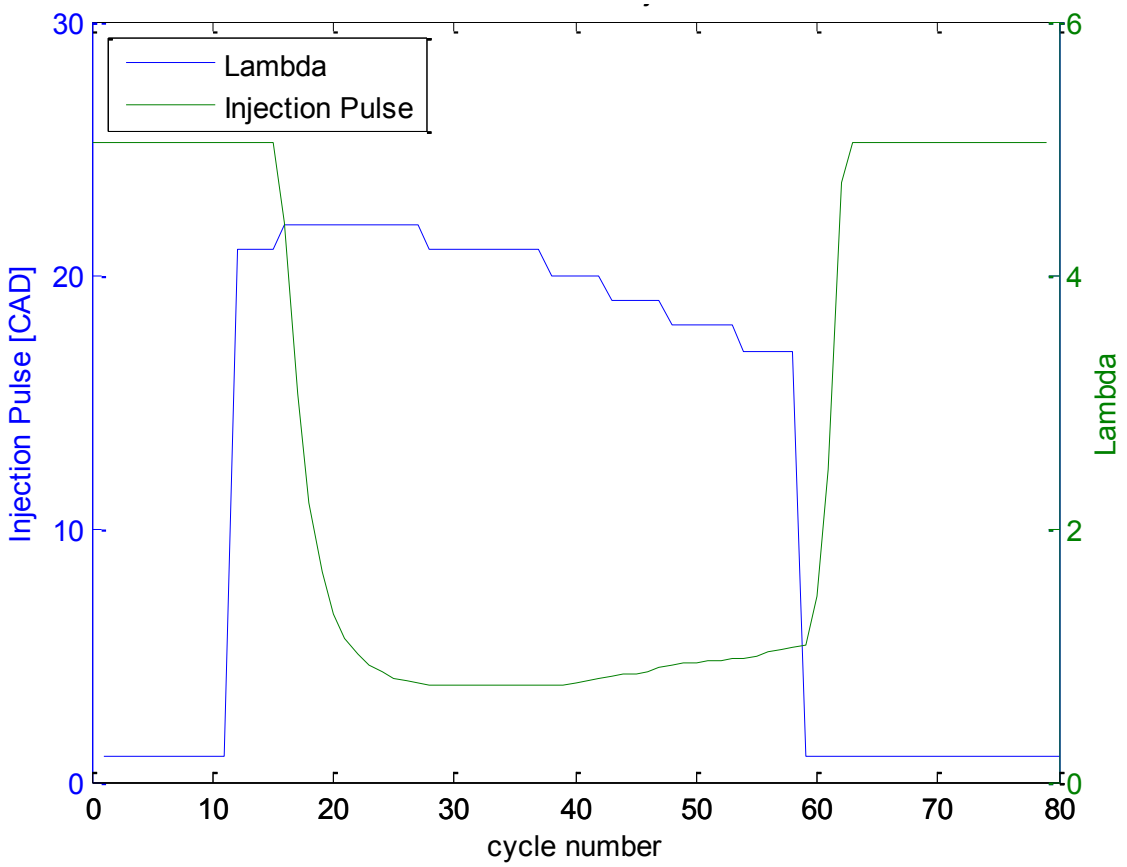

Figure 19: Variable Injection Pulse and Lambda Response

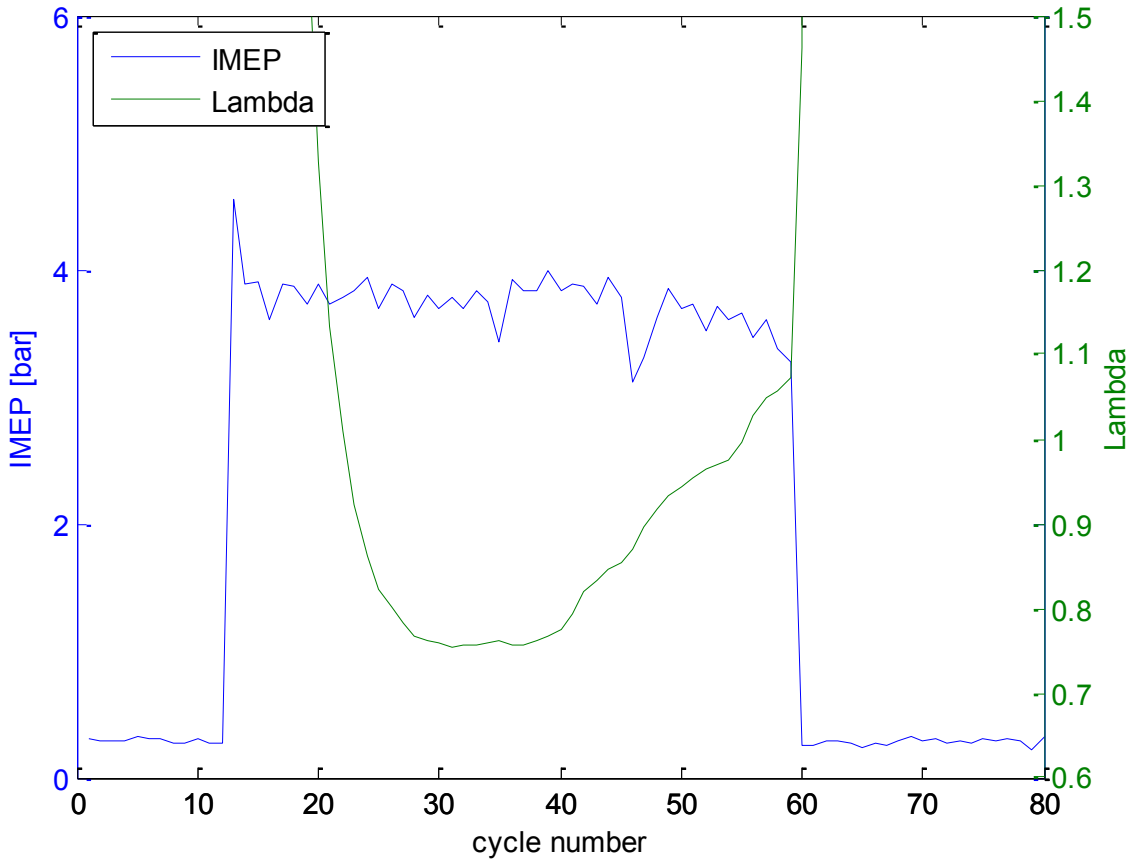

Figure 20: Lambda and Cycle-by-Cycle IMEP

The figure showing the IMEP response (Figure 20) also shows a more zoomed in view of the change in lambda once the pulse width is shortened. This detail shows that as lambda was ranged from around 0.75 to 1.05, IMEP remained relatively stable; the slight drop as the mixture is leaned out is subtle since the initial mixture was very rich and the end mixture was only slightly leaner than stoichiometric—it never got lean enough to see a significant drop in IMEP.

It is worth noting the reason for the jagged stepped appearance of the injection pulse trace. The CAS system used for data acquisition has a resolution of 1 CAD; at 1500 RPM, this gives it a

0.111 ms resolution. Thus, as the pulse is decreased, the CAS system rounds the value to the closest increment of that resolution. In reality, the pulse widths are changing at a constant rate rather than in the stepped way that the plots make it appear. Furthermore, the jump in pulse width at the beginning of the test during the 25 warm up cycles (when the pulse should be constant) is due to the fluctuation in RPM that occurs from the dynamometer fighting to absorb the sudden jump in power that comes from firing the engine. Figure 21 shows the RPM jumping from 1500 to 1560 RPM momentarily after the engine begins firing; as the speed jumps, the pulse is still held to a constant time, though it now takes place over a greater CAD period since the engine is spinning faster.

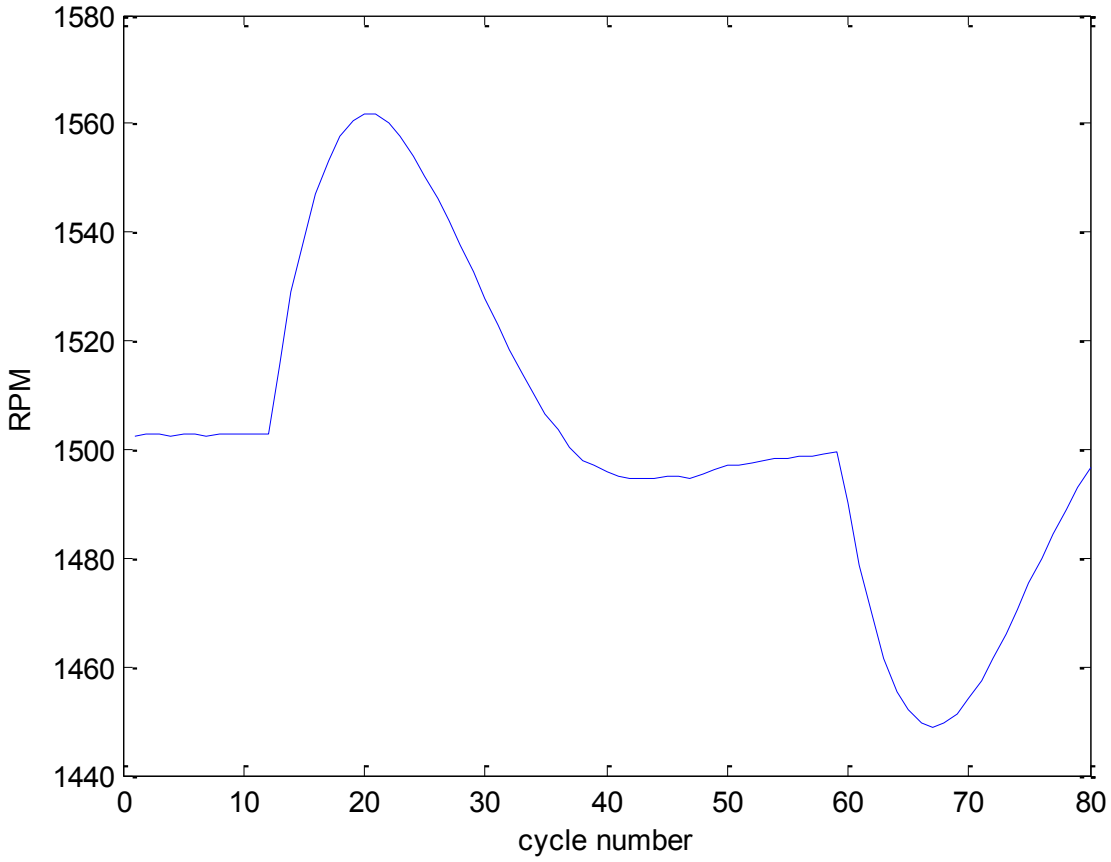

Figure 21: RPM Fluctuations due to Load Changes During Firing Test

From the high-speed images acquired from each cycle, the effects rich and lean combustion can be seen. The following plot shows a detail of the lambda trace and also highlights which cycles are shown in the following combustion images (Figure 22). The images are arranged by CAD, and each set of 6 images shows what the flame development looks like at that specific CAD for six different lambdas (Figure 23).

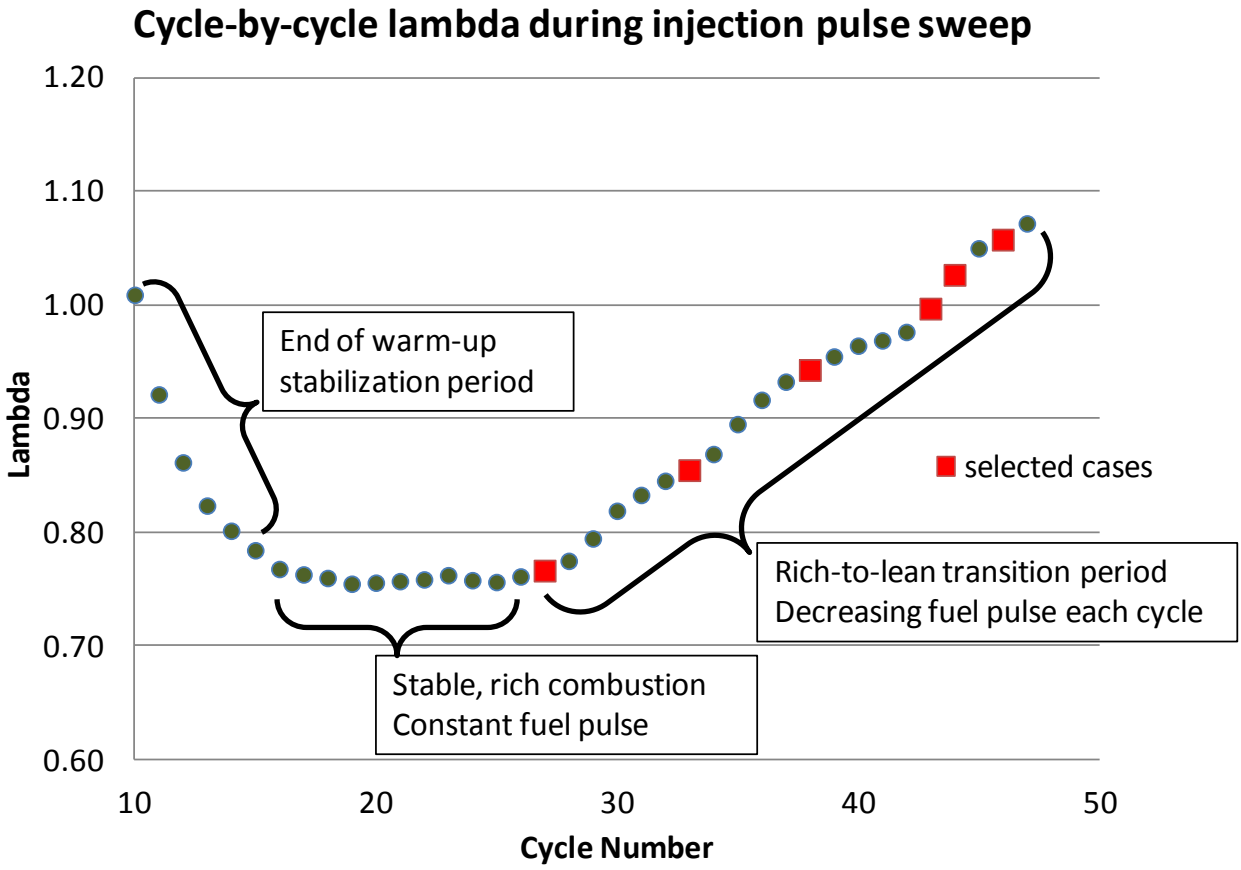

Figure 22: Cycle-by-Cycle Lambda during Injection Pulse Sweep with Selected Optical Image Cycles Noted

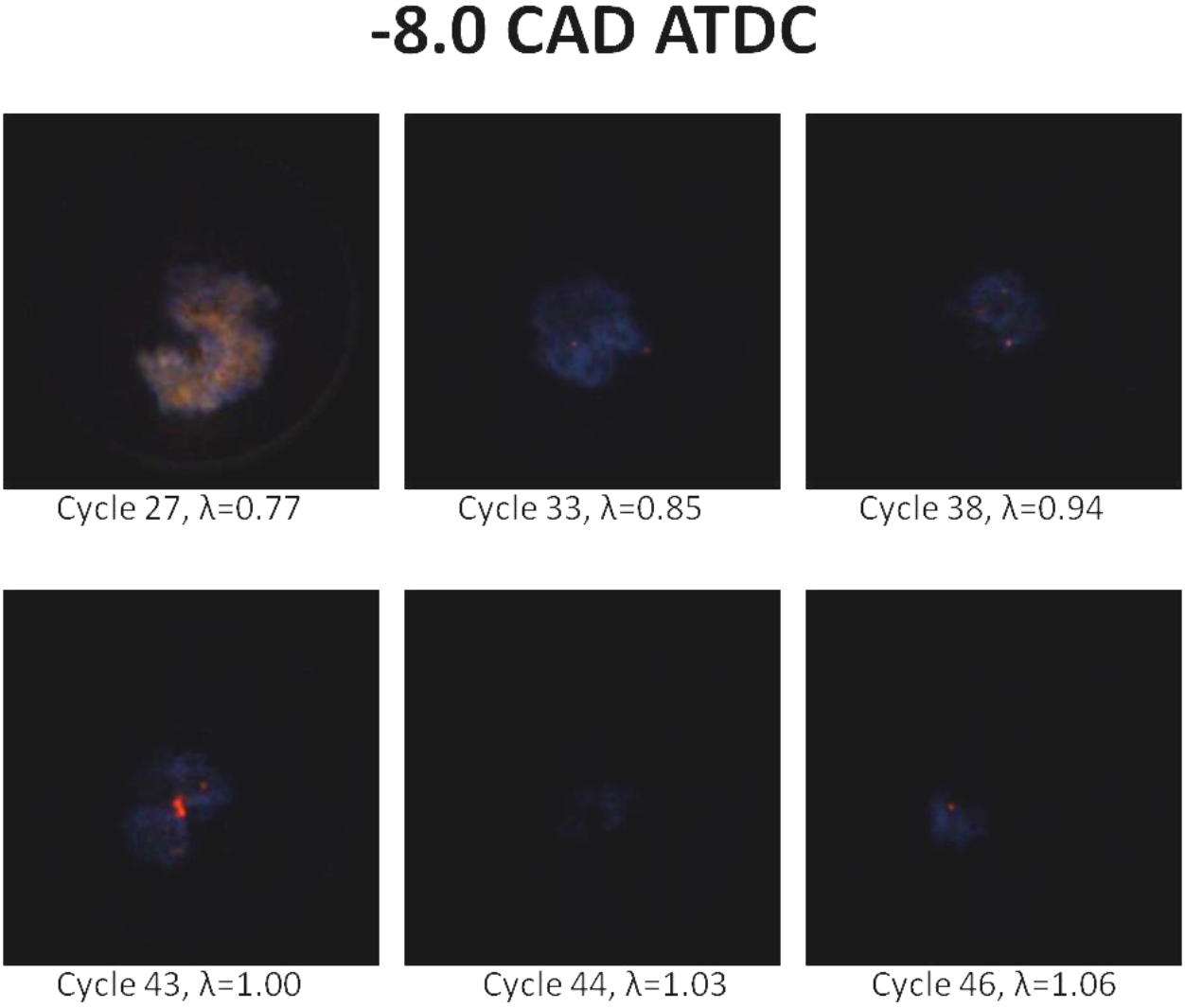

Figure 23: Visible Light Flame Images of SI Combustion at Varying Lambda

Figure 23 (cont'd)

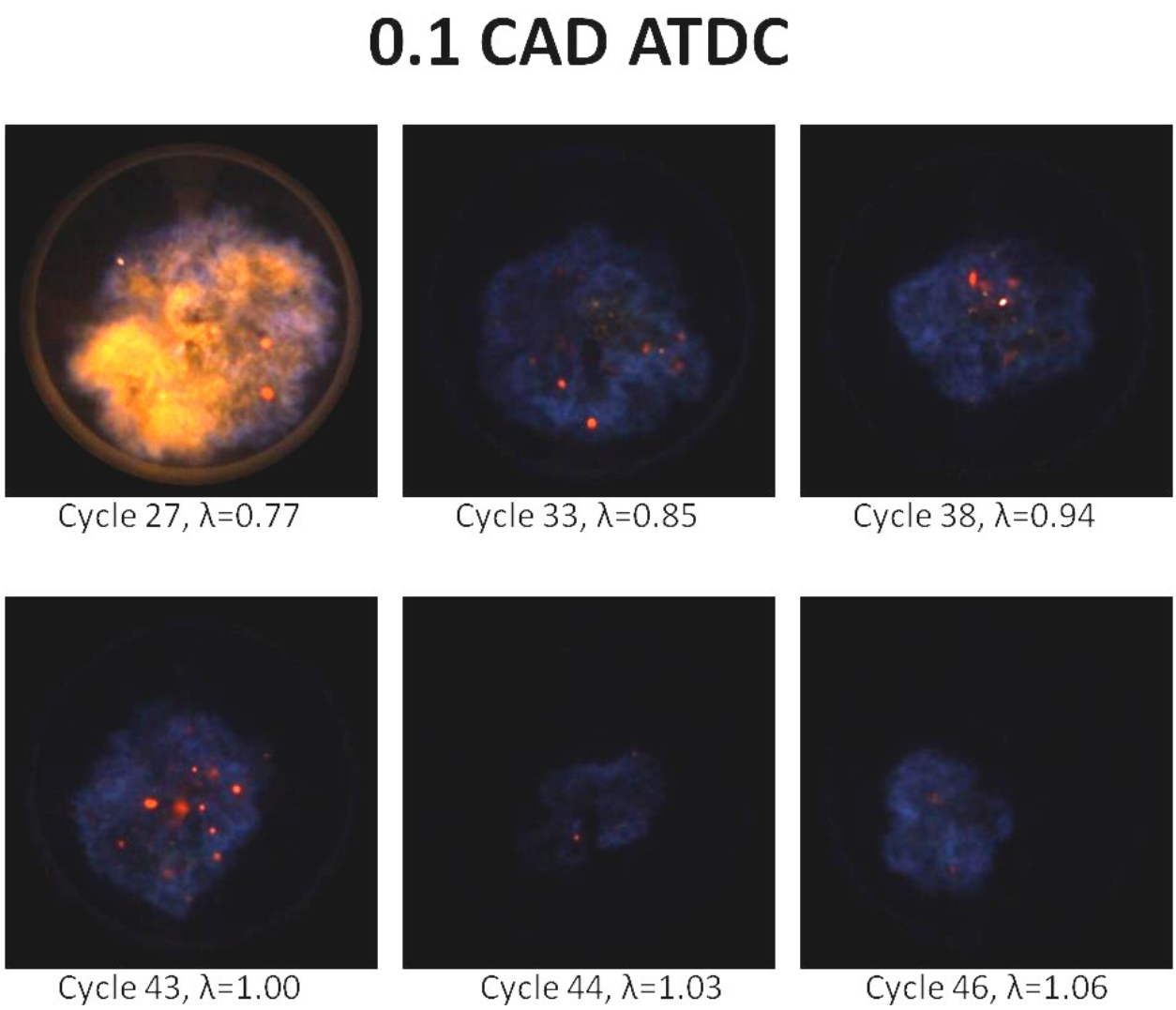

Figure 23 (cont'd)

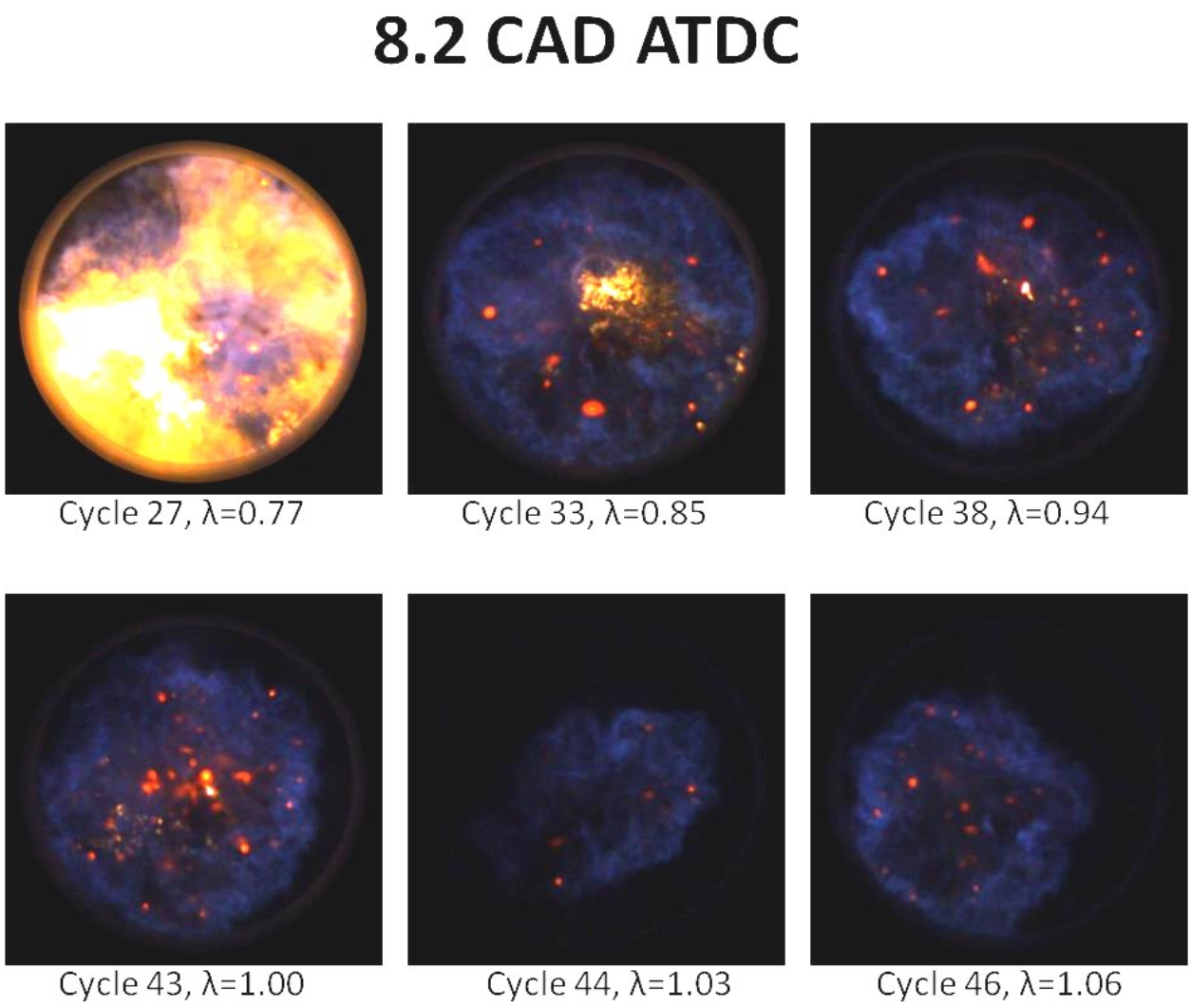

Figure 23 (cont'd)

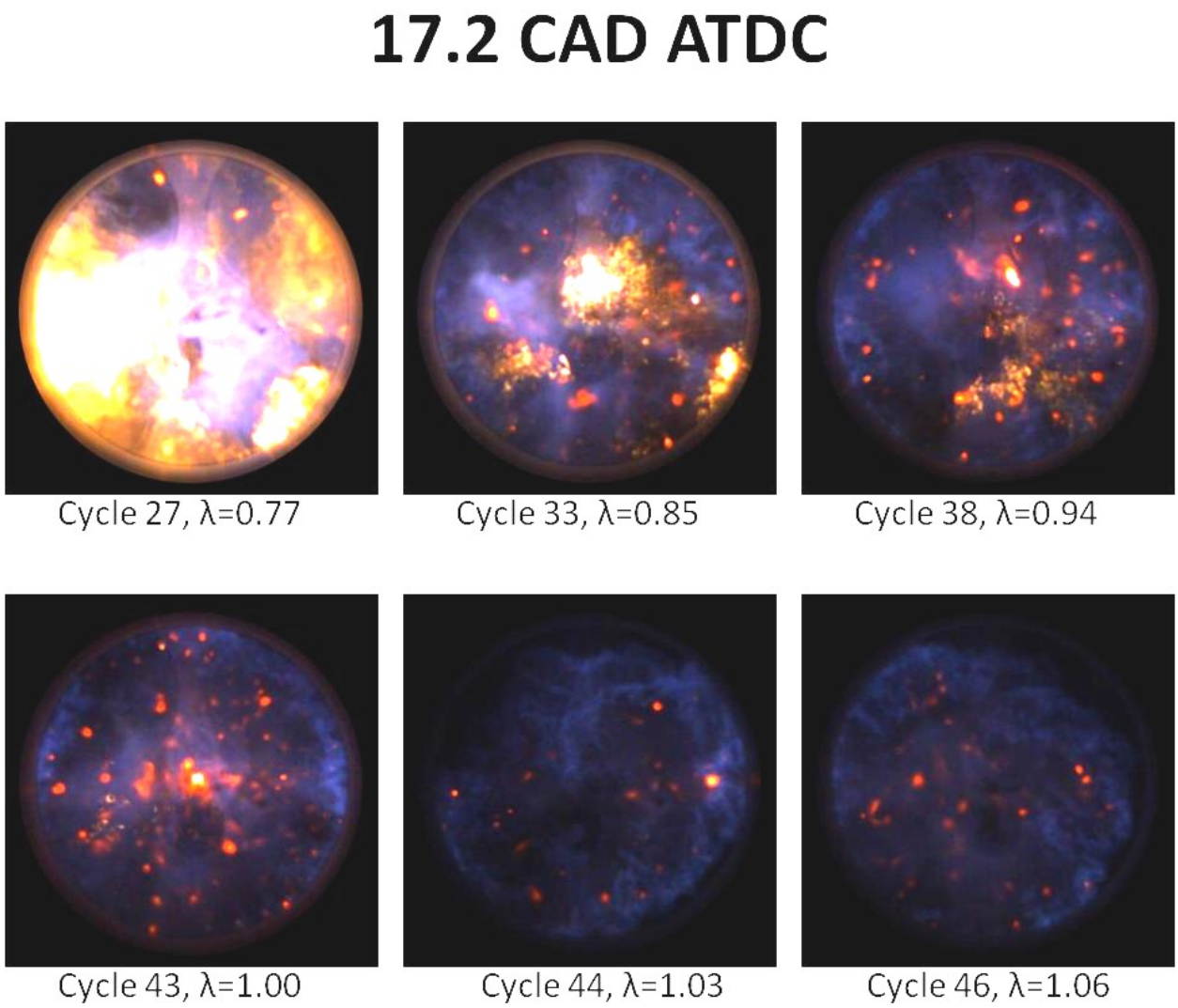

Figure 23 (cont'd)

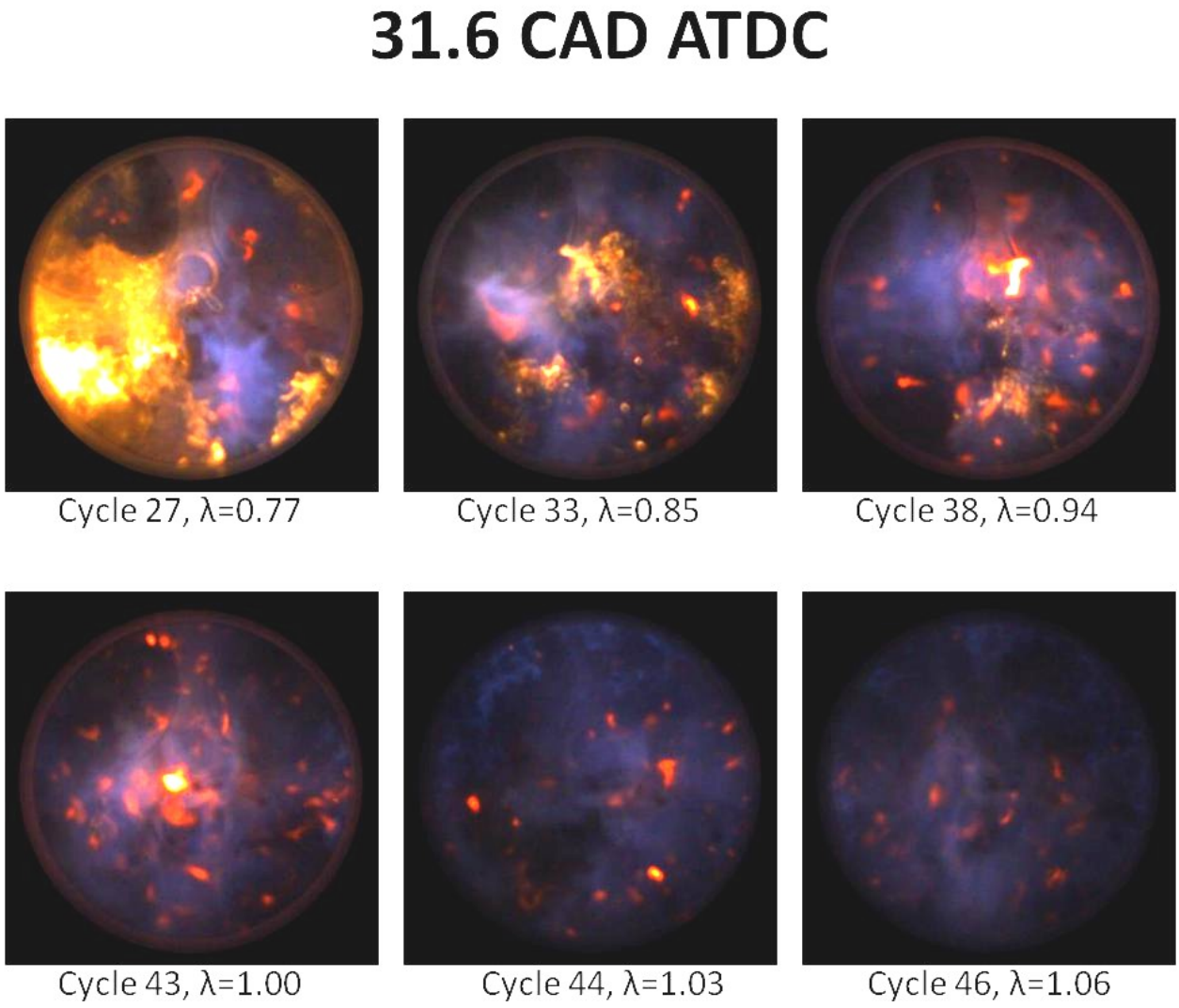

HCCI Tests

For initial optical engine HCCI tests, it was hoped that the setup would allow for a simple mode switch from SI to HCCI. Though the full details of smoothing of this switch were not to be worked out yet, the goal was to simple be able to run in SI mode for a few cycles to warm up the cylinder and to provide some exhaust gas that could be trapped to help initiate the first HCCI cycles. However, this method was never successfully achieved due to difficulties with the throttle plate.

It was hoped that the throttle plate would be strong enough to lower the intake pressure to acceptable SI levels even with a small amount of boost necessary for HCCI, but repeatability tests showed that the motor used to drive the throttle plate was not capable of controlling the throttle position against the force of the air flowing past it. After a few trials, the throttle plate motor burned out. A replacement motor fell victim to the same thing. Thus, the only HCCI tests performed involved trying to start the 50-cycle period with a spark-assist HCCI mode.

The first tests with indolene test fuel yielded very poor results with very little (if any) combustion; when combustion was achieved, it appeared in the form of a very late partial burn from the spark assist. The fuel was replaced with regular 87 octane pump gasoline, likely with 10% ethanol, in order to provide something that would more readily react under compression, with its lower octane rating being generally good for autoignition [17]. With this fuel, a series of tests were run with different intake air temperatures, boost pressures, and injection pulses (Table 3). With a temperature of 200°C, HCCI operation was achieved on roughly every 2-4

cycles with the remaining cycles consisting of misfires and partial burns. Optical images from these tests showed combustion initiating in multiple spots throughout the cylinder without the assistance of a spark. Most of the fully burned HCCI cycles followed high recompression pressure events—when a small amount of heat release was present during recompression, a fast-burning HCCI cycle usually followed. This result points to the likely benefits of using a recompression pilot injection strategy in the future in an attempt to induce a small amount of heat release during each recompression event.

Table 3: Optical Engine Test Result Overview with 87 Octane Pump Gasoline

	Intake air temp	**Exhaust cam advance**	**Manifold boost pressure**	**Injection pulse [ms]**	**Spark assist**	**Result**
Test063	185°C	42°	1.23 bar	2.4	none	No combustion
Test064	187°C	42°	1.75 bar	2.4	none	No combustion
Test065	188°C	43°	1.78 bar	2.0	25 cycles at -15°, 25 cycles at 5°	No combustion
Test066	203°C	43°	1.6 bar	2.4	25 cycles at -15°, 25 cycles at 5°	Some late combustion with early spark assist
Test067	200°C	45°	1.6 bar	2.4	25 cycles at -15°, 25 cycles at 5°	Combustion. Misfired approx every 3rd cycle. Cyclic combustion pattern with 7-8 HCCI cycles, always following partial burn cycle with high recompression
Test068	200°C	45°	1.25 bar	2.4	25 cycles at -15°, 25 cycles at 5°	Fired roughly every other cycle. Numerous HCCI cycles

Additional tests were run with PRF70 (Table 4) which is 70% isooctane, 30% n-heptane; this fuel should display an even more distinct two-stage heat release that can aid in the success of the main combustion event [18,19,20]. These tests showed just limited promise in this setup, with HCCI combustion achieved only roughly every 3rd cycle. Pressure rise rates in these tests were very high when the engine fired.

Table 4: Optical Engine Test Result Overview with PRF70 Test Fuel

	Intake air temp	Exhaust Advance	Manifold Pressure	Injection Pulse	Spark Assist	Result
Test083	190	60°	1.25 bar	2.4	25 cycles at -10°, 25 cycles at 0°	HCCI achieved on roughly every 3rd cycle. Very high pressure rise rates.

Test068 was the most successful HCCI test. The motoring trace for this case had a peak pressure of nearly 20 bar and a recompression pressure around 10 bar. The IMEP trace shows that roughly every other cycle produced at least some sort of combustion, though a closer look at the peak pressures and the actual pressure traces point to many of these being late or partial burns (Figure 24). For the first 25 fueled cycles, spark assist was on at 15° BTDC, while for the remaining cycles it was retarded to 5°ATDC. Combustion was more consistent after the spark was retarded, mostly likely due the increased operating temperature of the engine. A detailed summary of the cycles that fired with an HCCI-type pressure rise signature is found below (Table 5).

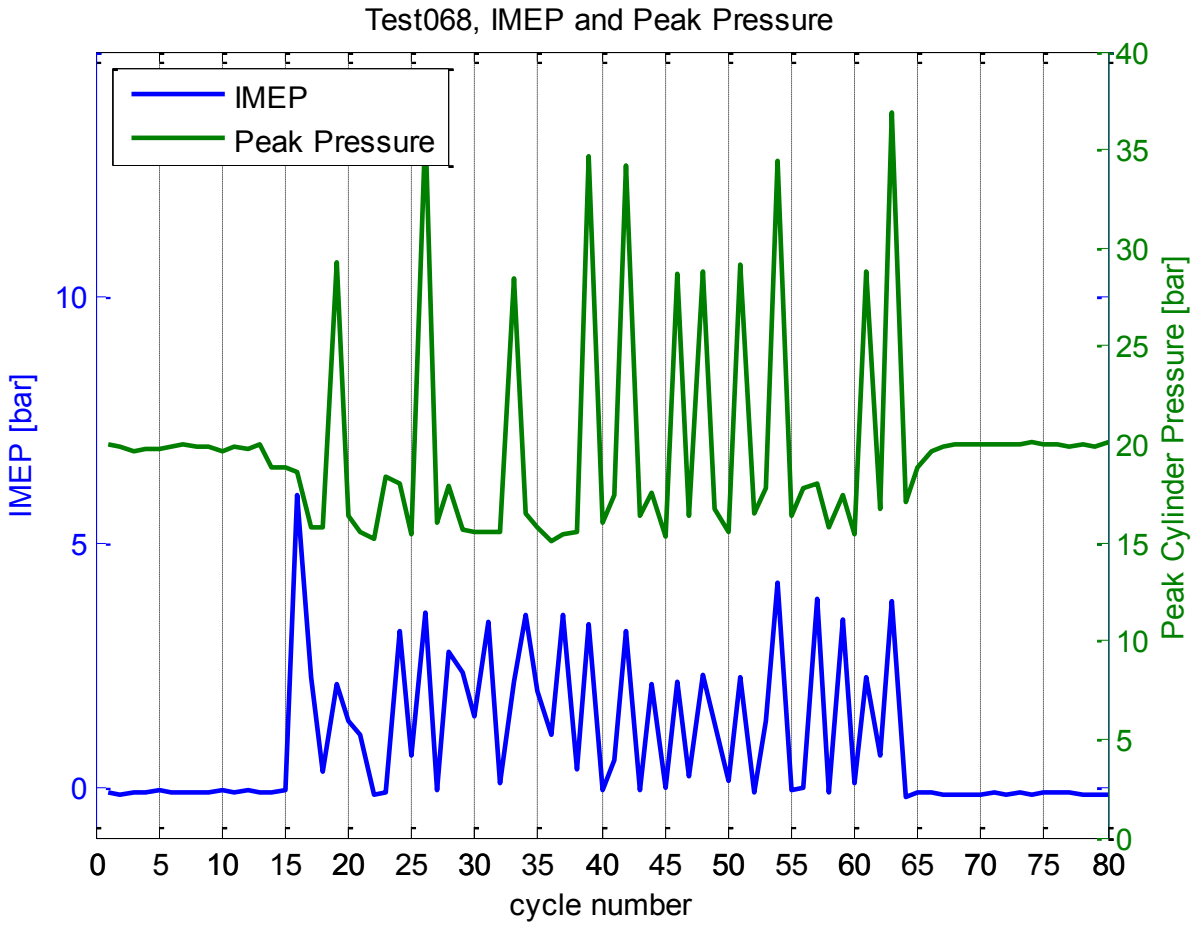

Figure 24: Cycle-by-Cycle IMEP and Peak Pressure during HCCI Test

Table 5: Data Summary, Optical HCCI Test068

Cycle	Spark Timing [CAD]	Peak P [bar]	Peak P location [CAD]	IMEP [bar]	Recomp. of previous [bar]	PMEP of previous recomp. [bar]	IMEP of previous firing cycle [bar]	Peak P of previous cycle [bar]	IMEP 2 cycles before [bar]	Peak P 2 cycles before [bar]
19	-15	29.3	-3	2.1	14.5	1.5	1.8	15.7	2.2	15.8
26	-15	36.0	-2	3.5	12.3	0.3	0.9	15.5	3.1	18.0
33	-15	28.4	0	2.0	15.8	1.7	1.8	15.5	3.3	15.5
39	5	34.7	-6	3.3	13.3	0.5	0.8	15.5	3.4	15.4
42	5	34.2	-2	3.1	13.3	0.1	0.7	17.4	-0.1	16.1
46	5	28.7	0	2.0	18.3	1.0	1	15.3	2.0	17.5
48	5	28.8	-1	2.2	18.6	0.9	1.1	16.3	2.0	28.7
51	5	29.1	-1	2.1	18.4	1.5	1.6	15.6	1.1	16.8
61	5	28.8	-1	2.1	19.0	1.2	1.3	17.7	3.3	16.4
63	5	36.9	2	3.7	11.6	0.3	0.9	15.5	2.1	17.4
Mean:		31.5	-1.4	2.6	15.5	0.9	1.2	16.0	2.2	17.8

Three cycles fired fully in an HCCI mode during the early spark assist period. The pressure traces of these cycles are shown below in Figure 25; in the plot, the blue curve is the motoring pressure trace, and the falling edge of the red signal shows the timing of the spark assist at 15° BTDC.

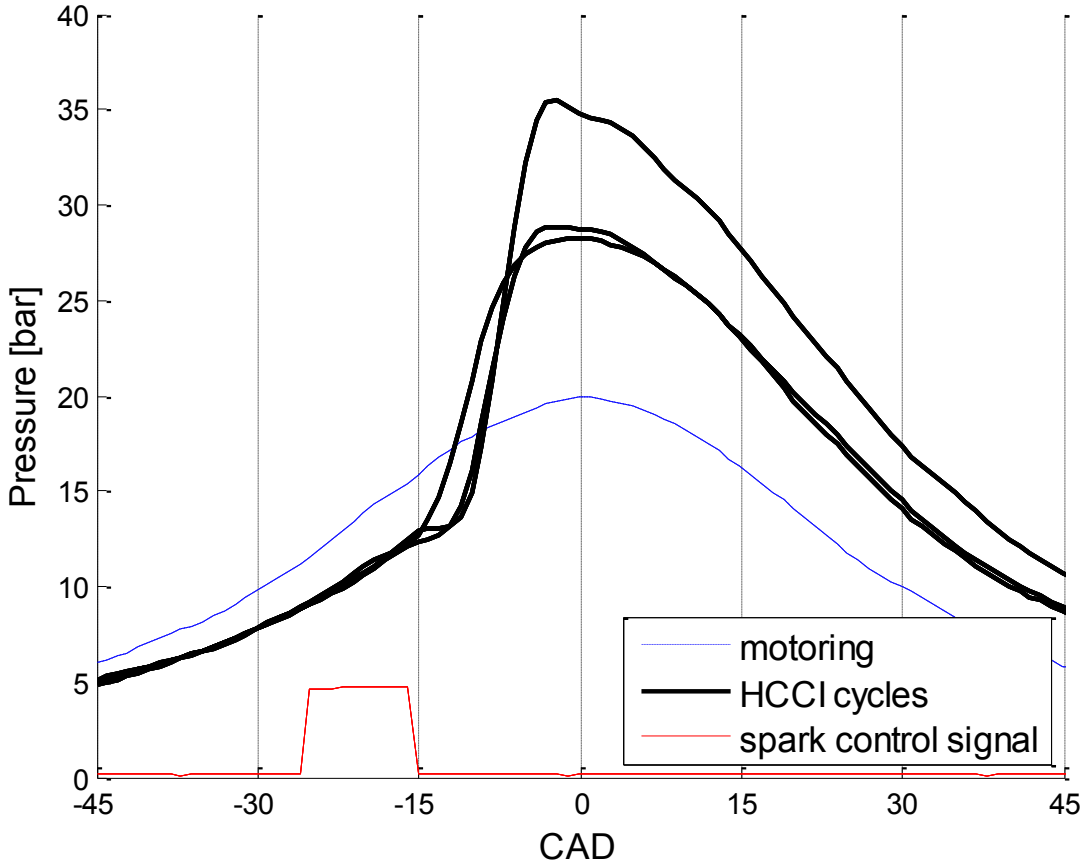

Figure 25: Optical Engine HCCI Cycles with Early Spark Assist

With the spark at 5° ATDC, seven HCCI cycles were recorded (Figure 26). Several of these cycles demonstrated very similar behavior, while one cycle showed much later combustion.

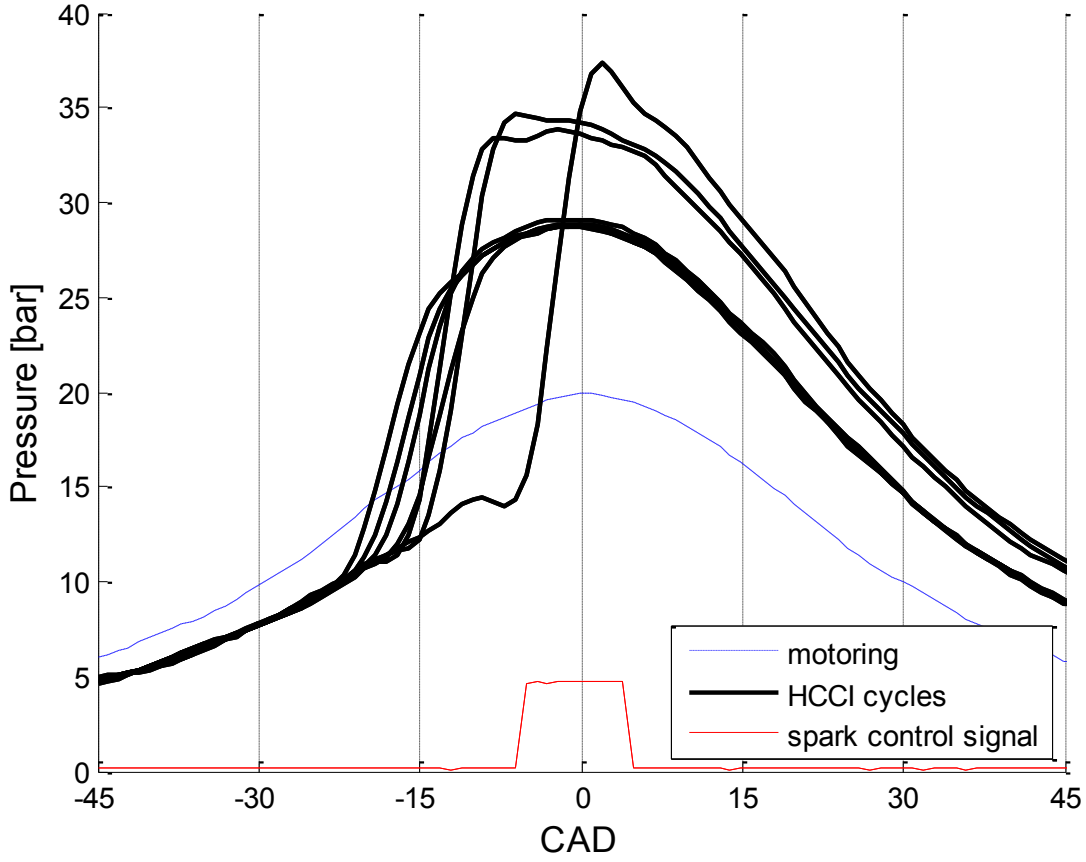

Figure 26: Optical Engine HCCI Cycles without Spark Assist

Looking at the full 720° cycles starting with the previous recompression event give insight into why the HCCI cycles fired the way they did. The following plot shows the early spark assist cycles with the recompression event that led to combustion. The recompression is significantly higher than the motoring recompression in all three cases (Figure 27). This is partly due to the higher pressure of the trapped exhaust gases compared to unburned air while motoring, but it also points to some amount of heat release happening during recompression. Indeed, the PMEP (essentially the IMEP of the 360 CAD pumping loop) is positive for these cycles, indicating heat release from unburned fuel left over from the previous cycle. This highlights an important key to achieving steady HCCI; using a pilot injection and possibly even spark assist during

recompression can help increase the likelihood that recompression pressures and temperatures are high enough to create conditions that will autoignite during the following compression stroke. This strategy has been used in works [12] and [13].

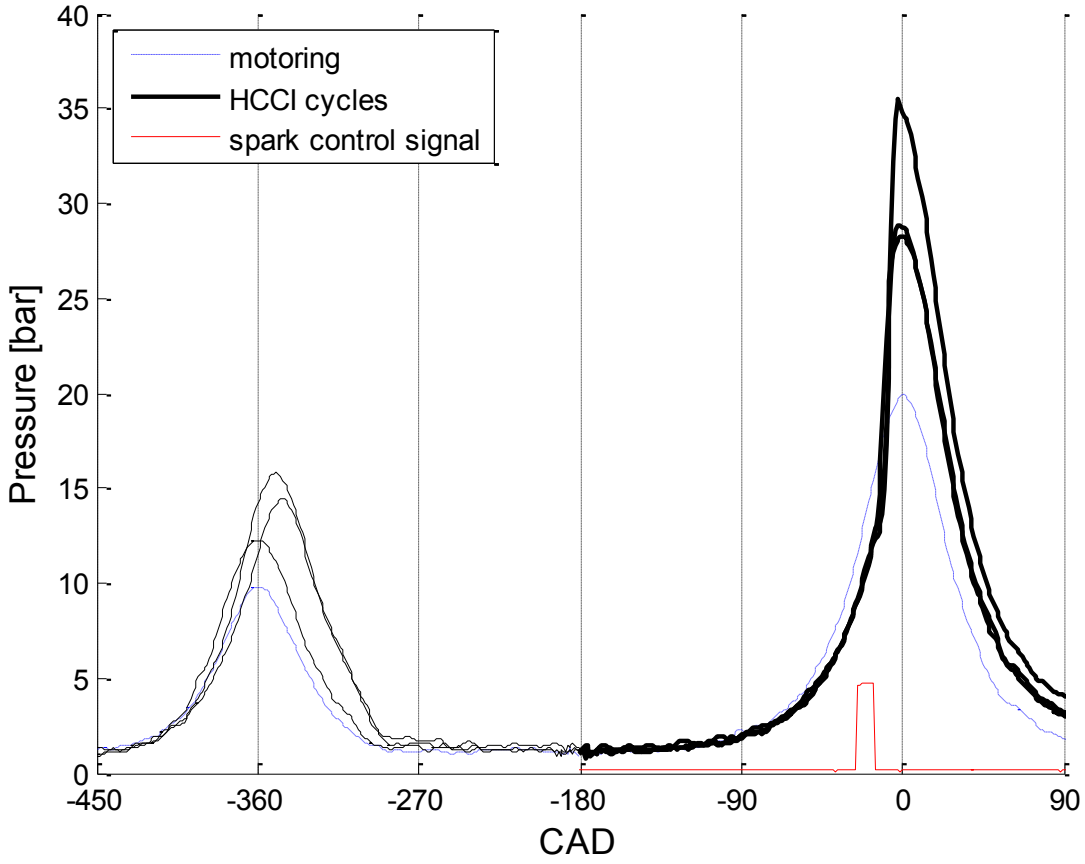

Figure 27: Recompression before Successful Spark Assist Optical HCCI Cycles

The same trend holds true for the HCCI cycles with the 5° ATDC spark assist, as shown below (Figure 28).

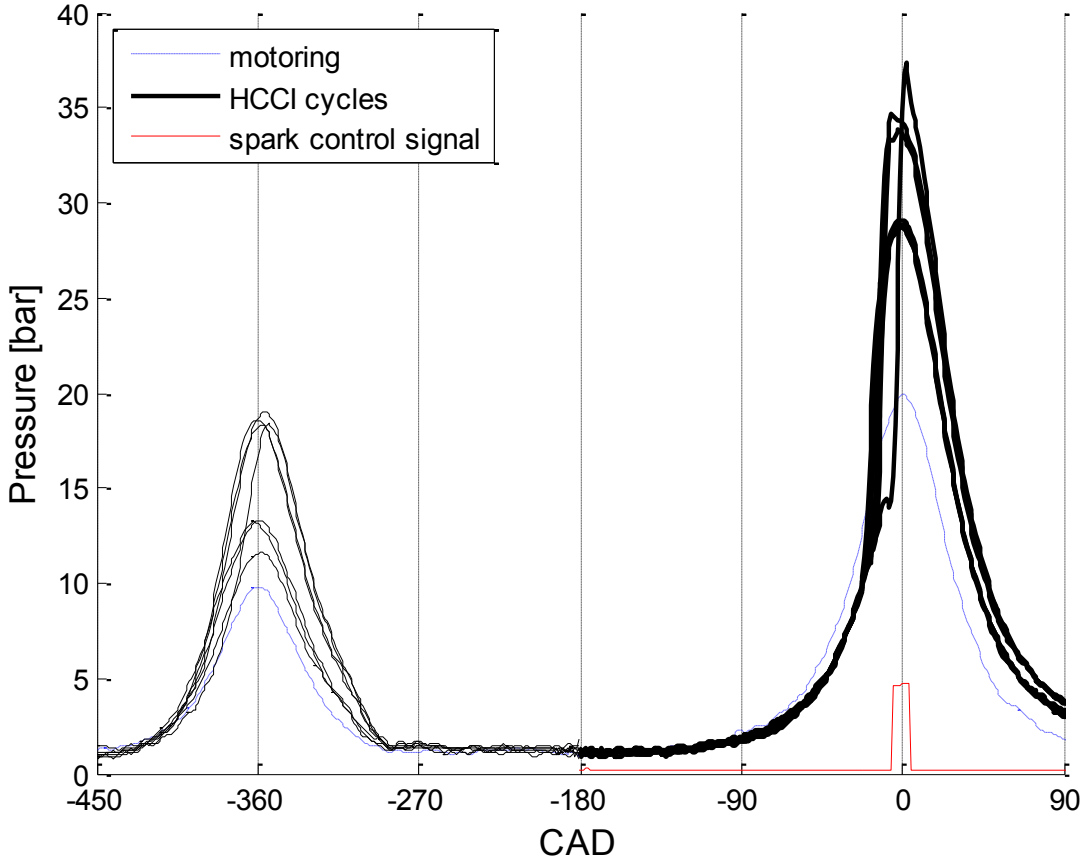

Figure 28: Recompression before Successful Non-Spark Assist Optical HCCI Cycles

In general, the combustion event that lead to the high recompression event prior to HCCI combustion was either a misfire or a very late partial burn. The following plots show the same recompression traces from cycles prior to HCCI as shown in the plots above, but this time they show the TDCF combustion (or lack of combustion) event that lead into the high recompression; almost all of them are misfires or late partial burns (Figure 29,Figure 30).

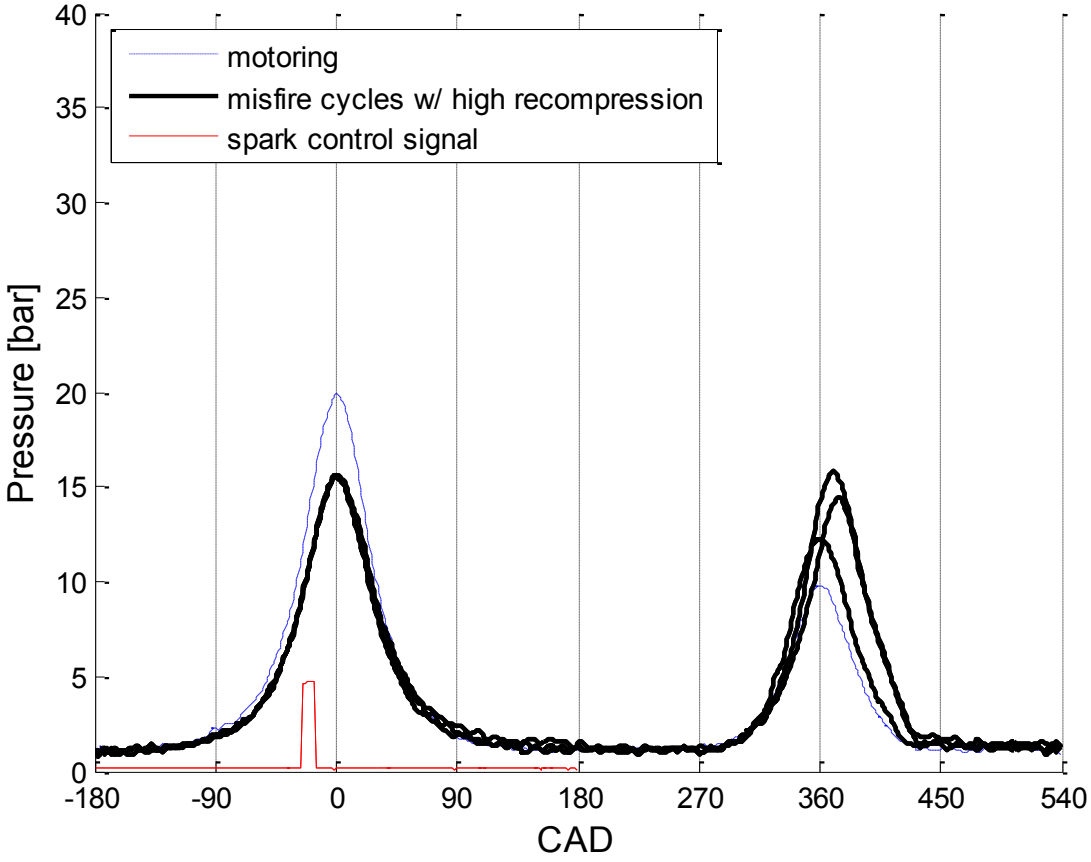

Figure 29: Misfires Before Large Recompression Events with Spark Assist

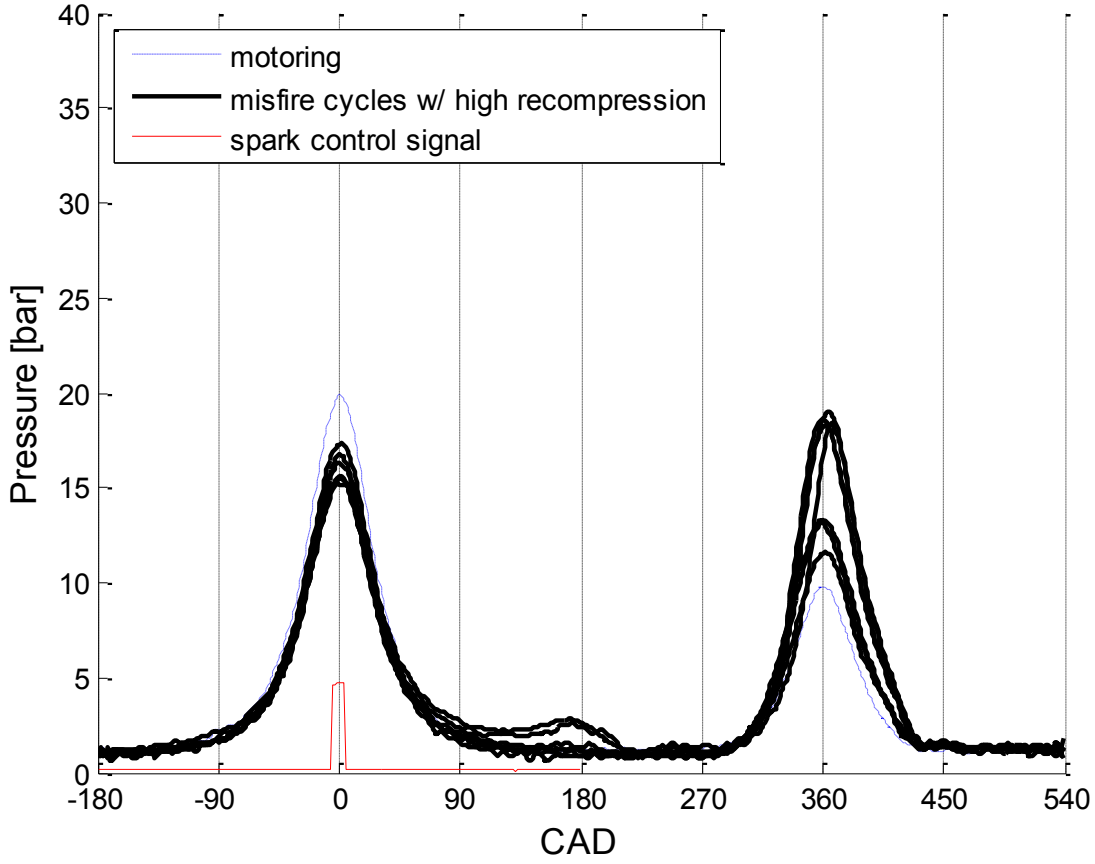

Figure 30: Misfires and Partial/Late Burn Cycles before Large Recompression, No Spark Assist

Cycle 39 of this test was chosen as an example cycle to show the formation of multiple ignition points at the start of combustion (Figure 31). Multiple initial ignition points are clearly visible in the first image, and as flame fronts from these points expand, additional separate ignition points form. Overall combustion is very fast, and phasing is earlier than desired with peak pressure occurring before TDC.

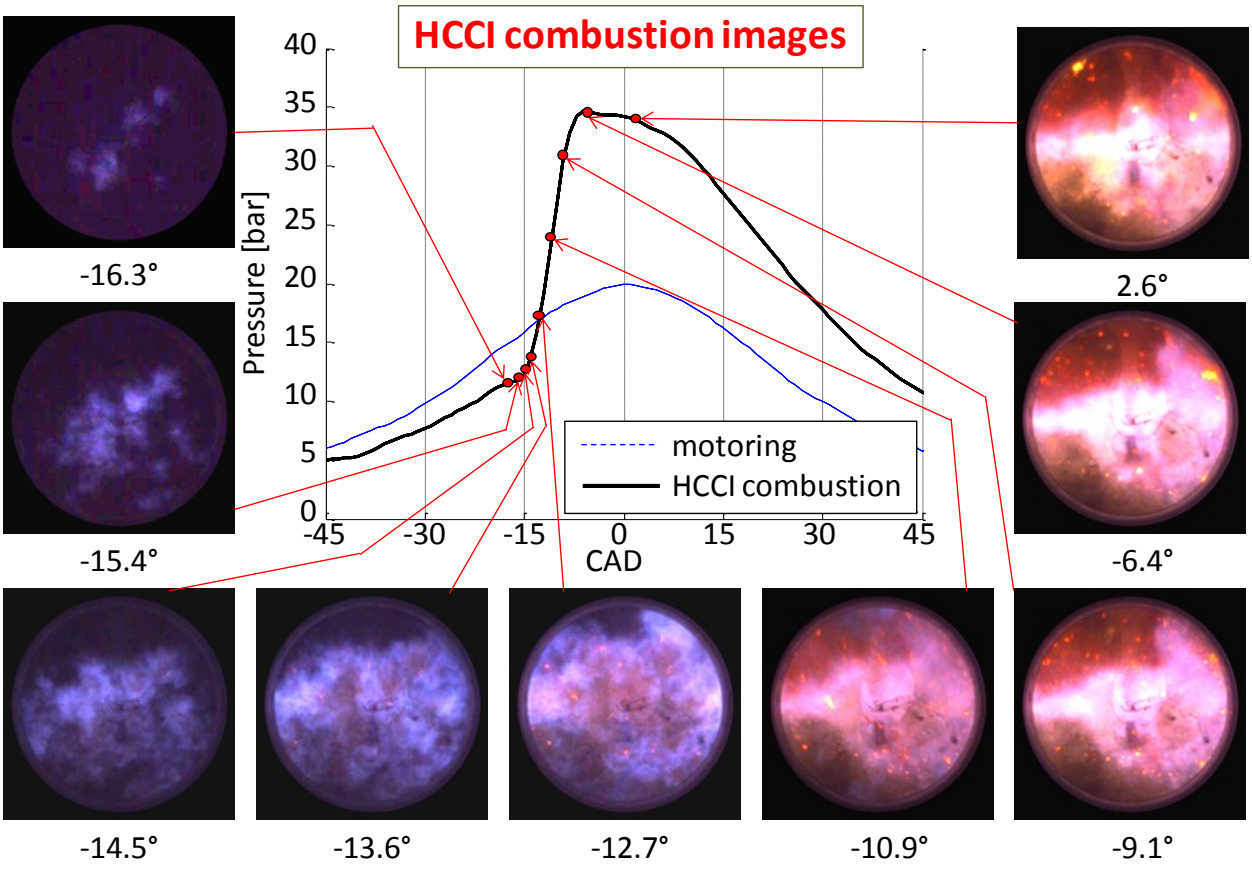

Figure 31: Single Cycle HCCI Combustion Images

A comparison of sample cycles (Figure 32) shows that combustion initiation can be seen in different locations throughout the cylinder and at different CAD timings in different cycles. This points out the difficulties of how cycle-to-cycle variations in flowfields and temperatures can effect HCCI operation drastically; they can affect the location and the timing of autoignition.

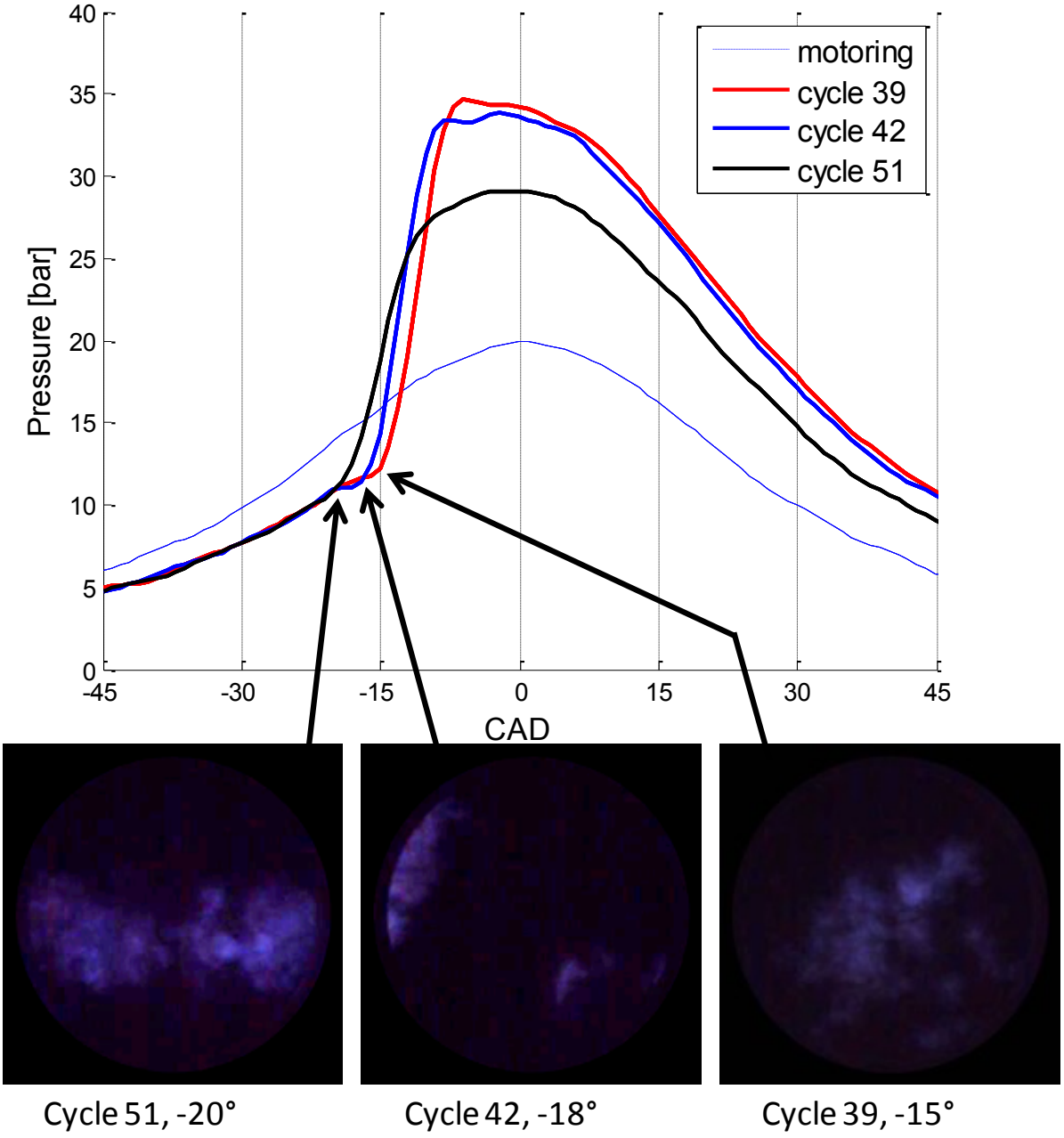

Figure 32: HCCI Ignition Points in Different Cycles

With the accomplishment of viewing the HCCI process in the optical engine complete, fabrication of the metal 4-cylinder engine became the priority, and the optical engine was partially disassembled to allow for this.

Chapter 4: METAL ENGINE

Upon completion of fabrication of the 4-cylinder metal engine and its test cell, the first motoring tests showed a significant difference in peak cylinder pressure between the cylinders, with cylinder 3 showing a particularly low pressure. This problem carried over into initial firing tests, and eventually led to the significant modification of converting the 4-cylinder engine into a 1-cylinder engine.

Blowby Issue Discovery

Firing tests with the original low CR pistons were run with both high- and low-lift cam conditions at 1500 and 2000 RPM (Table 6). These tests showed that blowby in cylinder 3 resulted in very poor combustion quality—the burn was late and slow, resulting in low peak pressure, low IMEP, and high COV. Adjusting the spark timing and fueling amount to cylinder 3 had little to no effect on improving this poor performance, nor did swapping hardware (injectors, spark plugs, pressure transducers, etc). Cylinder 2 performed well with low COV and the highest IMEP, while cylinder 1 was inconsistent with reasonable IMEP but sometimes a very high COV. Cylinder 4 showed a somewhat low IMEP but good COV.

Table 6: Initial Cylinder-by-Cylinder Firing Test Results, 4-Cylinder Engine

	MAP			IMEP [bar]				COV			
RPM	[kPa]	Lambda	Valve Lift	Cyl 1	Cyl 2	Cyl 3	Cyl4	Cyl 1	Cyl 2	Cyl 3	Cyl4
1500	45.5	1.03	low	3.53	4.59	2.61	4.10	20.2	2.7	12.1	2.5
1500	54.7	1.00	high	3.28	4.29	2.36	3.52	13.1	3.9	23.6	4.6
2000	52.1	0.97	high	3.69	4.44	2.94	3.75	3.9	1.9	8.8	1.4

A P-V diagram comparing the part load 1500 RPM performance of cylinders 2 and 3 demonstrates the blowby issue clearly (Figure 33). Note how the pressure trace of cylinder 3 deviates from that of cylinder 2 during compression and then results in a very weak burn. CAD-based pressure traces from a 2000 RPM test (Figure 34) show the drastically different peak pressure between the cylinders.

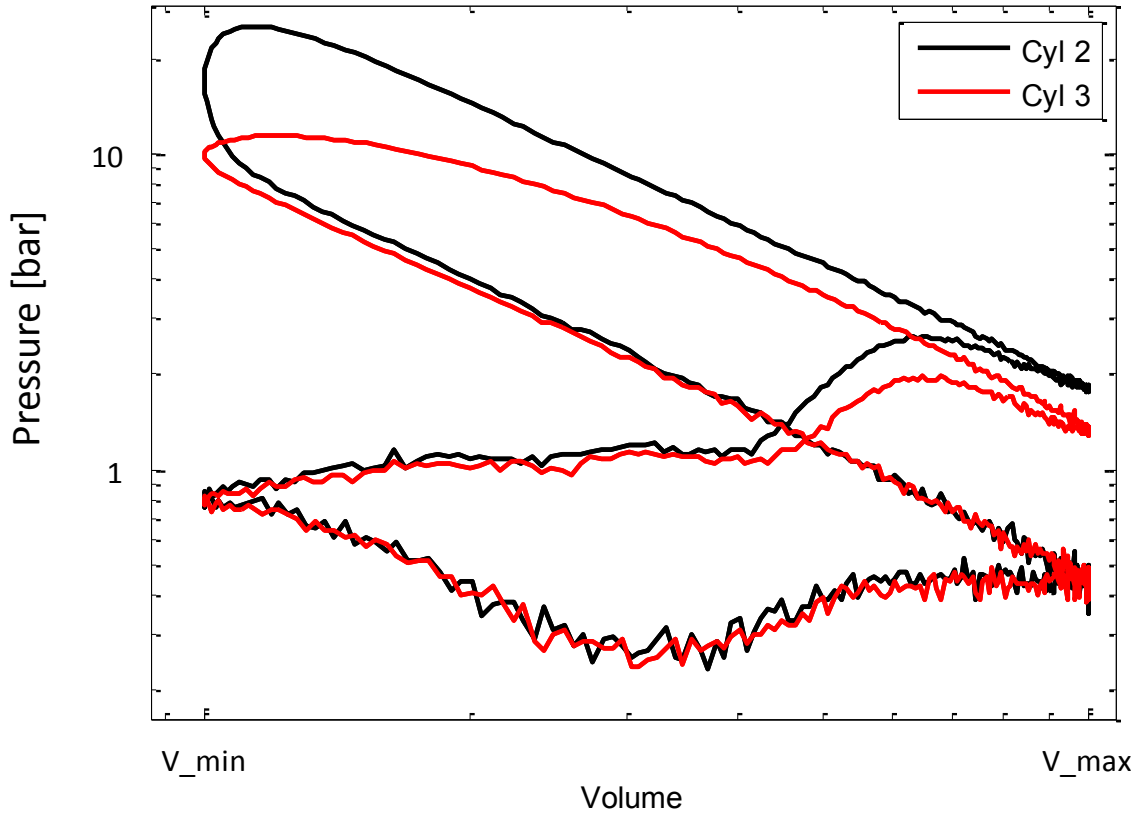

Figure 33: P-V Diagram Comparison of Cylinders 2 and 3 Firing, Low Lift Cams

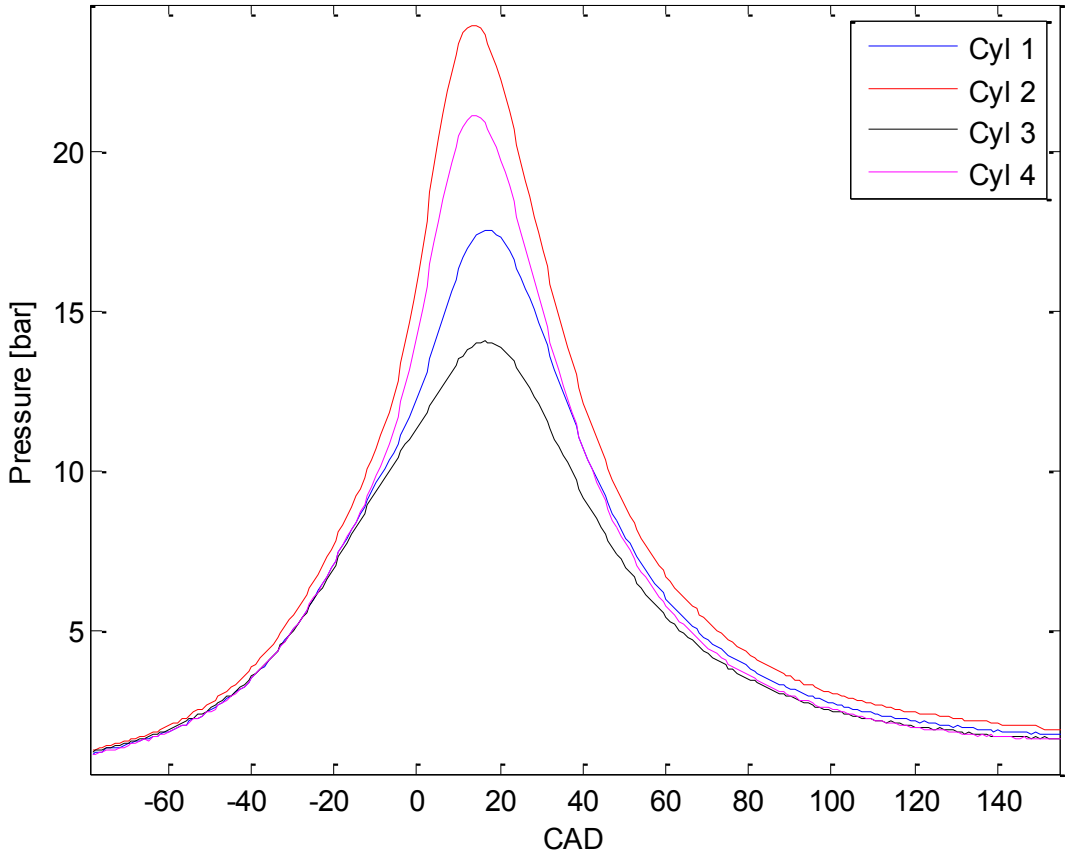

Figure 34: Firing Pressure Traces of all Cylinders, High Lift Cams

Despite the blowby problems in cylinder 3, performance of cylinder 2 was found to be very satisfactory. Control systems for fueling, ignition, valve lift, and cam phasing were verified to be working correctly, and a test point was run that closely mirrored previous test data provided by Chrysler, with considerations given the slightly different cam profiles with the 2-step valvetrain modifications that likely alter performance slightly (Table 7).

Table 7: Comparison of Cylinder 2 Performance with Existing Performance Data from Chrysler

	Speed [RPM]	MAP [kPa]	IMEP [bar]	NMEP [bar]	CA50 [CAD ATDC]	Peak Pressure [bar]	Injection Timing [CAD BTDC]	Spark Timing [CAD BTDC]
Chrysler Data Sample A	1856	53.1	4.48	3.99	5.1	26.6	299	22.5
Chrysler Data Sample B	2112	51	4.48	3.95	5.9	26.9	304	22.5
MSU Cylinder #2	2000	52.1	4.44	3.98	8.8	24.2	300	31

Motoring traces were examined in an attempt to better understand the low pressure problem in cylinder 3 (Table 8, Figure 35). Log-scale P-V plots also show a significant amount of blowby in cylinder 3. Though the peak pressure in cylinder 3 is close to those of cylinders 1 and 4 in higher speed and higher load motoring tests, the P-V plots from these tests still show significant blowby in cylinder 3, whereas the other cylinders arrive at their lower peak pressures by seemingly ingesting less intake air and losing less of it to blowby. A close look at a P-V diagram comparing cylinders 2 and 3 shows that at the start of the compression stroke, in-cylinder pressures are nearly identical, but the blowby in cylinder 3 causes a lower pressure by the end of the compression and expansion strokes (Figure 36).

Table 8: Motoring Pressure Tests, All Cylinders

Motoring Pressure Data							
Speed [RPM]	**MAP [kPa]**	**Valve Lift**	**Peak Motoring Pressures [bar]**				**Engine temp**
			Cyl 1	**Cyl2**	**Cyl3**	**Cyl4**	
1500	76.9	Low	17.8	18.6	16.2	17.0	Cold
2000	82.1	Low	19.7	20.1	19.2	19.3	Hot
2000	50.7	High	11.7	12.5	11.4	11.5	Hot

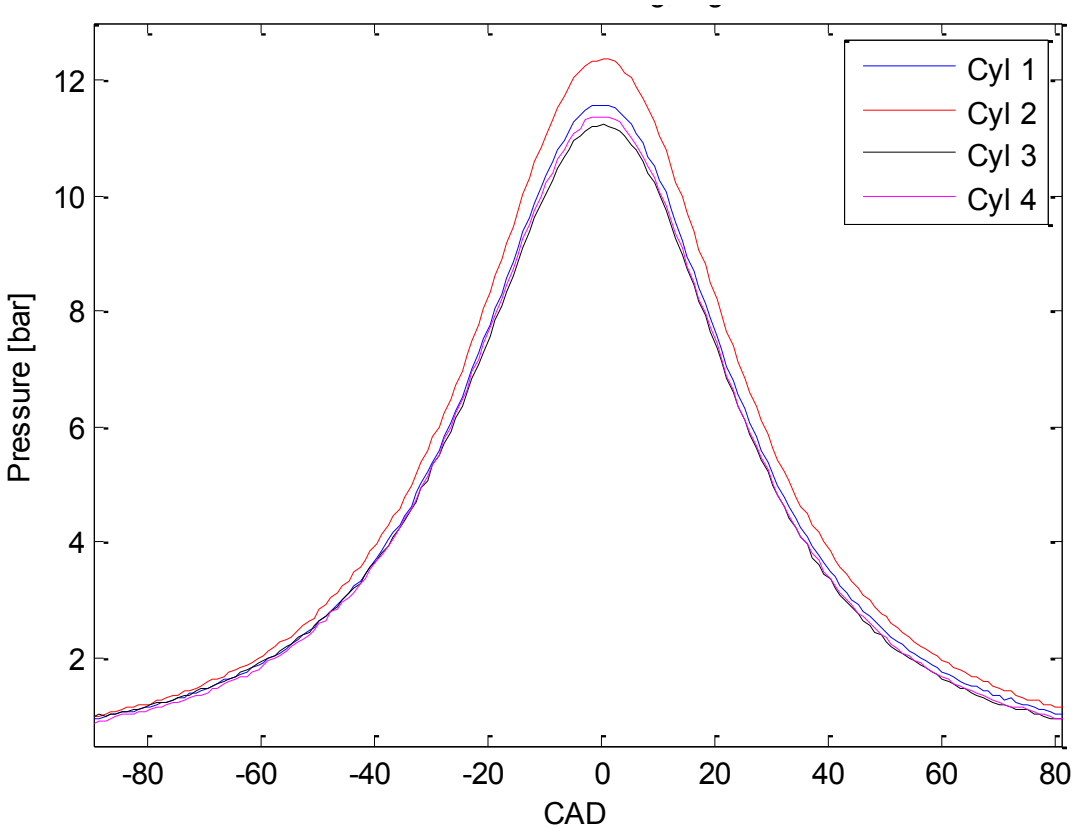

Figure 35: Motoring Pressure Trace Comparison of All Cylinders, Throttled with High Lift Cams

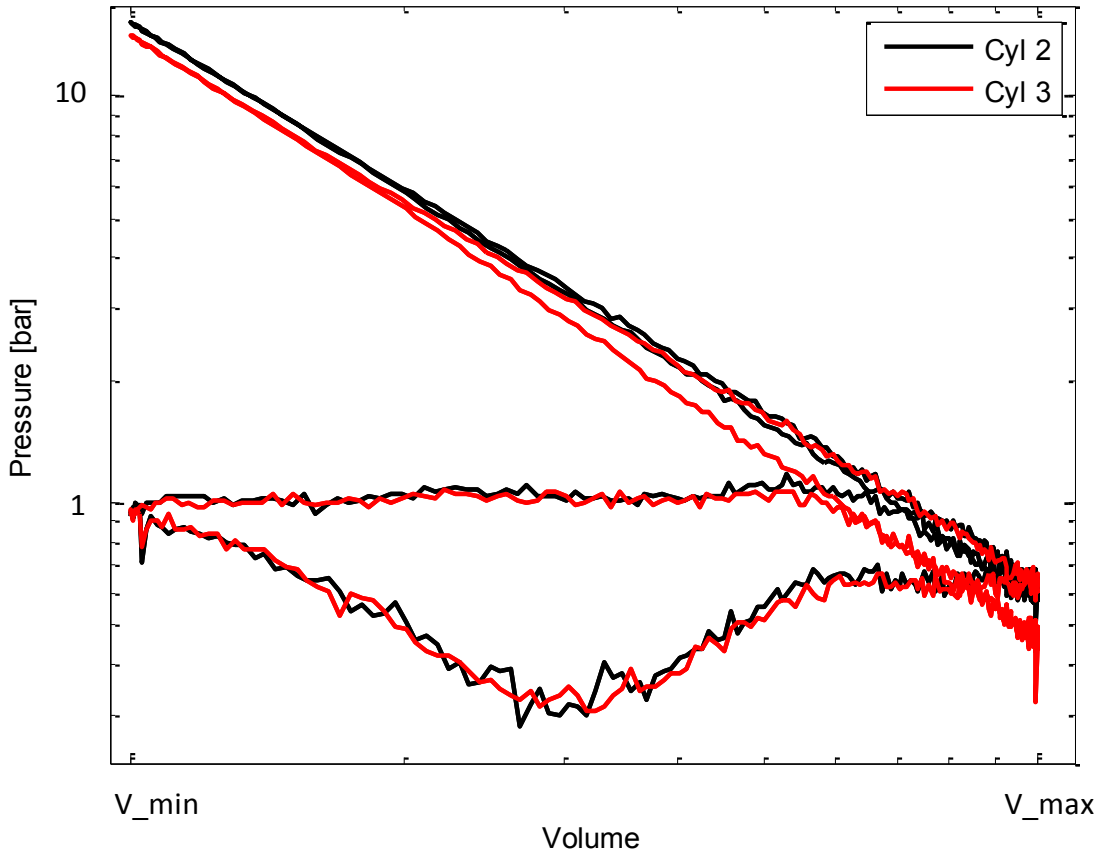

Figure 36: Motoring P-V Diagram Blowby Comparison, Cylinders 2 and 3, Part Throttle

Various tests were run to verify that the compression problems were due to blowby and not something else like head gasket leakage or valves seating improperly. A compression test was performed with a Mitvac Professional Compression Test Kit. With this device, the engine is motored at a low speed while a pressure gauge mounted to a cylinder through the spark plug hole; as the engine motors, the gauge reaches a maximum pressure. Cylinder 3 showed the lowest pressure at 195 psi, compared to a high of 240 psi for cylinder 2.

A second test was developed to determine if the leakage in each cylinder was indeed cause by air flowing past the rings and not the head gasket or valves. For this leak test, the cylinder was

filled with compressed air at a constant pressure of 95 psi through a fitting placed in the spark plug hole. All ventilation passages from the crankcase were blocked off except for one, which was outfitted with an airflow meter that could measure the flow rate of the compressed air that was leaking past the rings in standard cubic feet per hour (scfh). This test was performed with each piston at both TDC and BDC. Cylinder 3 allowed the greatest amount of leakage, showing that it experiences more ring blowby than the other cylinders. The results from both of these tests are show below (Table 9). Both of these tests help confirm what was seen in the motoring and firing pressure trace data.

Table 9: Compression and Leak Test Results

Cylinder number:	**1**	**2**	**3**	**4**
Compression test pressure:	225 psi	240 psi	195 psi	210 psi
Leak test flowrate at TDC:	11 scfh	11 scfh	16.5 scfh	9.5 scfh
Leak test flowrate at BDC:	15 scfh	13 scfh	19 scfh	12 scfh

Following these leak tests, the engine was disassembled, and the block, pistons, and rings were inspected for signs of abnormal wear that could be causing the blowby problem. Bore measurements were made, and nothing obviously wrong was observed with cylinder 3.

The new high compression ratio (CR) pistons were installed upon the rebuild of the engine, and further motoring tests were performed. Again, low peak pressures were observed in cylinder 3 (Table 10). It is noteworthy that the blowby seems to decrease with increasing speed and manifold pressure—the PV plots below show less blowby at the 2000 RPM WOT case than at

part load (Figure 37, Figure 38). At higher pressure, the ring may be forced to seat correctly, while at a lower pressure, it may not seat well, causing more blowby.

Table 10: Motoring Pressures with High Compression Ratio Pistons

RPM	MAP [kPa]	Peak Pressure [bar]			
		Cyl 1	Cyl 2	Cyl 3	Cyl 4
1000	67.9	18.5	19.3	16.8	17.3
1000	84.8	23.8	24.2	21.3	22.5
1500	55.6	15.6	16.2	14.5	14.9
1500	84.8	24.6	24.8	23.1	23.6
2000	46.2	12.9	13.5	12.5	12.5
2000	84.7	25.1	25.3	24	24.4

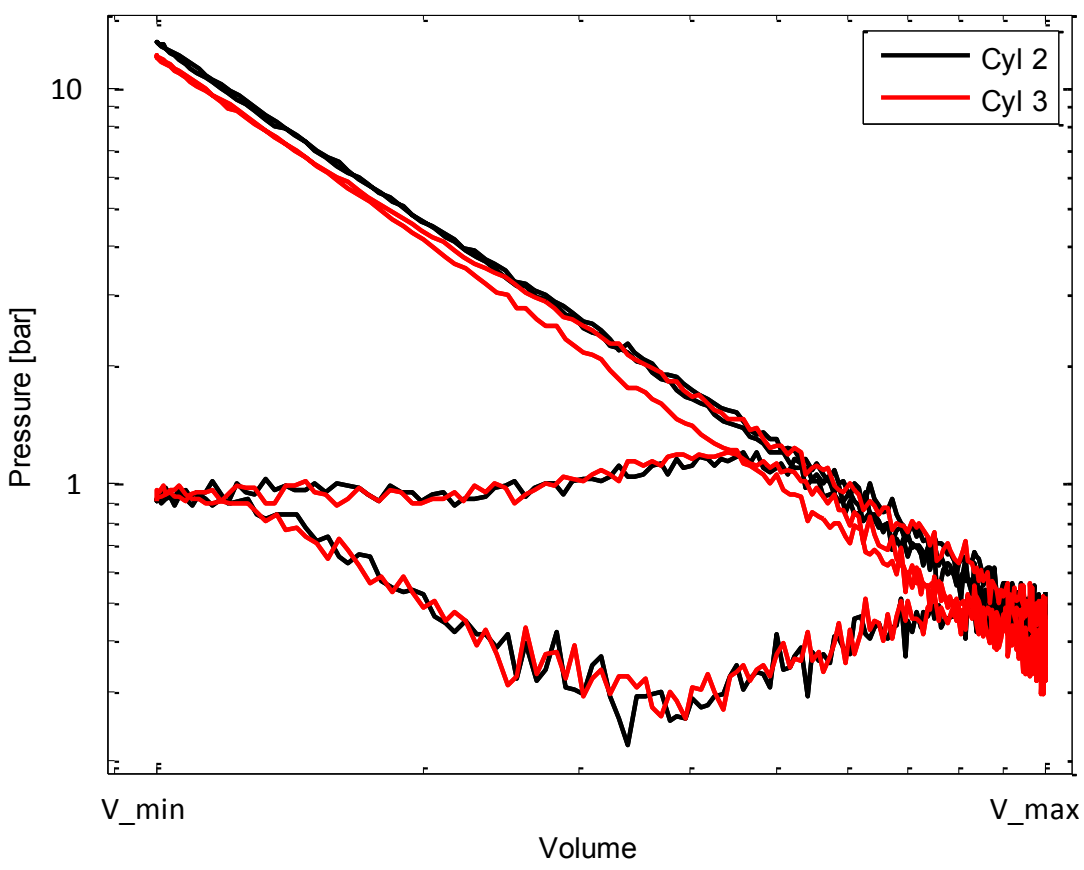

Figure 37: Throttled Motoring P-V Diagram Comparison of Cylinders 2 and 3, High CR Pistons

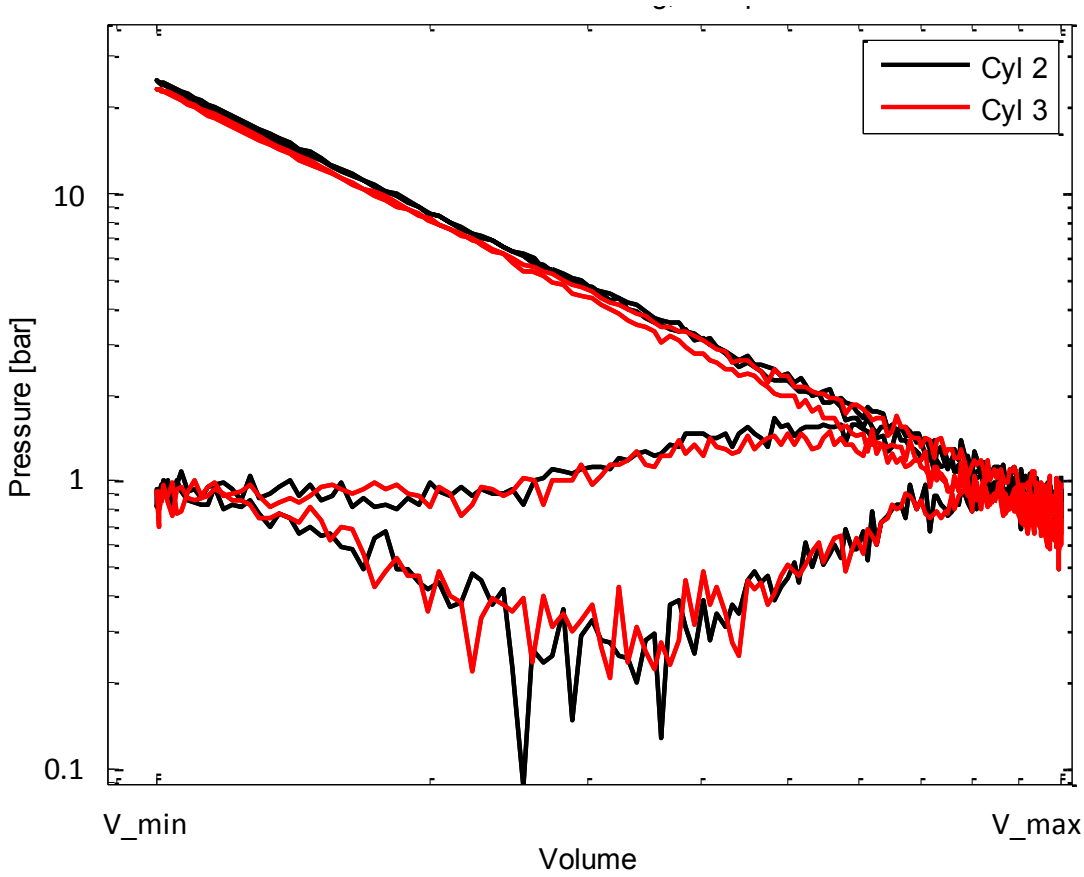

Figure 38: WOT Motoring P-V Diagram Comparison of Cylinders 2 and 3, High CR Pistons

In an attempt to eliminate the possibility that the valves were not seating fully (i.e. the lifter may still be lifting the valve stem slightly even when the valve is supposed to be shut), the engine was motored without camshafts in place. The results of this test was inconclusive—with no air entering through the intake valves, it appeared that random ring dynamics took over as the primary factor in peak motoring pressure as the peak pressures wandered significantly in each cylinder each time this test was attempted.

An attempt at eliminating exhaust valve seating was made by motoring with the exhaust valve rockers removed and with the intake throttle down significantly. The results of this test show poor compression in cylinder 3 and good compression in cylinder 2 (Table 11, Figure 39).

Table 11: Motoring Peak Pressure with Exhaust Valves Closed

		Peak Pressure [bar]			
RPM	**MAP**	**Cyl1**	**Cyl2**	**Cyl3**	**Cyl4**
750	22.5 kPa	5.1	5.9	3.32	4.41
1500	16.7 kPa	4.35	4.76	3.12	4.05

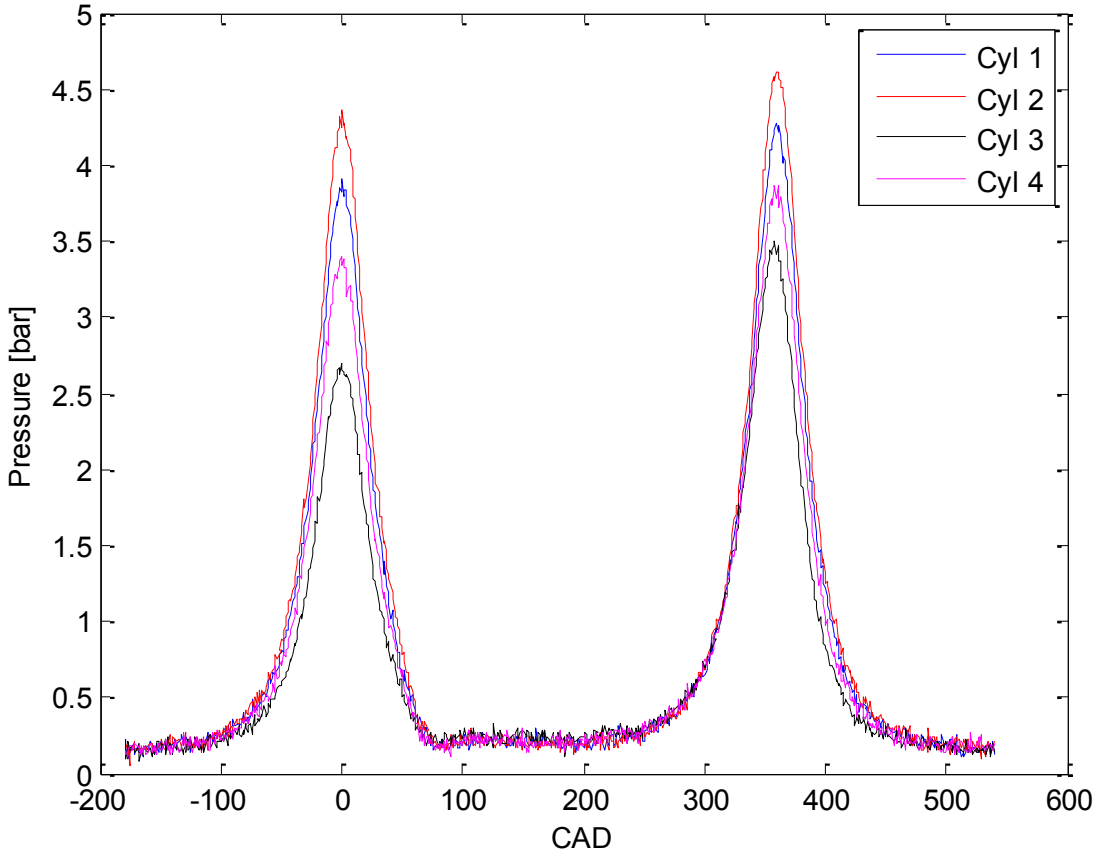

Figure 39: Motoring Pressure Traces with Exhaust Valves Shut

It was concluded that the likely reason for the blowby was a warped cylinder block that has caused different levels of bore distortion in the different cylinders. A second engine was delivered, but upon inspection of the block, a large gash was found in one cylinder bore; it was decided that it was not worth the effort to rebuild the engine with this block that contained visible damage and would likely cause compression and/or oil consumption problems. A third engine was also delivered, but time constraints prevented that engine from being disassembled for block inspection.

Multi-Cylinder SI Benchmarking Tests

The decision was made to proceed with tests with the new pistons and rings to see if breaking them in would improve the blowby problem enough to bring the performances of each cylinder close enough to each other to eventually run good HCCI tests. A series of benchmarking tests were run in order to map out a performance window of the engine at various loads and speeds, with the primary focus of these tests being the performance of cylinder 2.

The improvements from the increased compression ratio of approximately 12.5:1 were demonstrated by comparing performance of the old and new pistons at constant manifold pressure. The new pistons yielded a 5.2 bar IMEP verses 4.4 bar IMEP with the old pistons when air flow rate through the engine was held constant, air-fuel ratio was stoichiometric, and spark timing was adjusted to keep combustion phasing the same (Table 12).

Table 12: Performance Comparison of Low and High Compression Ratio Pistons, Constant MAP

	IMEP [bar]		COV		PeakP [bar]		CA50 [°ATDC]		Spark Timing [°BTDC]	
Piston:	**New**	**Old**	**New**	**Old**	**New**	**Old**	**New**	**Old**	**New**	**Old**
	5.2	4.4	1.7	1.9	29.4	24.2	8.7	8.8	25	30

Three test speeds (1500, 2000, and 2500 RPM) and three load points (4.5, 6.0, and 7.5 bar IMEP) were chosen as benchmarking test points for the high-lift cams in SI mode using 93 octane Shell premium fuel (Table 13). Optimal cam timings and injection timings in these tests were based off of previous test data provided by Chrysler. Spark timing was adjusted to keep CA50 timing at 8° ATDC for best IMEP and low COV. These test points not only give an understanding of how the engine responds to a broader window of operating conditions, but also help to establish parameters for the SI conditions needed during an HCCI-SI mode switch in the future. Sample P-V and Mass Fraction Burned (MFB) plots of the low, middle, and high load points from the 2000 RPM tests are shown below (Figure 40); these figures effectively show the reduction in PMEP as load increases, and they show the consistent combustion phasing. A careful look at the MFB plot shows the slightly faster 10-90% burn duration as the load increases. Also of note is how much of the fuel-air mixture is burned by the time the piston reaches TDC; in these cases it is around 15-20%. This parameter becomes useful when comparing SI combustion to HCCI combustion.

Table 13: Preliminary SI Benchmarking Test Points, Cylinder 2 Results, 93 Octane Fuel

Speed	MAP [kPa]	IMEP [bar]	PMEP [bar]	Spark [CAD BTDC]	Injection Pulse [ms]	CA50 [CAD ATDC]	B1090 [CAD]	COV of IMEP
1500	47.7	**4.54**	0.50	24	1.90	8	23	2.2
	57.7	**5.84**	0.42	22	2.20	8	22	1.5
	66.1	**7.51**	0.37	19	2.60	8	18	1.4
2000	46.0	**4.62**	0.53	27	1.85	7	23	1.2
	56.4	**5.98**	0.44	23	2.20	9	21	1.7
	65.4	**7.52**	0.35	20	2.55	7	19	1.2
2500	42.0	**4.51**	0.59	25	1.80	8	24	1.3
	52.8	**6.05**	0.50	22	2.20	8	22	1.8
	62.9	**7.77**	0.44	19	2.67	9	22	1.3

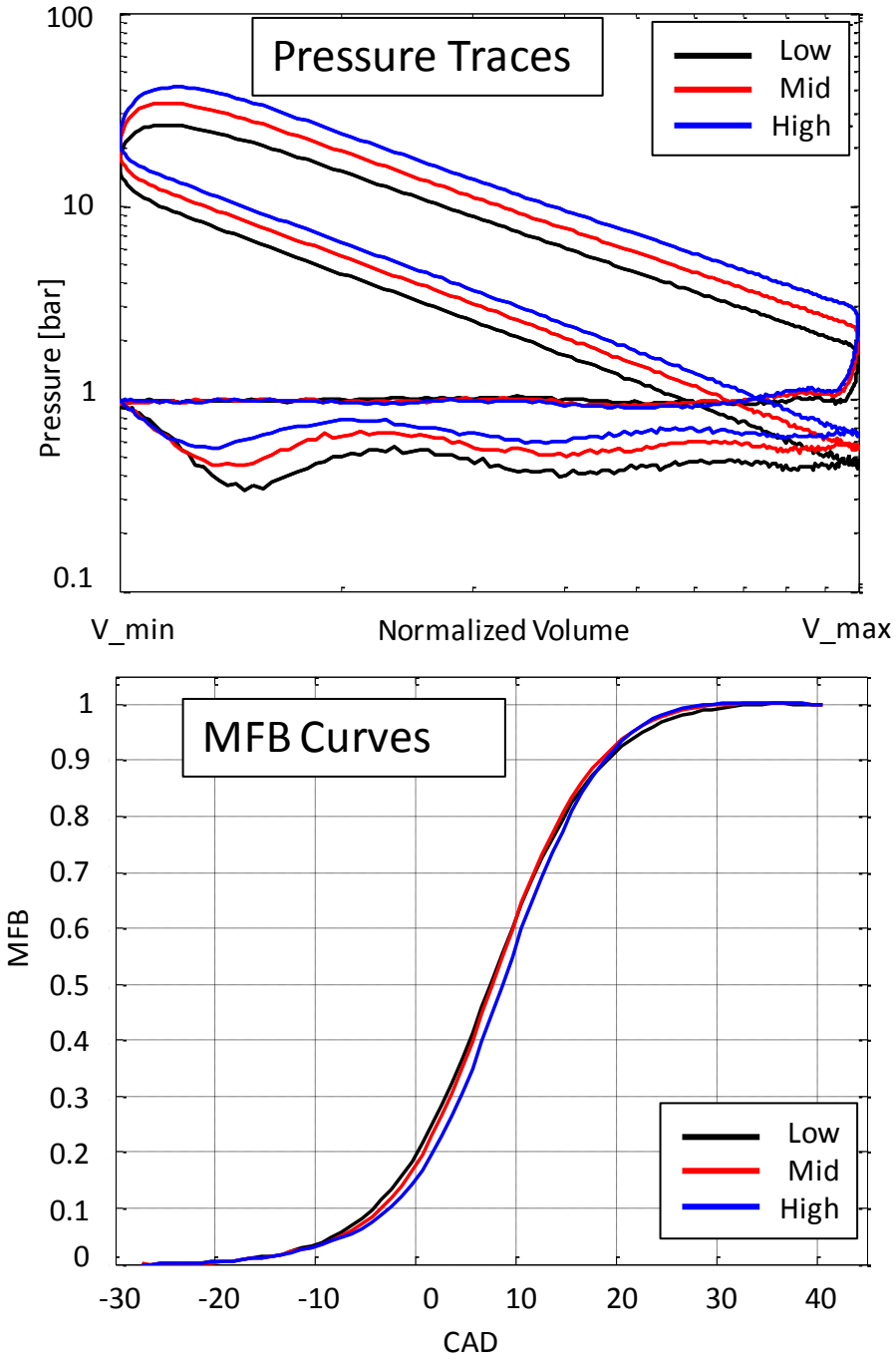

Figure 40: P-V Diagram and MFB Curves for 3 loads, 2000 RPM

Further studies were done to understand the performance using the low-lift cams. A first set of tests involved an injection timing sweep with the low-lift cams in their default retarded position. It was found that the same 300° BTDC injection timing used in the high-lift tests was

optimal based on IMEP and COV (Figure 41). This could imply that wall and piston spray impingement is the main factor that makes this timing optimal.

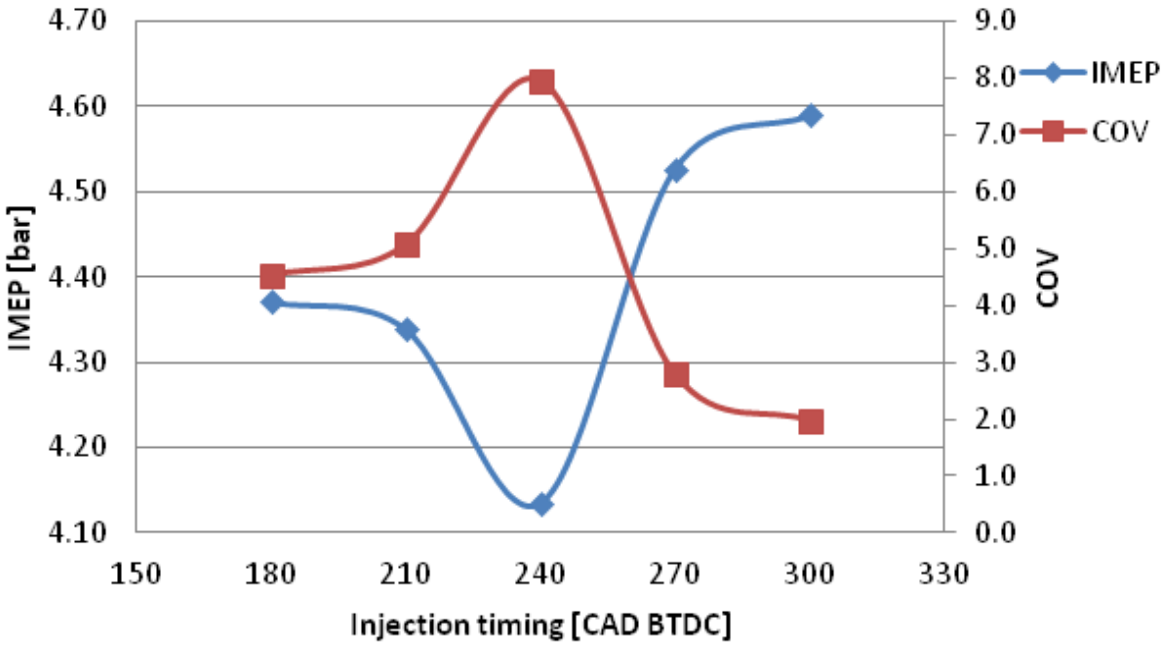

Figure 41: IMEP and COV During Injection Timing Sweep, Low Lift Cams

There are two main things of interest with the low-lift cams; for HCCI, the influence of the low-lift exhaust cam timing on EGR levels and recompression is important, while for SI operation the use of the low-lift intake cam as a way to reduce pumping losses is more typical. To study the behavior of both of these, numerous tests were run at the 2000 RPM/4.5 bar IMEP test point used in the high-lift SI tests. This load/speed point was decided as the target for HCCI testing and mode transition testing as well, so exploring potential efficiency gains from other operating modes possible with the valvetrain at this test points was important.

Two sets of exhaust timing sweeps were performed by advancing the exhaust over a 70° window. For the first sweep, all parameters were kept constant to see the effect of the increased EGR on combustion speeds, lambda, and engine load; for the second, spark and fuel were tuned to keep lambda and CA50 constant. These tests represent realistic conditions that could be present while cam phasing is in motion during a mode transition event. It is clear that exhaust cam advancement slows combustion significantly, but spark and fuel adjustments can yield stable performance with favorable combustion phasing over this entire 70° window of exhaust cam timing even as EGR levels increase significantly (Figure 42, Figure 43). Of note is the reduction of PMEP as the exhaust valve is advanced, and the also the slightly faster combustion, as evidenced by the later spark timing, when the exhaust valve is advanced 20° (Table 14).

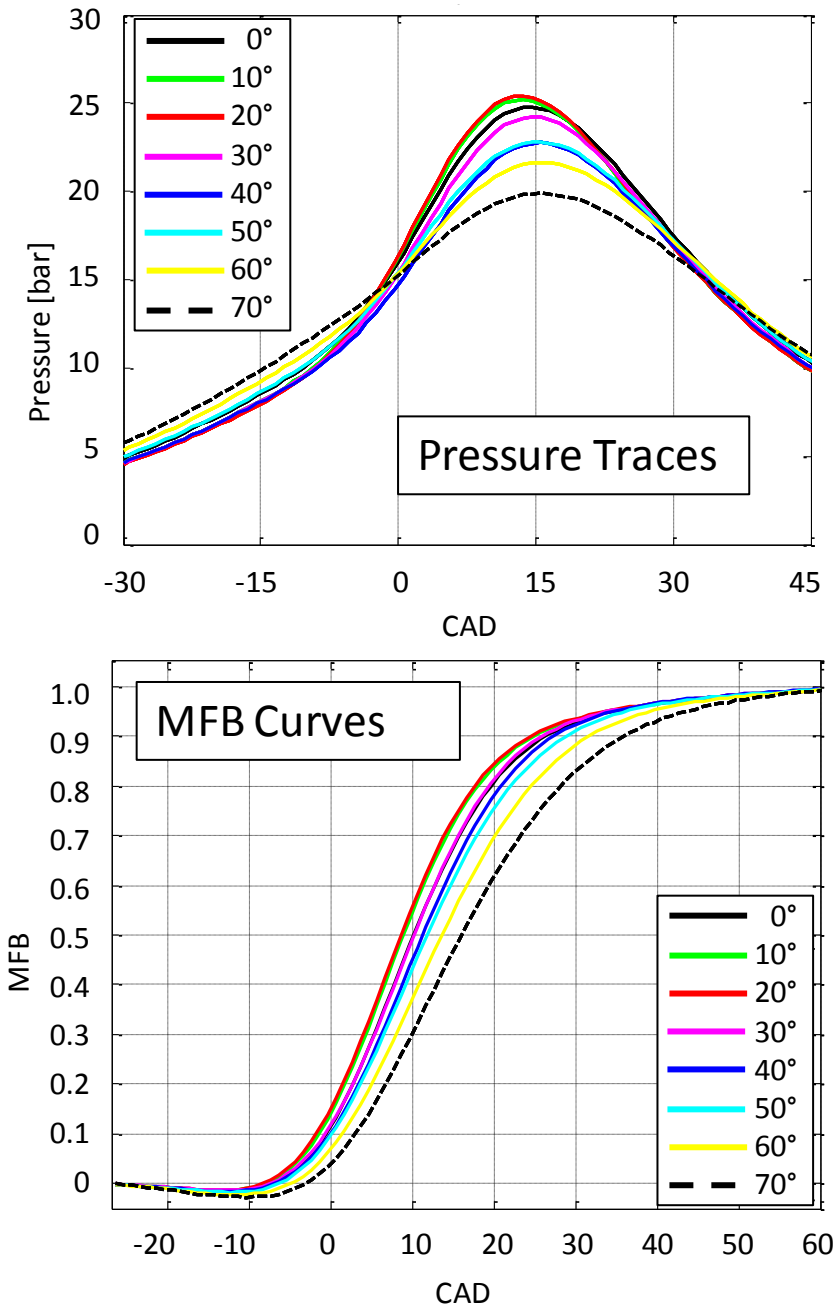

Figure 42: Pressure Traces and MFB Curves, Low-Lift Exhaust Cam Sweep from retarded to 70° Advance, Constant Spark and Fuel

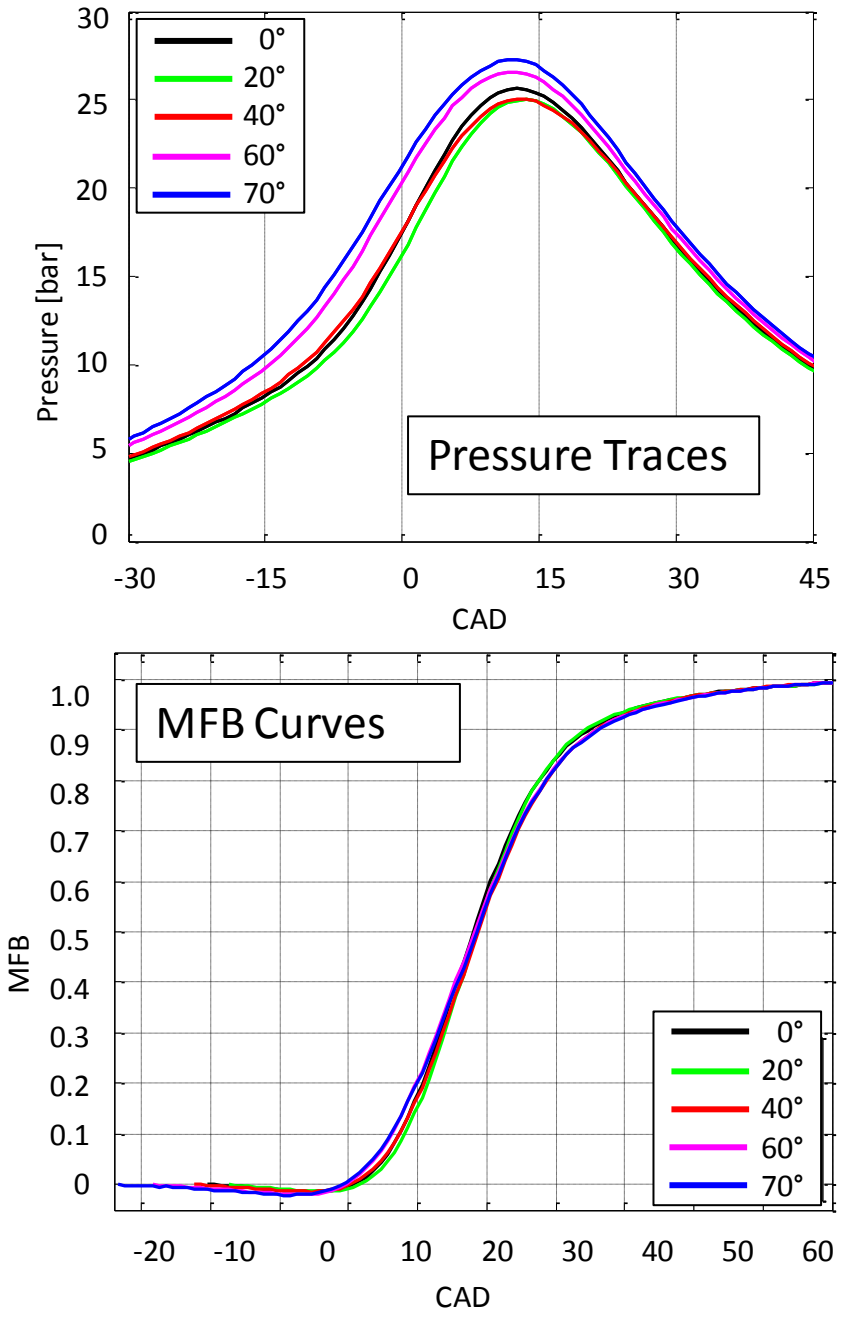

Figure 43: Pressure Trace and MFB Curve, Low Lift Exhaust Cam Sweep from retarded to 70° Advance, Constant Lambda and CA50

Table 14: Low -Lift Exhaust Cam Timing Sweep Data, Constant Lambda and CA50

Exhaust Advance	IMEP [bar]	NMEP [bar]	PMEP [bar]	COV	CA50 [°ATDC]	Lambda	MAP [kPa]	Spark timing [°BTDC]
0°	4.54	3.09	1.45	1.5	8.1	0.98	39.8	33
20°	4.52	3.41	1.11	1.3	8.6	0.99	39.0	31
40°	4.51	3.67	0.84	1.4	9.0	1.01	41.4	36
60°	4.44	3.84	0.59	1.5	8.3	1.01	47.9	42
70°	4.42	3.91	0.51	1.8	8.9	0.98	52.6	47

Table 15 shows a comparison of high-lift and low-lift performance at 4.5 bar IMEP and 2000 RPM. The low-lift setup slows combustion and requires a much larger spark advance, especially at extreme exhaust cam positions that cause high levels of EGR. At this load, the high-lift cam is superior with a greater IMEP from the same fuel pulse and a much lower PMEP, meaning that more of the engine's work will actually be output to the shaft. Advancing the low lift cam 70° lowers the PMEP to the level seen with the high-lift cam, but combustion speed decreases significantly, and IMEP is reduced despite the longer fuel pulse demanded in this condition.

Table 15: High and Low Lift Cam Performance Comparison

Speed	Cam lift	Exhaust Advance [CAD]	MAP [kPa]	IMEP [bar]	PMEP [bar]	Ignition [°BTDC]	Injection Pulse [ms]	CA50 [°ATDC]	B1090 [CAD]	COV of IMEP
2000	high	6	46.0	4.62	0.52	27	1.85	7.3	23.2	1.2
2000	low	20	39.0	4.52	1.11	31	1.85	8.6	26.6	1.3
2000	low	70	52.6	4.42	0.51	47	1.90	8.9	30.9	1.8

Also of interest from the exhaust cam sweep is the amount of recompression (Figure 44) from negative valve overlap during the pumping loop, which becomes a key component of HCCI combustion. Recompression at TDC from early EVC begins to appear with about 40° of exhaust

advance. By 70° of advance, there is over 5 bar of recompression; this will increase significantly under WOT operation for HCCI. Though this is not a typical strategy for running in SI mode, it does show that the engine is able to run in throttled SI mode with a valve timing scheme that would be typical of WOT NVO HCCI operation, which is useful information for designing a mode switch.

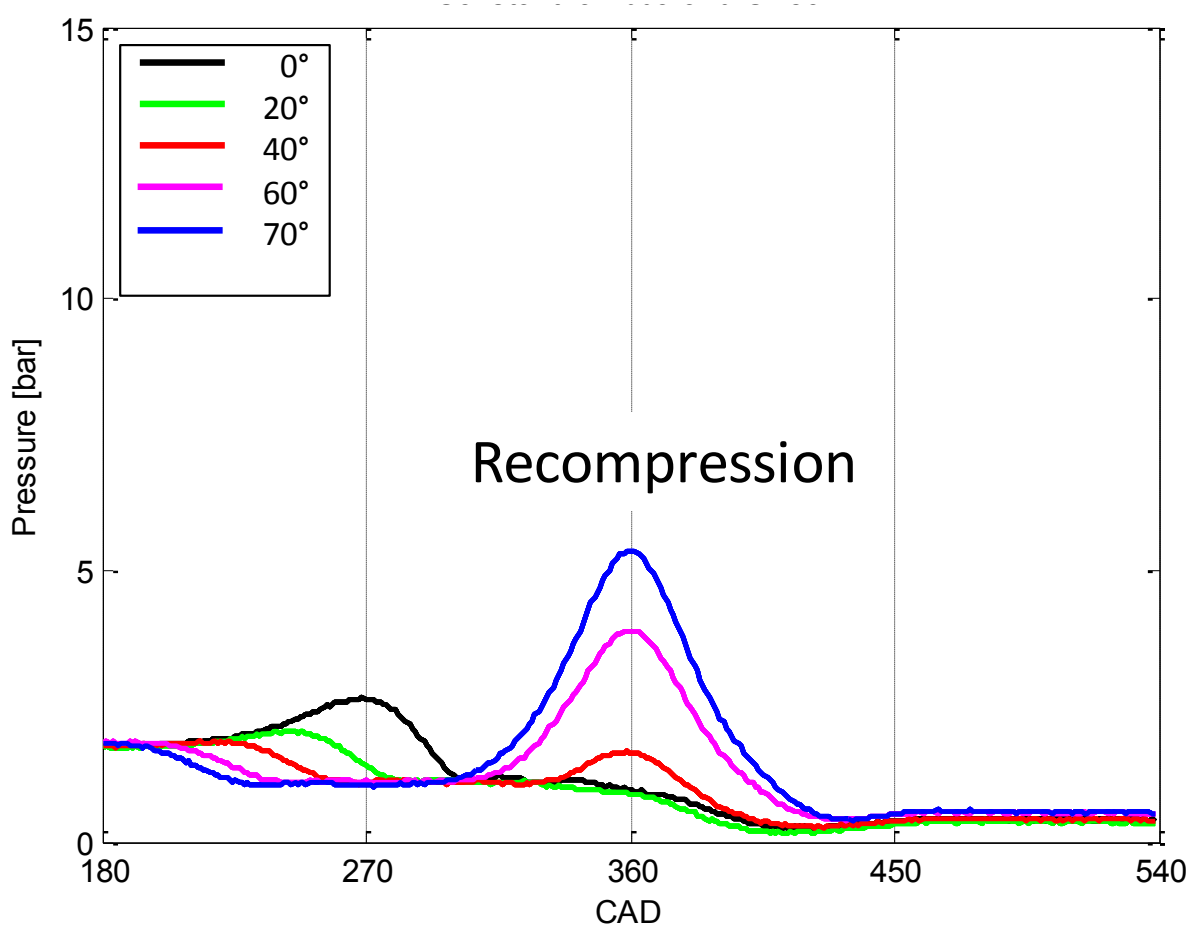

Figure 44: Recompression from NVO as Exhaust Cam is Advanced

A P-V plot of these same tests shows how recompression builds with increased exhaust valve advance, and also displays the shift in pressure during the main compression stroke as more EGR is trapped by the advanced exhaust valve timing (Figure 45). The final curve with the

exhaust valve advanced 70° previews the type of P-V curve shape that is expected with HCCI, with the primary difference being the pressure during the intake stroke following IVO. This will greatly reduce the pumping loss under HCCI operation.

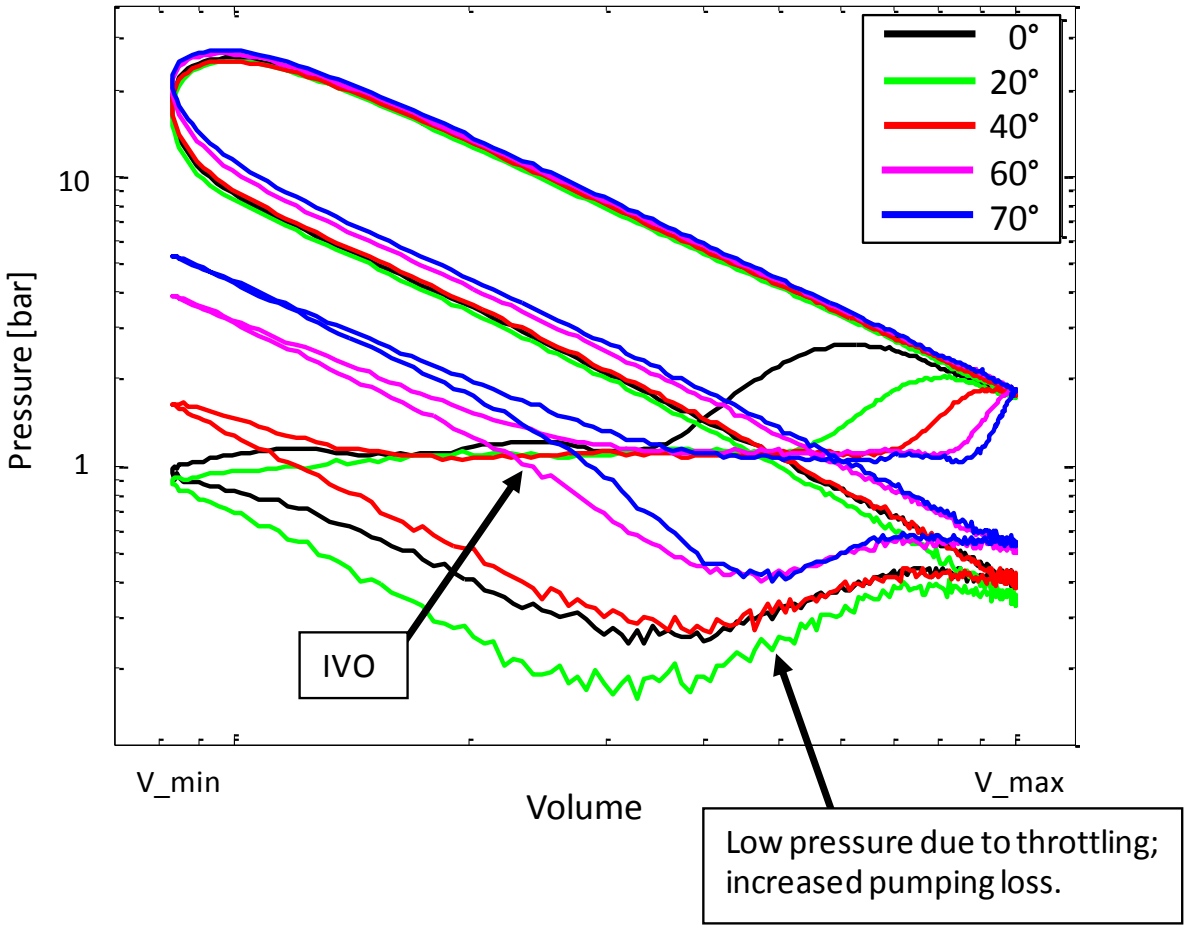

Figure 45: P-V Diagrams of Increasing Recompression with Exhaust Cam Advancement

As mentioned above, a more typical way to use a low-lift cam in SI operation is by intake valve throttling. Using the high-lift exhaust cam allows for an easier low-pressure exhaust stroke since the high lift cam allows for a less restrictive opening and a longer duration to push the exhaust gas out through. Advancing the low lift intake cam timing allows for early IVC (EIVC), which helps to limit the amount of fresh intake air that gets into the cylinder while allowing for

more open throttle positions and higher manifold pressure, and thus a reduction in pumping work during the intake stroke. A good overview of such a system is given by Sellnau et al. [21]. They provide a simulation plot showing the theoretical benefit of the shrunken pumping loop from EIVC throttling (Figure 46). Proper use of EIVC can produce a similar result from firing tests with the metal engine.

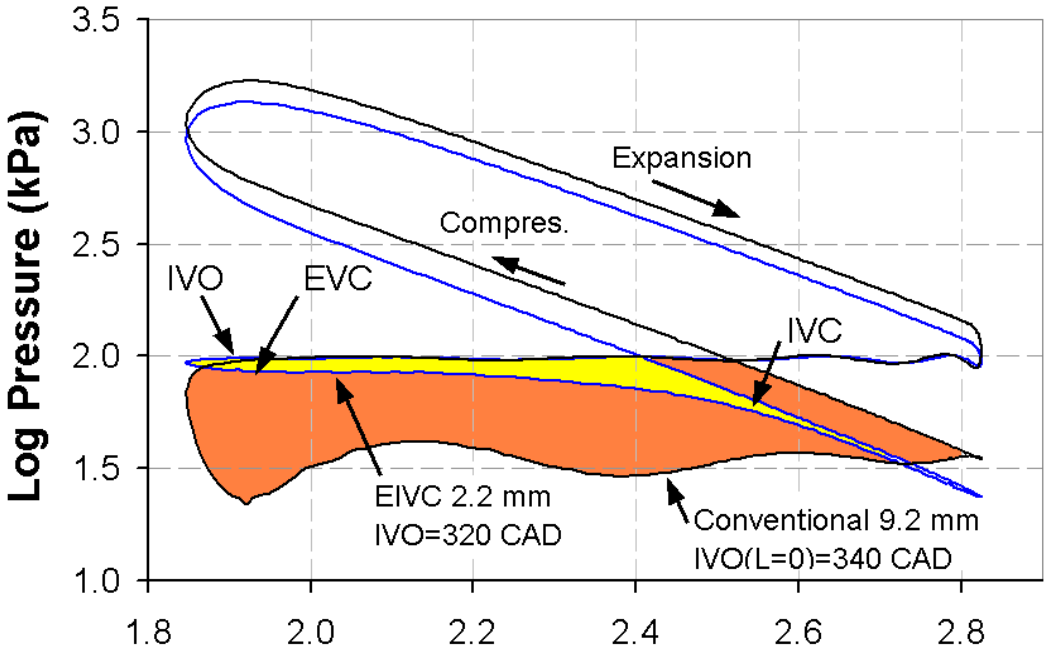

Figure 46: Simulated Pumping Loop Minimization from EIVC (Sellnau et al.)

P-V plots from firing cases run with a low-lift intake cam sweep are shown below (Figure 47), along with a table of the data from these cases with the key to the test number labels in the plot (Table 16). Exhaust advance timing was fixed at 6°, the same as what was used for high-lift benchmarking tests at this load. Though the many curves make it somewhat difficult to see, the main thing of note from this figure is the increased pressure during the intake stroke due to less throttling with more advanced intake timing. With the intake cam advanced 60° from the

default position, PMEP was reduced to 0.31 bar, down from the 0.52 bar PMEP seen in the high-lift base case. A test with the intake advanced 70° was attempted, but cylinder 1 began knocking and misfiring badly, and operation was stopped.

Pumping efficiency, which is calculated as (NMEP/IMEP)*100%, describes how efficiently the engine uses the gross power made during the compression and expansion. The base case with high-lift cams had a pumping efficiency of 89%; this improved to 93% with the use of early IVC, meaning that only 7% of the gross power made is being used for pumping air and exhaust in and out of the engine. The goal for HCCI operation is to improve upon this even further.

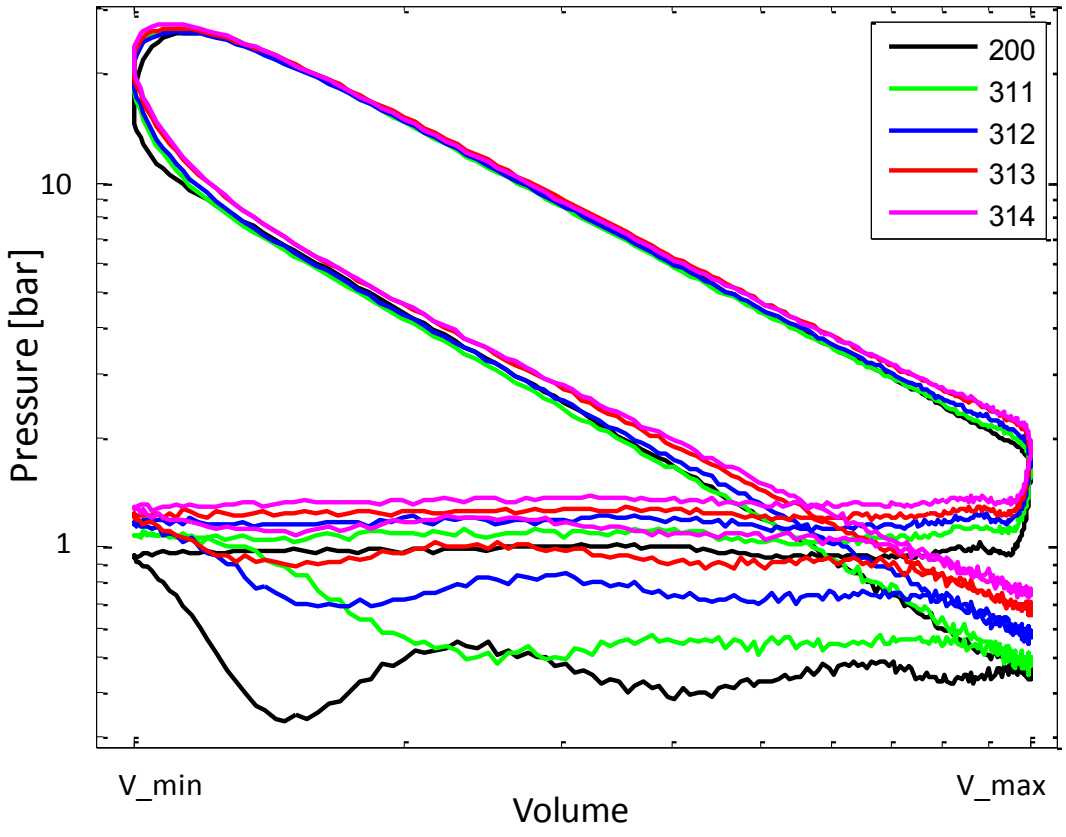

Figure 47: P-V Diagram, Pumping Loss Reduction from EIVC Throttling

Table 16: EIVC Throttling Performance Data

Test	Intake	Exhaust	IMEP	CA50	B1090	PMEP [bar]	Pump effic.	MAP [kPa]	Spark [°BTDC]
200	43 high	6 high	4.58	7.6	23.6	0.52	89%	45.7	27
310	0 low	6 high	4.52	8.9	28.8	0.55	88%	43.9	34
311	20 low	6 high	4.57	8.6	31.8	0.52	89%	48.1	42
312	40 low	6 high	4.51	9.5	34.5	0.44	90%	57.1	51
313	50 low	6 high	4.57	10.0	36.6	0.36	92%	66.9	57
314	60 low	6 high	4.49	8.3	35.9	0.31	93%	75.4	58

A simplified figure with just the two “best case” SI P-V curves shows the original high-lift case (Test 200) and the 60° advance low-lift case (Test 314) together (Figure 48). This is similar to the idealized plot from literature referenced above, with the main difference being higher average cylinder pressure of the low-lift case. In the simulation diagram, the power loop has a higher pressure in the high-lift case because the low-lift pumping loop takes place at a much lower pressure. This is because the simulated case is comparing NMEP—that is, it is matching the output over the whole 720° engine cycle, while the case from this work is matching the 360° IMEP while reducing the pumping work. Were the NMEP matched in these two tests, it would be expected that the curve from the low-lift case would shift to a lower pressure as shown in the simulation figure.

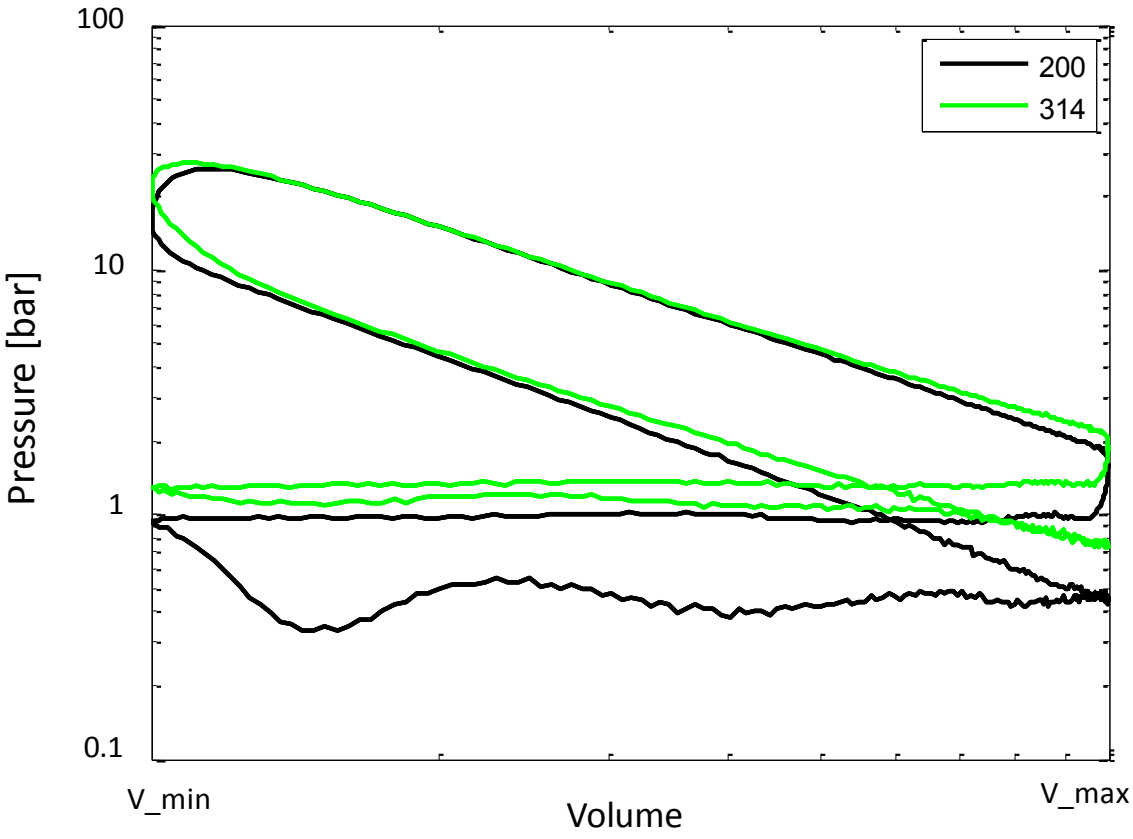

Figure 48: P-V Diagram Comparison of Baseline High Lift and EIVC at constant IMEP

Modification to 1-Cylinder Operation

As previously mentioned in the Engine Setup section, the 4-cylinder engine was modified to be run as a 1-cylinder engine because of the ongoing blowby problems. While this was not the ideal way to conduct tests originally planned for a multi-cylinder engine, it eliminated some of the difficulties of trying to run with essentially four different operating conditions at once, particularly when trying to discover the parameters that could lead to successful HCCI operation, which is very dependent on in-cylinder conditions.

The potential for misfires was seen as a significant problem in attempting HCCI with some poorly performing cylinders. While cylinder 2 might have performed well, cylinder 3 might not have done the same, and this could have caused difficulty in understanding the air-fuel ratio since the O2 sensor would be seeing a mixture of burned and unburned gases from the different cylinders. Running the engine with one cylinder while still allowing the others to pump air through would cause a similar difficulty with the O2 sensor reading a mixture of exhaust and fresh air. Furthermore, under certain conditions, such as the low-lift intake valve throttle case discussed above, cylinder 1 displayed very erratic behavior with knocking and misfiring. Cylinders 3 and 4 did not always respond as expected to changes in spark timing or valve timing either. Thus, the switch to 1-cylinder operation greatly simplified the process of isolating which parameters actually are affecting operation.

With the lower airflow demands of the 1-cylinder setup, a new more restrictive throttle was designed. The old throttle plate was replaced with a much smaller diameter plate, and the surrounding space was filled in with a donut-shaped piece of aluminum press-fit into the original throttle pipe. This design allows the manifold pressure to drop low enough for low-load SI operation.

Preliminary HCCI Setup

As discussed in Chapter 3, it was found during the optical engine tests that successful HCCI combustion depended very much on not only the pressure conditions in the cylinder during the compression stroke, but also on what had happened in the previous recompression period during NVO. Recompression with little or no heat release often led to misfires or partial burns, while recompression with large heat release led to violent autoignition which was frequently phased earlier than desired. For successful operation, it was known that this heat release needed to be controlled more strictly so that it could be more consistent and lead to more consistent conditions in the cylinder at the start of the next compression stroke. The control parameters available to do this are cam position, fuel delivery, and spark timing.

The fuel delivery strategy involves utilizing a split pulse during HCCI. A pilot pulse is introduced during NVO recompression, while a main pulse is left at the tradition timing early in the intake stroke to create a mostly homogeneous mixture in the cylinder; in this case, the main pulse timing was left at the same 300° BTDC that was used in the SI tests. The purpose of the pilot

pulse is to introduce a small amount of fuel into the higher pressure and temperature environment of the recompressed exhaust gases. Ideally, if the pressure and temperature were high enough, the pilot fuel would begin breaking down and going through a reforming process in which radicals are formed that can help trigger ignition of the rest of the fuel during the following compression stroke. However, depending on the valvetrain capabilities, the peak temperature and pressure during recompression may not be high enough to consistently produce these radicals. With a fully variable camless valvetrain such as a pneumatic system, NVO can be expanded to very long periods independently of EVO timing; this can allow for very large levels of trapped residuals and thus very high pressure and temperature during recompression that could feasibly allow for this reforming process to take place. However, with an actual cam-operated valve train, there is a tradeoff between lengthened NVO and EVO timing; the larger NVO demanded, the earlier EVO timing becomes. If EVO is too early, the expansion stroke is effectively shortened, and large amounts of exhaust gas can exit the cylinder quickly before the early EVC timing has a chance to trap it for recompression. While this problem could be addressed by designing cam profiles that open the valve for only a short period, the current setup was designed for flexible operation in multiple modes, and thus has a cam profile that effectively limits the use of extreme NVO periods of over approximately 180°.

With the current setup and its limited NVO period, it is beneficial to also fire the spark plug during recompression to help this fuel reformation process along in a more consistent and aggressive manner. The spark is used to actually initiate combustion during recompression. This combustion will be small, as there is only a small amount of oxygen in the trapped exhaust

mixture from the lean operation of the main combustion event; this is actually desirable, as it limits the actual amount of combustion heat release—too much heat release, and HCCI turns into more of a violent knock on the following compression stroke—but does allow for the potential of some of the remaining pilot fuel to begin the reforming process due to the extra heat that is trapped in the combustion chamber due to the spark and small combustion.

To prepare for using this split injection pulse, some injection pulse experiments were done to learn about the injection pulse behavior. With no fuel flow meter on the engine setup—it is particularly difficult to get usable readings on fuel flow for the small and pulsing flow rates present in part-load single-cylinder operation—the fueling amounts of different pulses were calculated using lambda and mass air flow (MAF) sensor data.

Since fuel delivery during a pulse is not a linear process—that is, there is an opening time in which fuel flow rate ramps up followed by a steady flow rate period—tests were done to determine the minimum pulse width that would deliver a detectable amount of fuel. This was done by running the engine stoichiometrically with a standard single pulse, and then gradually increasing the size of the pilot injection until lambda changed; this pulse width was then known to be the minimum threshold that allowed a detectable amount of fuel to flow. Unfortunately, repeatability of this threshold pulse was not good; this was the first hint that the control of small pulses was not particularly repeatable with the prototype injector used in the tests.

With the use of a MAF sensor mounted on the intake air pipe, the actual mass of fuel per injection could be calculated for different pulse widths. This allowed a rough fuel mass-per-pulse-width curve to be formulated. The relationship was found to be fairly linear for large pulses, but somewhat unpredictable for small pulses.

By starting with a single pulse, the fueling rate was calculated from lambda and MAF sensor readings. Starting with the basic relationship:

$$\lambda = \frac{{}^{A}/_{f_{main}}}{\left({}^{A}/_{F}\right)_{stoich}}$$

where f_{main} is the fueling rate resulting from a single main injection, A is the MAF rate, and $(A/F)_{stoich}$ is 14.7 for gasoline. From this, f_{main} was calculated:

$$f_{main} = \frac{A}{14.7\lambda}$$

This gave the flow rate of fuel, which was converted to a mass-per-cycle basis using the engine speed of the test; thus the total fuel per injection was known.

Introducing a pilot injection that alters λ allowed calculation of the flow rate (and fuel mass per injection) of the pilot injection:

$$\lambda = \frac{{}^{A}/_{(f_{main}+f_{pilot})}}{\left({}^{A}/_{F}\right)_{stoich}}$$

Solving for f_{pilot} gives the fueling rate from the pilot injection:

$$f_{pilot} = \frac{A}{14.7\lambda} - f_{main}$$

Figure 49 shows the results from using these calculations on the data generated from a simple sweep of a single injection pulse width from 1.85 ms to 2.05 ms. The result was a fairly linear relationship between pulse width and injected mass. The trendline in this figure is also present in Figure 50, which shows the calculated results from adding small second pulses. This shows that at small pulse widths, the behavior deviates significantly away from this linear relationship seen with the larger pulses. Furthermore, there is much more variability at these small pulse widths, an issue that will be discussed later in more detail.

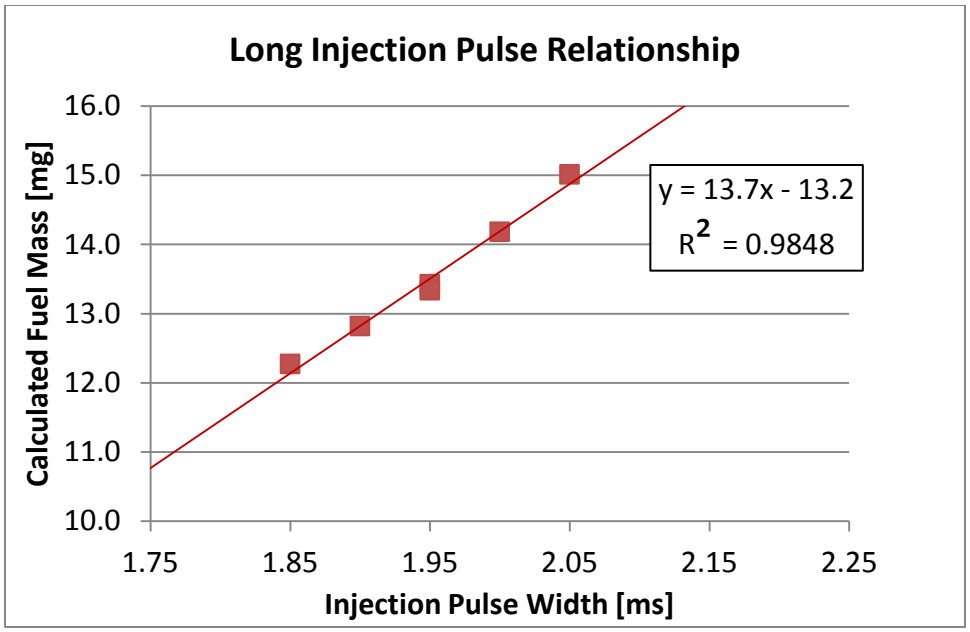

Figure 49: Injection Pulse Width and Fuel Mass Relationship, Long Pulses

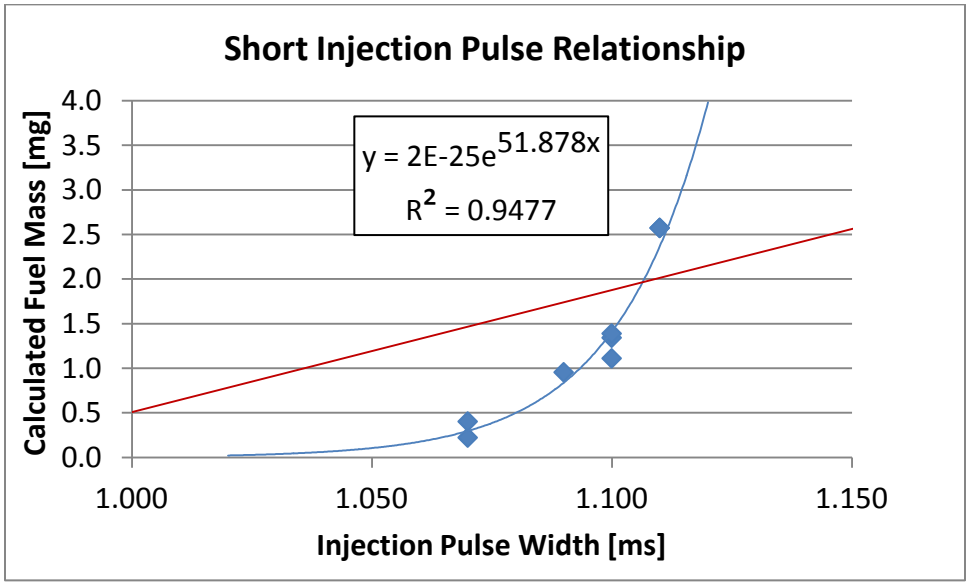

Figure 50: Injection Pulse Width and Fuel Mass Relationship, Short Pulses

Wermuth et al. [12] performed HCCI experiments with a 1-to-1 split and a 5-to-1 split between main and pilot pulses, though those tests were run at a lower engine load. Their findings were

that the smaller pilot pulse led to better efficiency, retarded CA50 timing, and lowered COV. The results of these tests help to determine the size of a pilot pulse that is needed if a similar 15-20% of the fuel is desired in the pilot pulse. Unfortunately, the variability that shows up in the small pulses continued to be a difficult issue to deal with, leading to necessary frequent adjustments to fuel pulse widths to keep the desired ratio in tact on a test-by-test basis. For example, in the above plots, a pilot injection of 1.11 ms paired with a main injection of 1.95 ms would lead to approximately 19% of total fuel being injected in the pilot pulse. However, repeatability of such a setup was found to be very poor, as this 1.11 ms pulse width appears to be right on the edge of stable operation for this injector. Sometimes, this pulse width would result in a much larger amount of fuel than anticipated, and other times, it resulted in less. With no other injector available for these tests, there was nothing to do but make the best attempts to adjust the pulses as necessary on a test-by-test basis.

Preliminary Mode Transition Setup and First HCCI Attempt

Motoring tests were done to prove the capabilities of the control system to handle the cycle-by-cycle changes needed during the mode transition. While the original ideal transition plan called for a 5-cycle total transition period, these motoring tests confirmed what was found with the optical engine cam phaser tests, which is that the transition may need closer to 9 cycles for completion of a large phasing event.

Figure 51 summarizes the components of the mode transition by showing cycle-by-cycle details of the motoring pressure trace (black), MAP (red), and injection pulses (blue). In the cycles prior to the ones shown in this figure, the cams were in their standard high-lift SI position, and the engine was motored with a part-load throttle position. From cycle 43 to 44, the peak cylinder pressure drops, indicating that the cams have begun to phase and are changing the amount of intake air that the engine is ingesting. At cycle 45, MAP begins to increase, indicating that the throttle has started to open. For cycle 46, the cams have switched from high-lift to low-lift, and some recompression is now visible in the pressure trace. This is followed by the addition of a pilot injection during recompression in cycle 47. Finally, by cycle 49, the cams are fully phased, recompression is at a maximum, and the manifold pressure has stabilized at a near WOT condition.

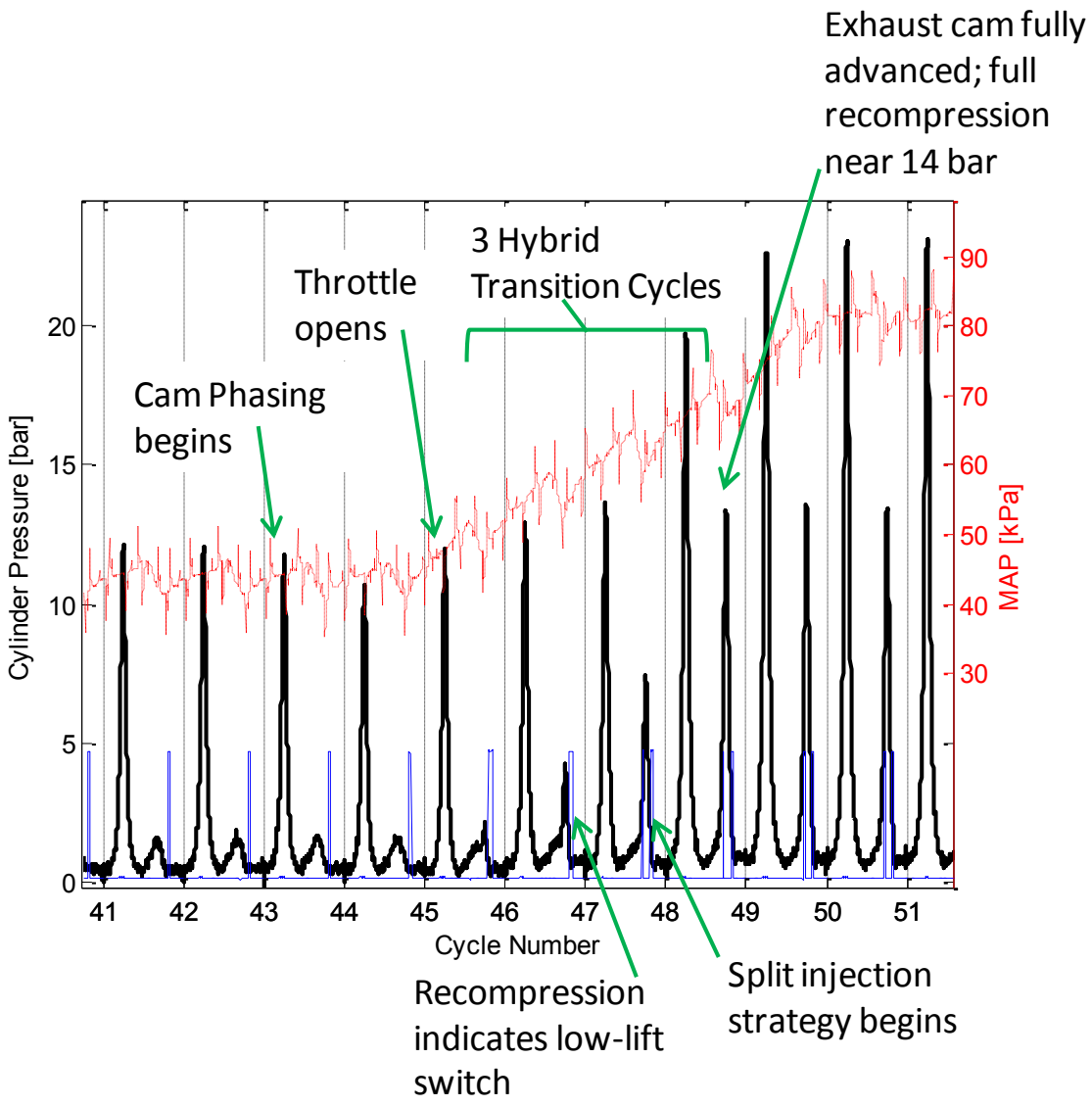

Figure 51: Detail of Motoring Mode Transition Test Setup

While the original proposal for the mode-transition assumed a switch from a standard high-lift cam profile SI condition as is shown in these initial transition setup figures, the flexibility of the valvetrain could potentially allow for mode transitions to exist with other starting points, each with various advantages and tradeoffs. For example, a transition from low-lift EIVC to HCCI would only need to involve an exhaust cam lift switch as the intake cam would already be in low-lift mode. SI operation was also demonstrated with the low-lift NVO strategy used for

HCCI; a transition from this mode to HCCI might involve just a small phasing adjustment and a simple throttle opening as the spark and fuel delivery are adjusted.

Four potential mode switches were identified based on the potential SI operation modes available with the setup of the valvetrain that were explored during the SI benchmarking tests. These modes and their tradeoffs are summarized in Table 17 along with the required phasing and cam lift demands of the transition process.

Due to time and hardware constraints, efforts were focused on only two of these strategies. Development of the standard high-lift SI transition was continued, and eventually efforts were redirected toward a transition with both cams starting in low-lift mode already during SI operation. This was done because of a malfunctioning cam lift system that would not allow the exhaust cam to be run in high-lift mode.

Table 17: Summary of Potential SI Modes Preceding an SI-to-HCCI Mode Switch

SI Strategy	Advantage	Disadvantage	SI cam and throttle setup	Total cam change in transition
Standard—both high lift	Most traditional way to control low to mid loads	All things are changing at the same time—both phasers, both cam lifts, large throttle change	Intake: high 43° Exhaust: high 6° MAP: ≈45 kPa	Intake: switch to low, retard 43° Exhaust: switch to low, advance 64°
Early IVC (intake low lift)	Intake valve throttling, so smaller jump in MAP in transition; low PMEP	Both cams must phase a long way before recompression builds	Intake: low 60° Exhaust: high 6° MAP: ≈75 kPa	Intake: retard 60° Exhaust: switch to low, advance 64°
Late IVC (intake high lift)	Intake cam needs little if any phasing; throttle slightly more open	Throttle still needs to open a lot in transition, large phasing for exhaust cam	Intake: high 0° Exhaust: high 0° (?) MAP: ≈55 kPa	Intake: switch to low, no phasing Exhaust: switch to low, advance 70°
Both low lift	Can phase cams nearly all the way to NVO HCCI positions with stable SI operation; throttle becomes main initiator of HCCI	Unconventional way of running in SI mode—getting there with phasing essentially becomes part of the transition; throttle becomes main initiator of HCCI	Intake: low 0° Exhaust: low 70° MAP: ≈53 kPa	Intake: minimal phasing Exhaust: minimal phasing

With the control strategy components needed for the mode transition in place, the strategy had to be tuned through actual firing tests to determine how to adjust the details of the sequencing of each parameter to avoid misfires during the transition. However, without knowing the parameters for a stable HCCI condition to shoot for at the end of the transition, this was very difficult. After some small tweaks to the strategy, initial attempts at running the transition strategy resulted in numerous misfiring cycles during the transition (Figure 52, Figure 53) and an unstable final operating point (Figure 54) similar to the one seen previously in the optical engine tests. Not shown in Figure 52 is the retarding of spark timing from the initial -25° SI timing; it first transitions to -15° for cycle 52 for the hybrid mode cycles, and then to -5° for cycle 55 once transition process is finished. These tests and all following HCCI tests were run with 85 octane test fuel.

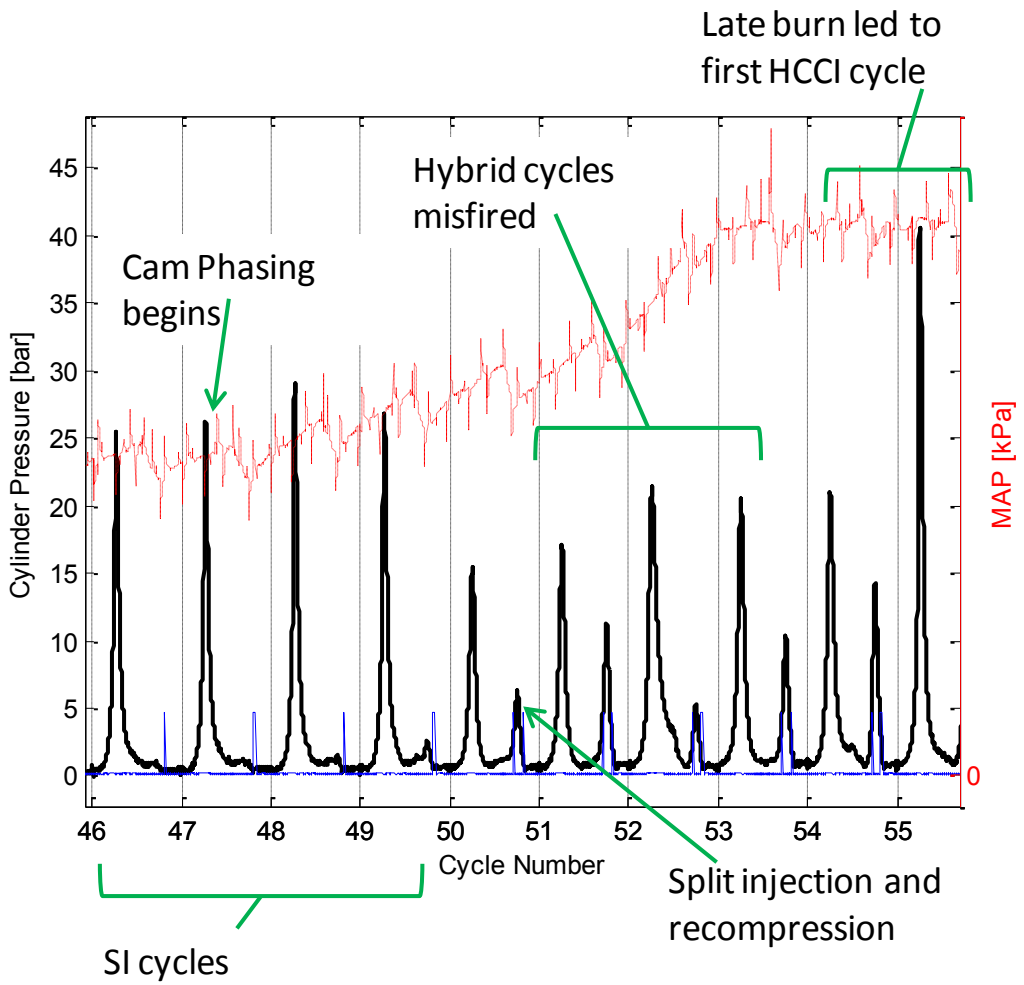

Figure 52: Detail of Misfires in First Attempted Firing Mode Transition

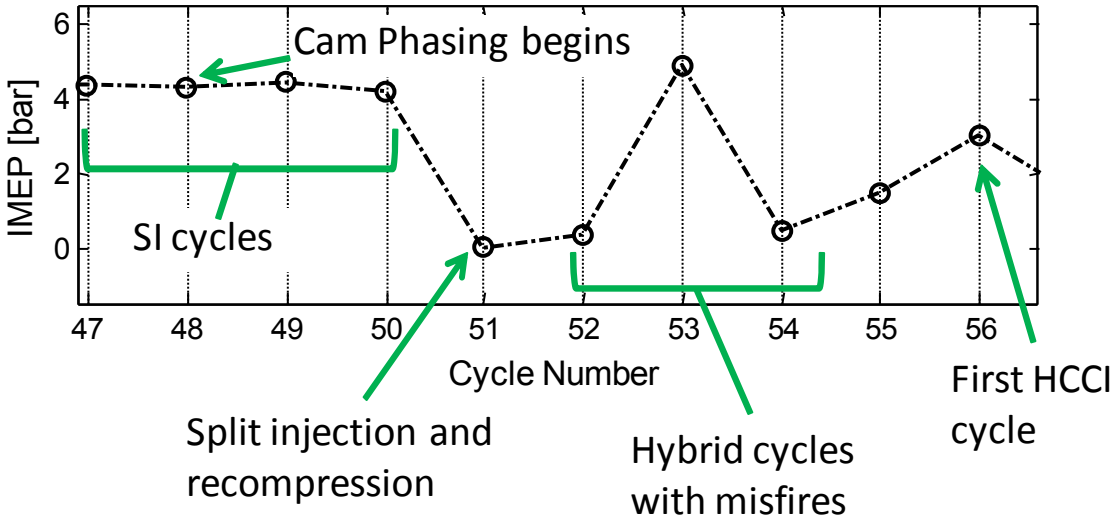

Figure 53: Cycle-by-Cycle IMEP during First Attempted Firing Mode Transition

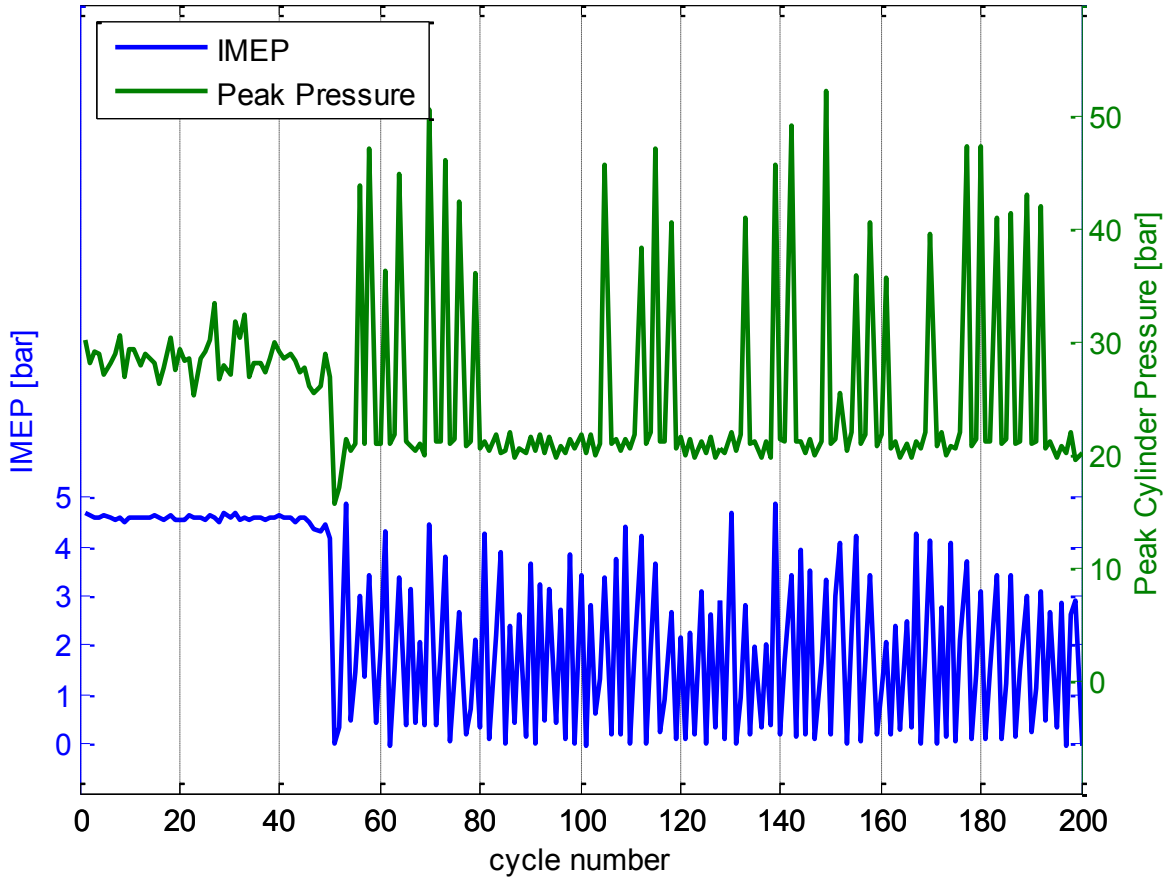

Figure 54: IMEP and Peak Cylinder Pressure of Initial HCCI Attempt

Despite the shortcomings of this test, it was a milestone test from which important information was derived that helped lead to improvements in future tests. During the mode transition, it was clear that a re-mapping of the throttle and the spark timing were necessary to keep more stable combustion leading up to the hybrid cycles. Spark timing must have sufficient advance to sustain normal SI combustion, and throttle must not be opened too early so that the mixture will not grow too lean too quickly and suffer from slow burn durations.

In Figure 54, the HCCI cycles are evident from their high peak cylinder pressure. Following the transition zone near cycle 45, all cycles with peaks over 30 bar were cycles which autoignited; approximately 1 in 6 cycles fired in this way, though some short periods showed more consistent cyclic behavior of alternating autoignition and misfires. As was seen in the optical engine tests, the misfires frequently led to a large heat release during recompression, which led to violent autoignition in the following cycle. A key difference between this and the previous optical engine work was that it was achieved here without the aid of the intake heating or boost; neither electric heaters from the optical engine setup nor the removable coolant-fed heat exchanger for the metal engine were used in this test. This test was run with a pilot injection, which was not previously used in the optical engine, but the pilot spark discussed previously was not yet utilized here. Thus, this test helped show that the recompression heat and pressure alone were not enough to initiate pure fuel reformation in a way that stabilized the HCCI process.

The relationship between misfiring/partial burn cycles, recompression heat release, and the rather violent HCCI cycles that followed is demonstrated in Figure 55. This plot, which shows the average HCCI cycle with the average preceding misfire cycle, clearly shows a large difference in the recompression pressure. Note the obvious late burn and recompression heat release present in the pre-HCCI cycles in the P-V diagram (Figure 56). The P-V diagram also very effectively shows how the late and slow combustion of misfiring cycles leads to this large recompression pressure. The mixture is still burning at BDC when the exhaust valve opens, and presumably some of that burning mixture is also still trapped when the valve closes at the start

recompression; thus the fuel injected during the pilot injection likely joins in with this combustion that is already going on, leading to a substantial amount of recompression heat release.

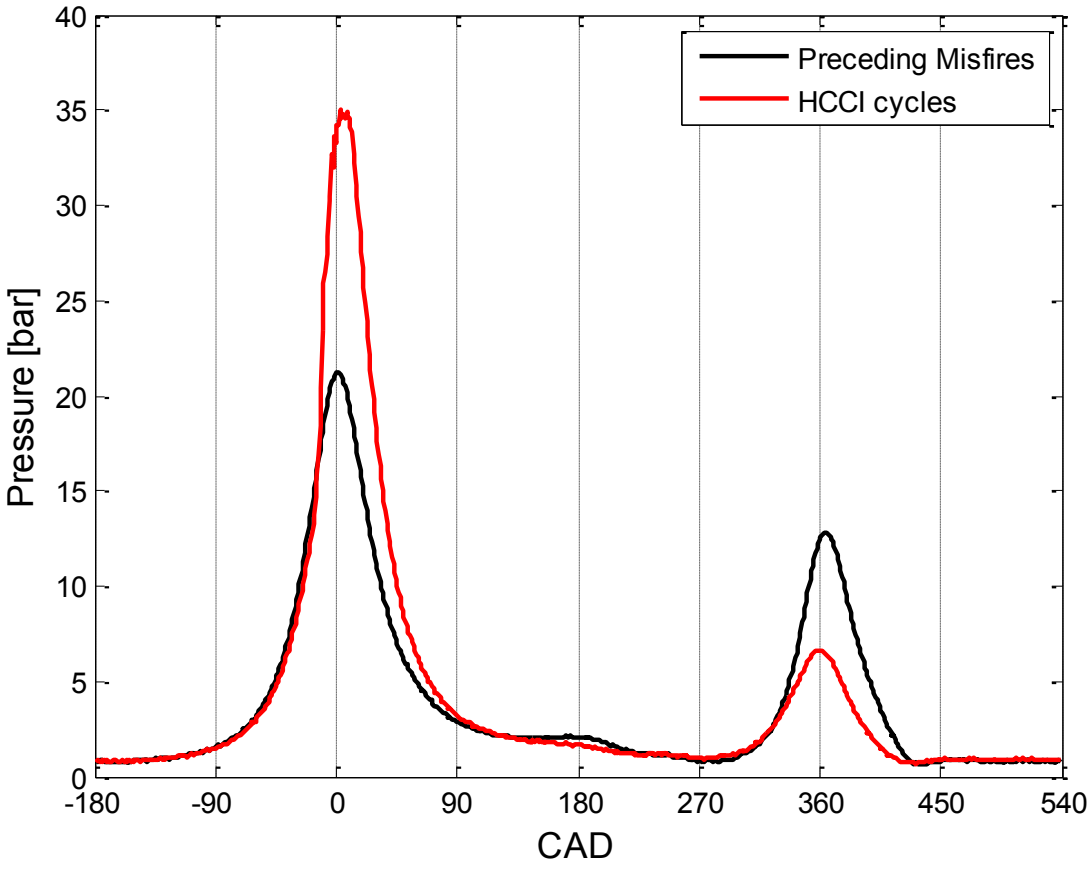

Figure 55: Average Successful HCCI Cycle and Preceding Misfire Cycles

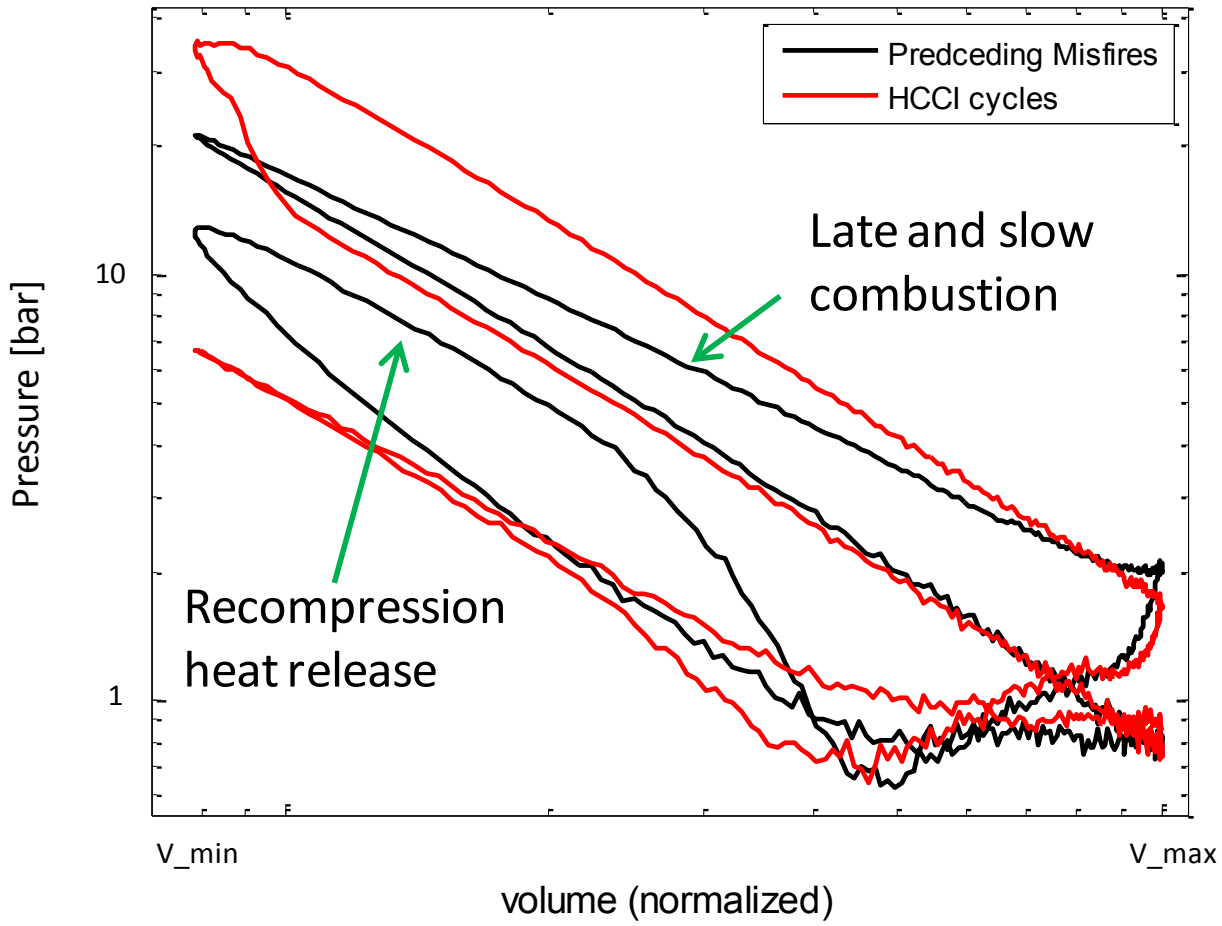

Figure 56: P-V Diagram of Average HCCI and Pre-HCCI Cycles

Combustion timing in many of the HCCI cycles was earlier than desired (Figure 57), which limited the IMEP despite high peak pressures; the average IMEP for HCCI cycles was 3.4 bar, compared to 4.6 bar during SI operation with roughly the same fuel mass.

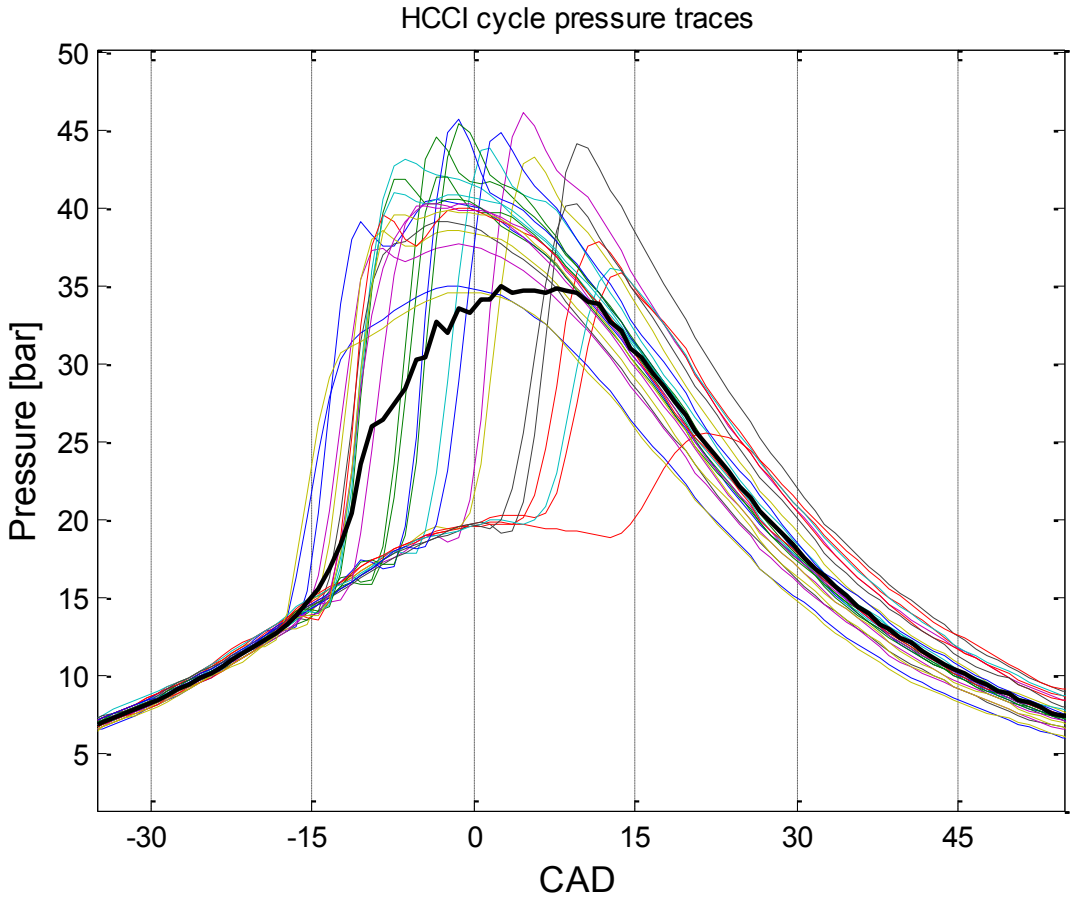

Figure 57: Overlay of all HCCI Cycle Pressure Traces and Average HCCI Trace

For steady operation, the autoignition process needed be slowed down; retention of more exhaust gas following HCCI cycles could help do to this, and was also necessary to bring recompression pressures up high enough to help initiate combustion more consistently on the following cycle. The best solution to accomplish this was to modify the cam positions to allow for a longer NVO period. Furthermore, altering the control system to allow for a spark during recompression was seen as a vital change following this test.

Cam Repositioning and Successful Manual Transition to HCCI

Following the difficulty of the initial HCCI test, the cam shafts were repositioned to provide a longer NVO period that could trap more exhaust gas and recompress it to higher pressures and temperatures. Each cam was jumped by 2 teeth on the timing chain in opposite directions, with the exhaust cam advanced by 2 teeth and the intake cam retarded by 2 teeth. The cam shaft gear contains 54 teeth, so each tooth represents a 13.5 CAD change in cam timing. Total practical NVO increased by approximately 54 CAD to 173 CAD. The new and old valve profile limits of the low lift cams are shown in Figure 58; the new opening and closing specs of all profiles is found in Table 18.

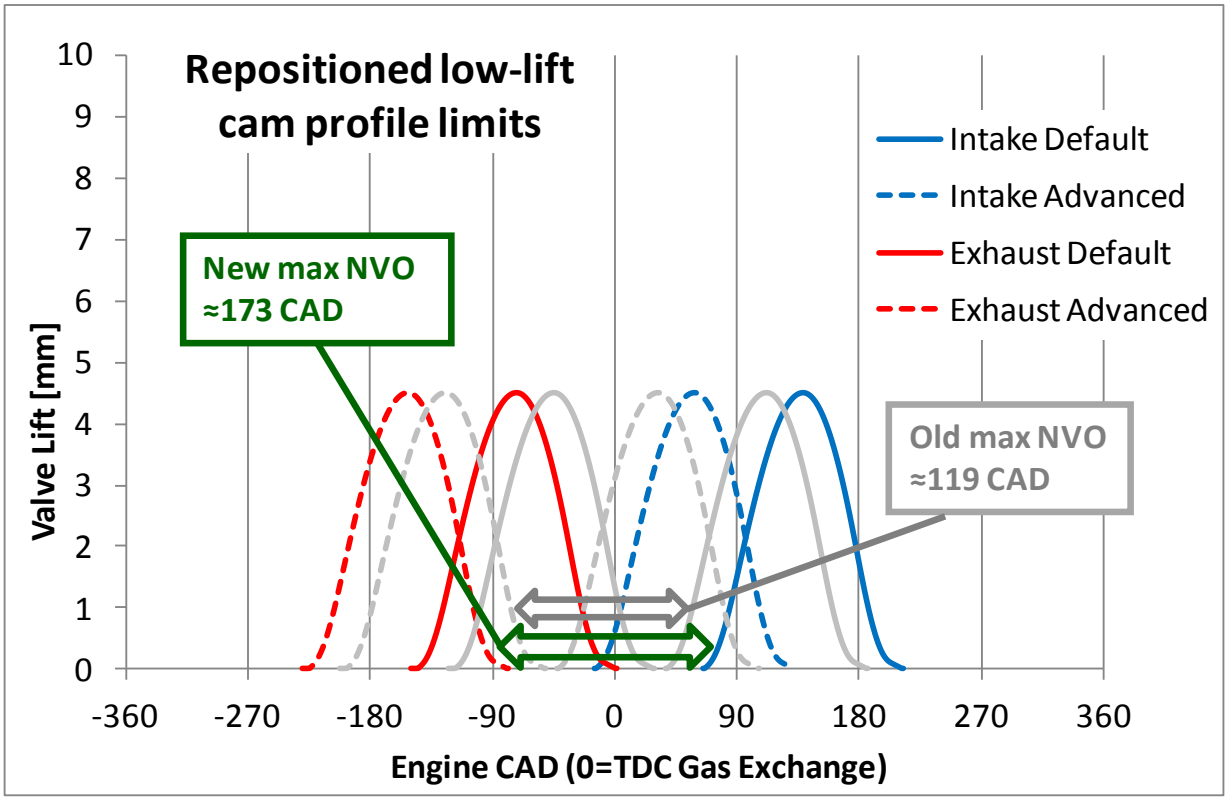

Figure 58: Low-Lift Cam Profile Limits, Before and After Cam Repositioning

Table 18: Valve Timing Specs, Fully Retarded Position after Cam Repositioning

		Open Spec	Open effective	Center line	Close effective	Close Spec
Fully Retarded 0° Position	**Intake High**	63	73	183	305	315
	Intake Low	65	80	139	198	213
	Exhaust High	-237	-227	-105	5	15
	Exhaust Low	-146	-131	-72	-13	2
Fully Advanced 0° Position	**Intake High**	-17	-7	103	225	235
	Intake Low	-15	0	59	118	133
	Exhaust High	-317	-307	-185	-75	-65
	Exhaust Low	-226	-211	-152	-93	-78

As was the case prior to the cam repositioning, the recompression is asymmetric, with 93° of the NVO occurring on the exhaust side and 80° of it occurring on the intake side.

With the cams repositioned, it was decided that the best way to explore a stable HCCI point would be to slowly transition the engine from an SI condition into HCCI by manually adjusting parameters in small increments until a stable autoignition point was found. This would result in a known end condition that could be applied to the mode transition code in the future, and would also give some understanding about the hybrid combustion cycles in the middle of the transition; it is easier to design a transition strategy if the end point of that transition is known.

To begin this process, the engine was run with both cams in low-lift with just a moderate level of NVO. The cams were slowly phased a few degrees at a time to gradually increase NVO until a split injection could be applied; as more exhaust gas was trapped, the throttle was gradually

opened wider. With a significant NVO period and a sufficiently opened throttle, spark timing was retarded toward TDC in small increments until the first signs of autoignition occurred. At this point, the cams were phased to their limits (most advanced for exhaust, most retarded for intake), the throttle was opened fully, and the spark timing was dialed back to just before TDC.

The first attempt at doing using this manual transition after the cam repositioning resulted in an improved but still unstable condition in which HCCI was achieved on roughly every third cycle. Over the 200 cycle sample taken, consecutive autoignition cycles occurred 5 separate times. For this test, the recompression spark was utilized for the first time (see the spark and injection strategy in Figure 59), and its effect on recompression heat release was somewhat noticeable. While the previous attempts resulted in numerous misfires of essentially 0 bar IMEP, the misfires in this attempt did show at least some positive work output (Figure 60). The P-V diagram of Figure 61 shows HCCI cycles again resulted in a very low recompression heat release compared to what was seen in the misfiring pre- and post-HCCI cycles. An overlay of all of the autoigniting cycles shows ignition frequently occurring around 15° BTDC, which resulted in peak pressure being reached before TDC. Variability in autoignition timing and peak pressure timing was large.

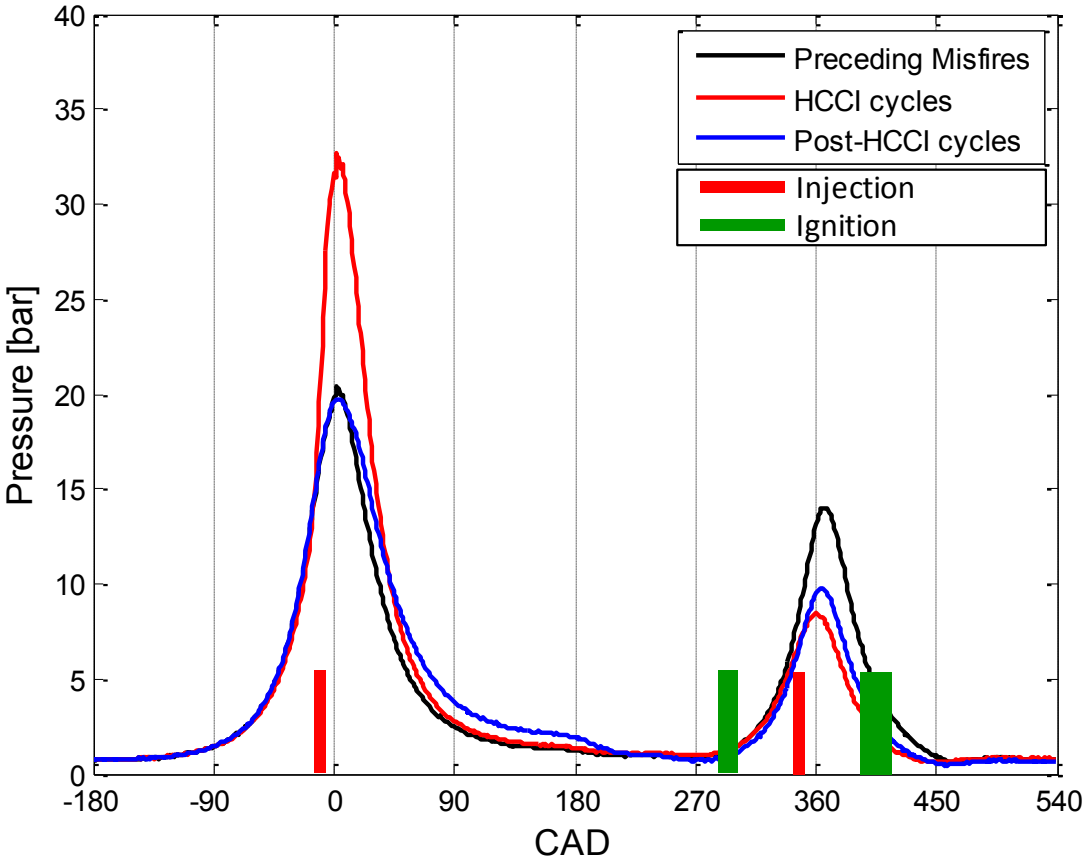

Figure 59: Average HCCI Cycle with Pre and Post HCCI Cycles, Initial Slow Transition

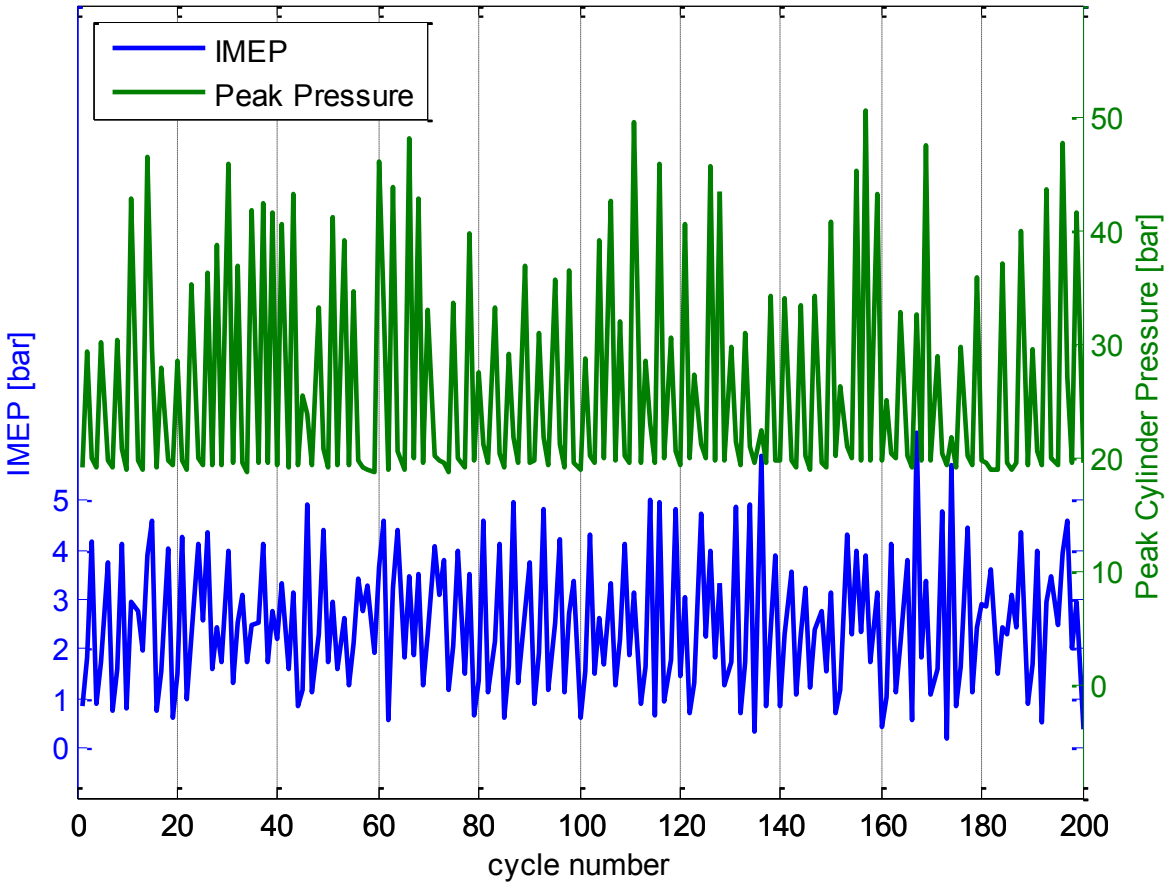

Figure 60: IMEP and Peak Cylinder Pressure of Initial Slow Transition HCCI Attempt

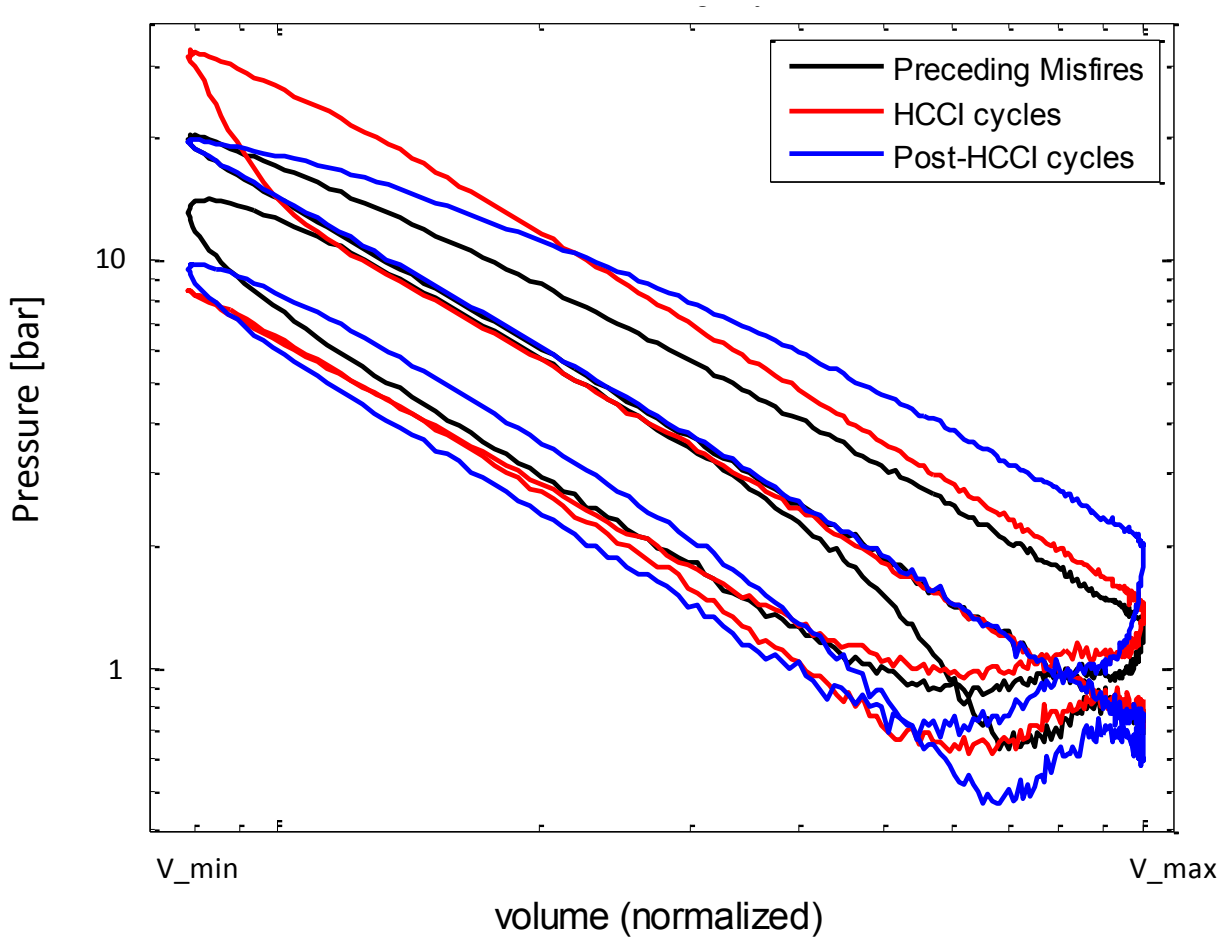

Figure 61: P-V Diagram of Average HCCI Cycle with Pre- and Post-HCCI Cycles, Initial Slow Transition

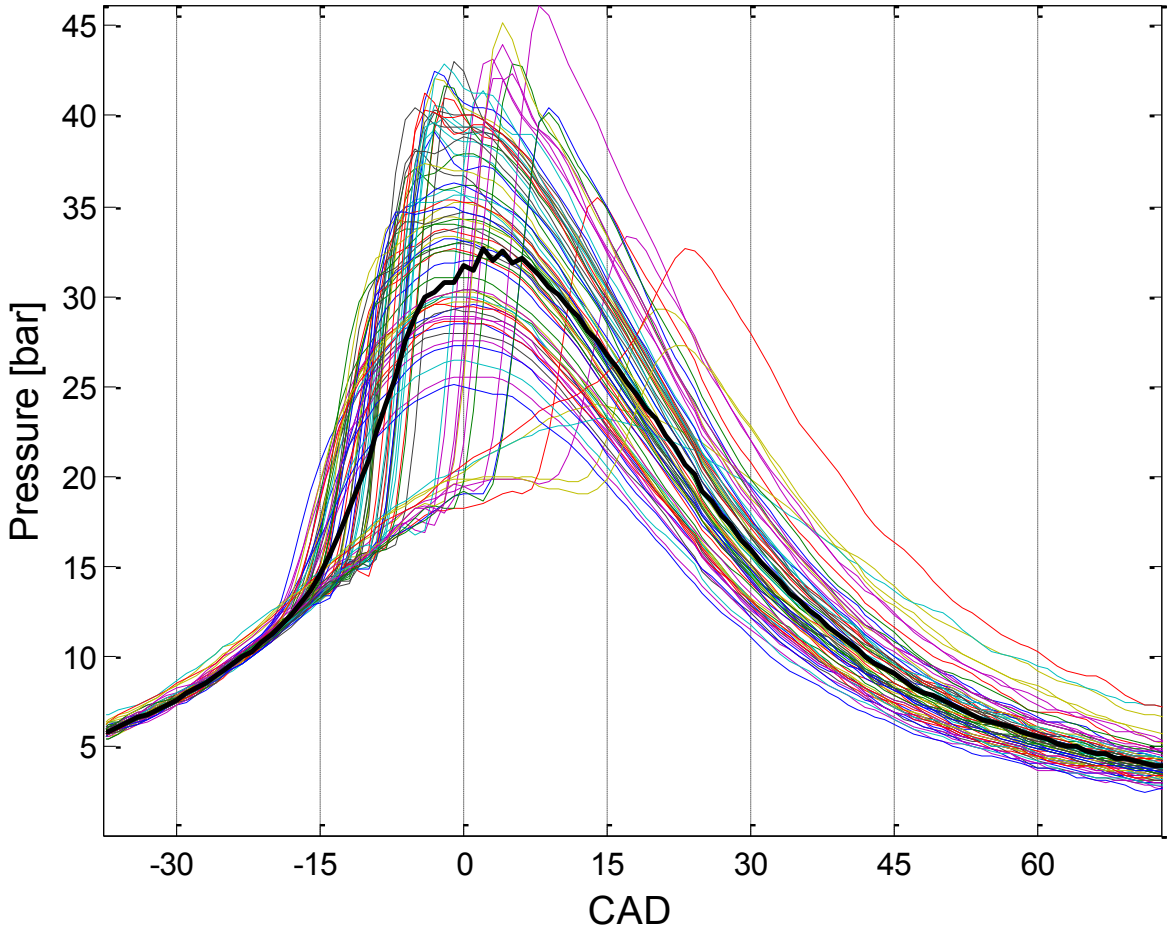

Figure 62: Overlay of HCCI Cycles and Average HCCI Cycle, Initial Slow Transition Test

This initial slow transition test was not done with the maximum NVO timing. Due to a control system shortcoming following the cam repositioning, the exhaust cam was only advanced by 63°, which created the largest symmetrical NVO period possible at 156°.

A second attempt was made at a manual transition with the full 80° phasing of the exhaust cam available. Other modifications to the setup for this test included the pilot injection timing and the addition of heat to the intake air. In the previous attempts, pilot injection timing was set at 60° BTDC GE with the intention of allowing the fuel extra mixing time during recompression

before the pilot spark was fired. For this attempt, the pilot injection timing was changed to 25° BTDC; with the extremely high level of exhaust gas dilution present during recompression, it was hoped that spacing the pilot injection and spark closer together might lead to a zone of fuel concentrated more near the spark plug that could readily begin combustion for more consistent recompression heat release. For intake air heat, the coolant-fed heat exchanger was re-installed in the intake manifold. This resulted in intake air temperatures in the range of 165-175° F, depending on the engine coolant temperature.

The same method as before was used to get to the first signs of autoignition. Once there were a significant number of cycles showing autoignition, the cams were phased to the extremes for the full 173° NVO, and spark timing was dialed back toward TDC. The resulting point showed consistent fast-burning autoignition characteristics, acceptable COV, high IMEP, and very low PMEP. This stable HCCI point was run at λ=1.16.

An average pressure trace of a 200 cycle sample of this steady HCCI point is shown in Figure 63 along with the injection and ignition strategies. The injection strategy shows a short pilot injection pulse ending at 25° BTDCGE and a longer main pulse ending at 300° BTDCF, the same timing used in single-injection SI tests. The spark, which fires at the falling edge of the control signal shown, is 10° BTDC during both recompression and main compression events. The P-V diagram of Figure 64 is useful for showing the small positive heat release that comes as a result of the pilot injection and spark.

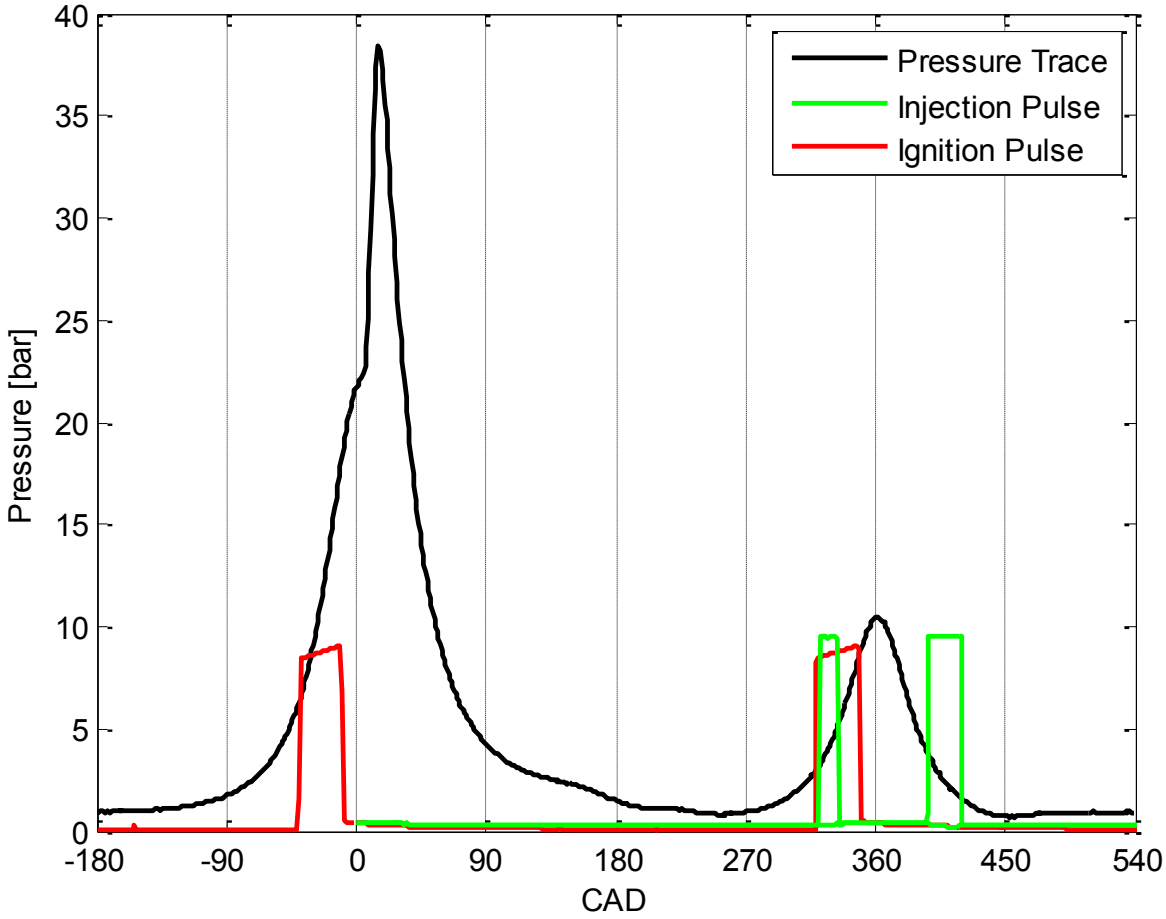

Figure 63: Average Pressure Trace of Stable HCCI, Second Slow Transition Test

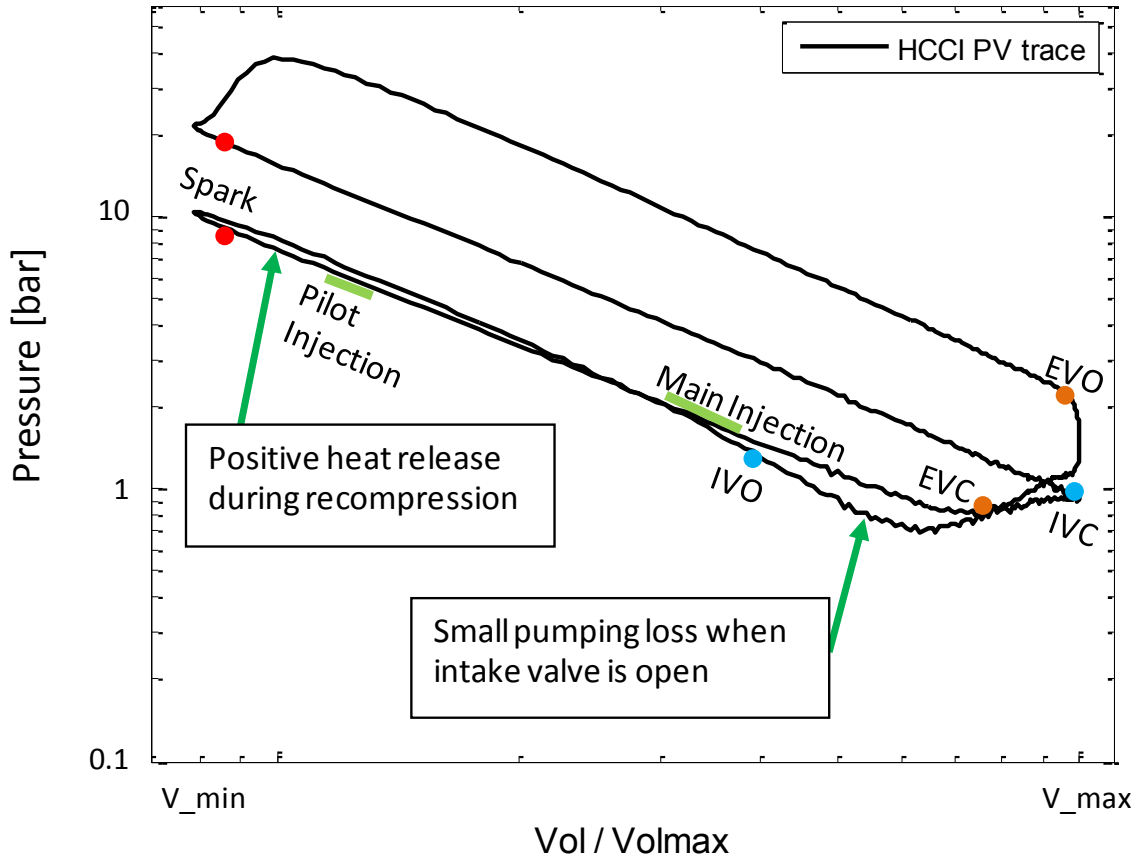

Figure 64: P-V Diagram of Steady HCCI with Small Heat Release in Recompression

A detailed overlay of all 200 cycles sampled shows some variation in peak pressure and peak pressure location, but overall a consistent trend of fast combustion initiating just after TDC (Figure 65). While the peak pressure varies a fair amount due to the timing of combustion, load fluctuations are quite small (Figure 66), with the COV of IMEP at just 2.1% over this 200 cycle sample. Also of note in this figure is the virtually nonexistent PMEP.

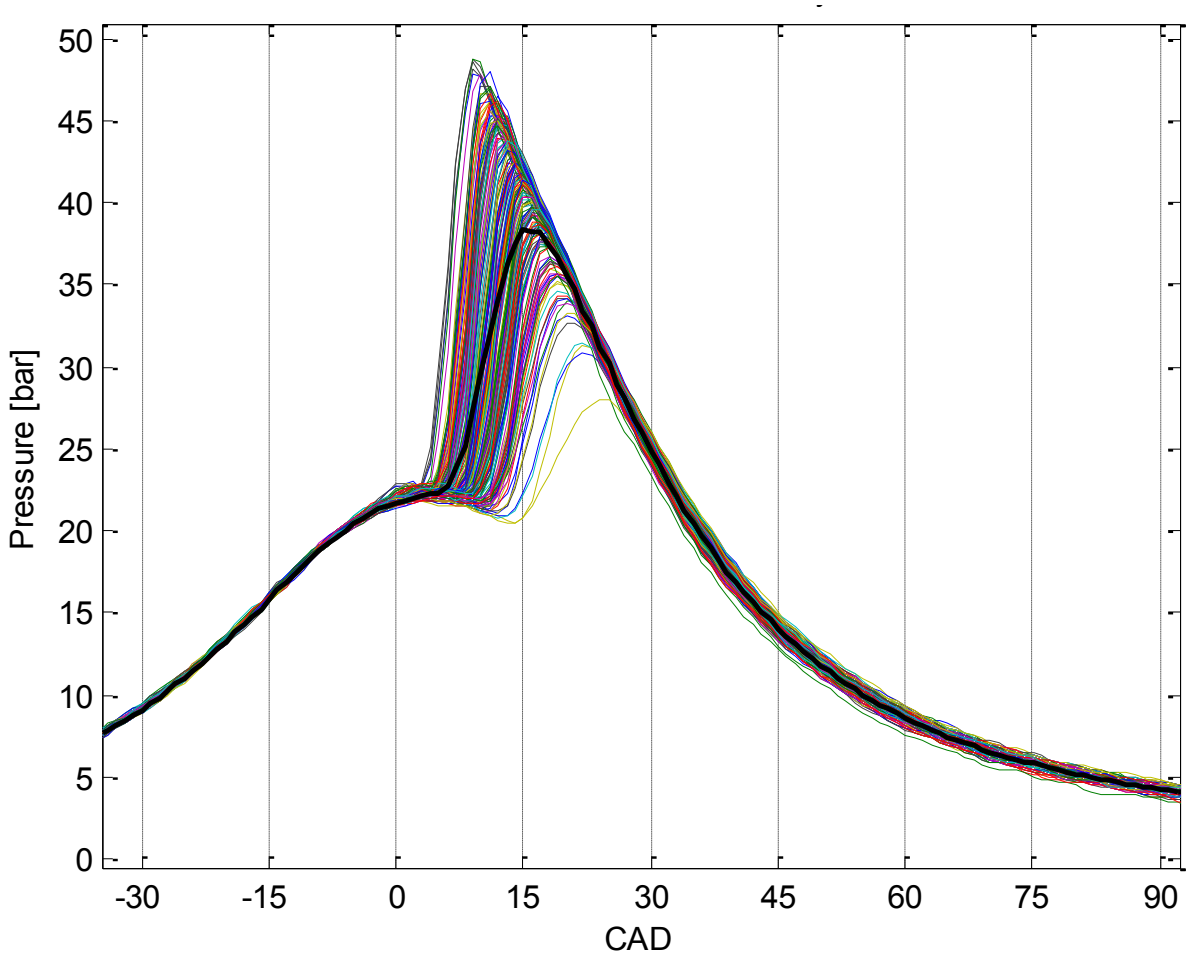

Figure 65: Pressure Trace Overlay of 200 Consecutive Steady HCCI Cycle

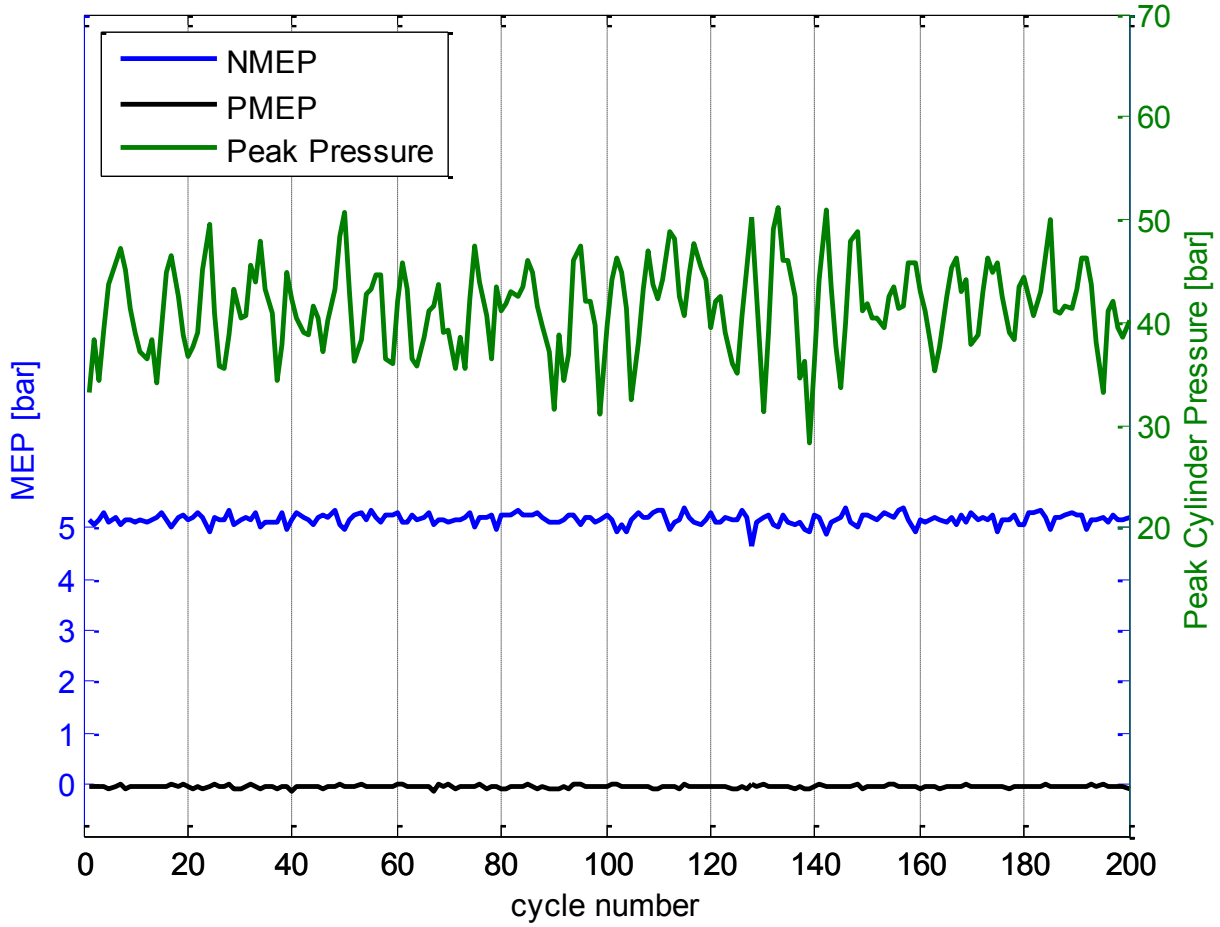

Figure 66: Peak Cylinder Pressure, IMEP, and PMEP of Stable HCCI

With the case-by-case fuel pulse variability issue mentioned previously with the injectors, it is hard to say with confidence how much fuel the two injection pulse widths used were injecting using during this test. However, in an attempt to best demonstrate the benefits of running in HCCI considering the injector shortcomings, a test was run at a standard SI benchmark point at 4 bar NMEP was first run with a single injection immediately prior to running the HCCI point. With the engine still running, a second pulse was added until lambda dropped from 1.0 to 0.94, and then the original main pulse was reduced to bring lambda back to 1.0. This resulted in approximately 6% of the fuel being injected in the second small pulse. Again, with the engine

still running, the cams were transitioned to low lift and phased to provide a moderate level of NVO, and second injection pulse during intake was replaced with a pilot pulse during recompression of the same size. These pulses were left alone for the remainder of the transition into HCCI, ensuring as accurately as possible that the amount of fuel in HCCI mode was the same as that in the SI case. This yielded equivalent fueling rate test points which were used to assess the performance of the HCCI point (Table 19).

Table 19: SI and HCCI Test Point Comparison

	SI (single pulse)	***SI (dual pulse)***	***HCCI (dual pulse)***
Main Inj Pulse [ms]	1.93	1.90	1.90
Pilot Inj Pulse [ms]	----	1.12	1.12
IMEP [bar]	4.60	4.54	5.21
PMEP [bar]	-0.59	-0.59	-0.04
NMEP [bar]	4.01	3.96	5.17
COV of IMEP	0.9%	0.9%	2.1%
λ	0.99	1.00	1.16
MAP [kPa]	50	50	96
CA50	8.2	8.3	12.5
B1090	25.2	25.1	12.1
PRRmax [bar/CAD]	1.4	1.4	4.1
Peak Pressure [bar]	27.3	27.0	41.4
Peak P loc [°ATDC]	13.1	13.1	15.0

The P-V diagram (Figure 67) and MFB curves (Figure 68) demonstrate the differences between the SI and HCCI cases effectively. The difference in pumping work is immediately apparent in the P-V diagram, as are the higher peak pressure, later initial burn, and faster overall burn rate. The MFB curves of the two cases also demonstrate the difference in burn rate.

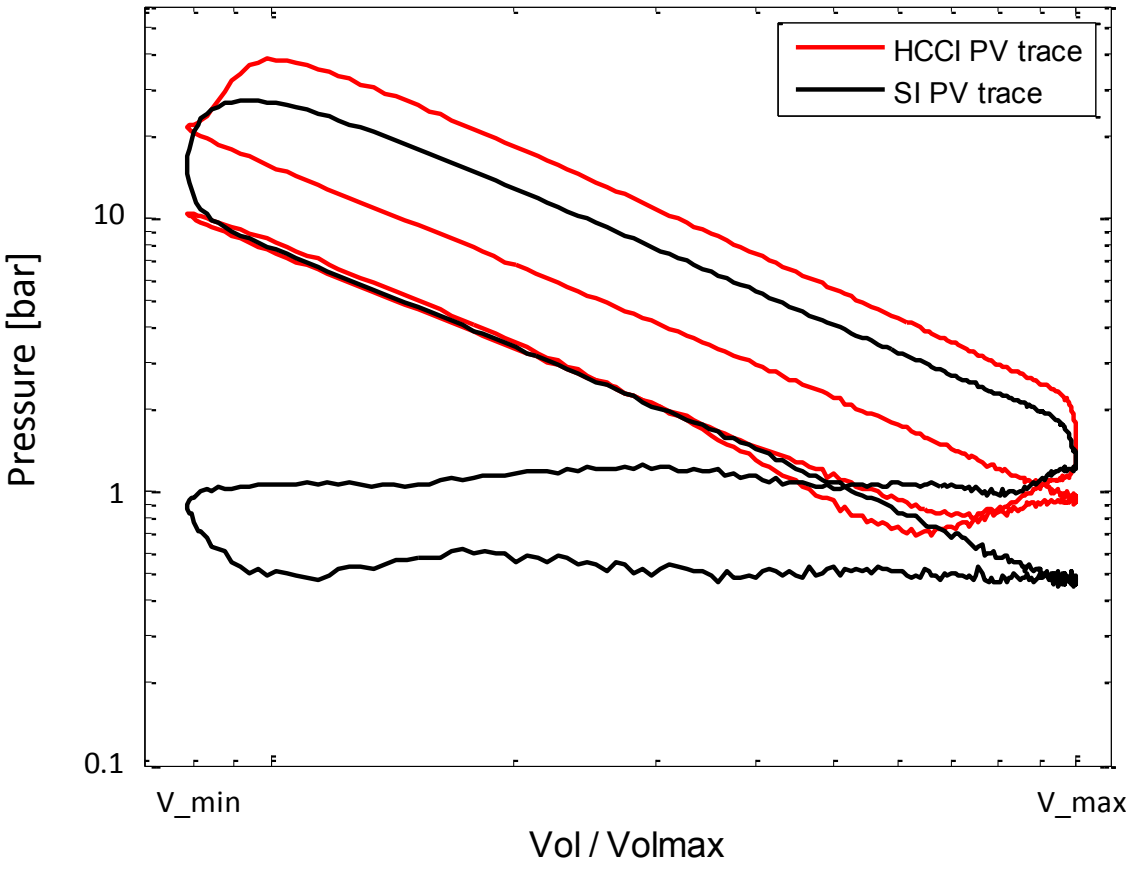

Figure 67: P-V Diagram Comparison of SI and HCCI Operation

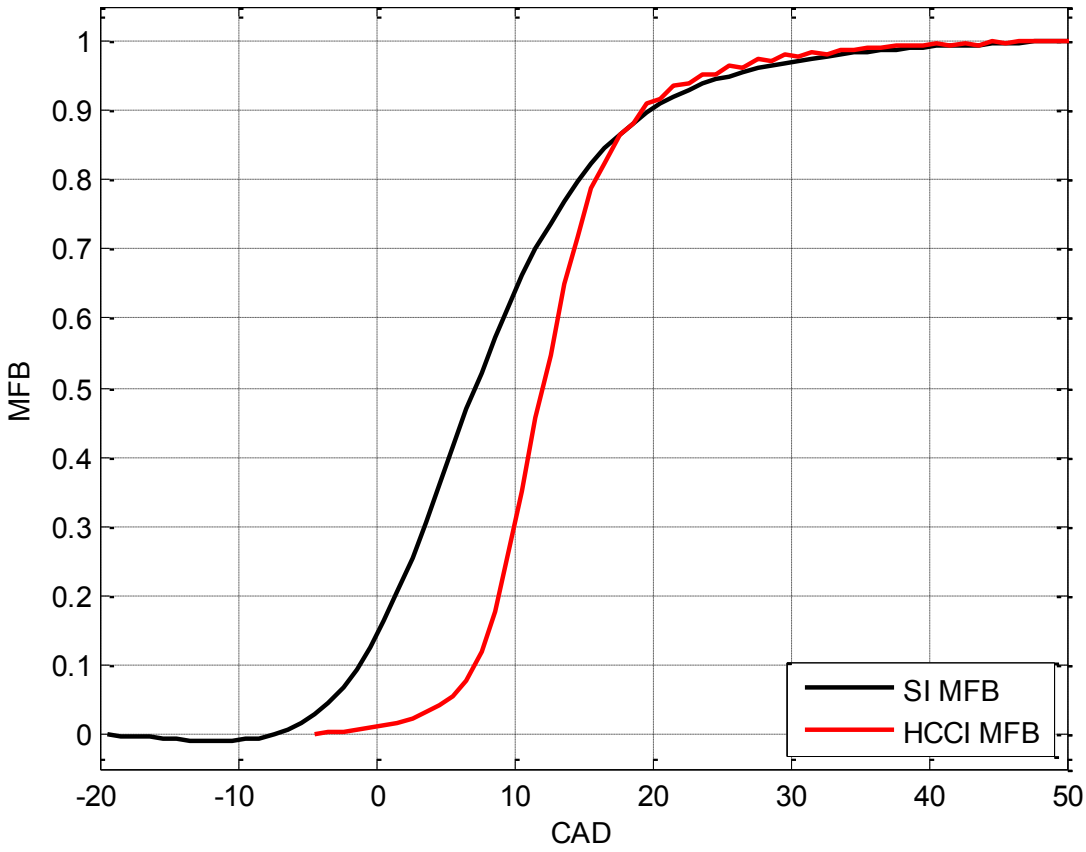

Figure 68: MFB Curve Comparison of HCCI and SI Operation

While the near elimination of pumping losses is an obvious efficiency advantage of this HCCI point when looking at output in NMEP over the entire 720 CAD engine cycle, what is less obvious at first glance is how much the fast burn duration and the fact that nearly all of the combustion happens after TDC also adds to efficiency of the gross 360 CAD IMEP. The change in IMEP from 4.6 bar to 5.2 bar using the same amount of fuel is a significant improvement. While the higher operating pressure in the HCCI case requires more work to complete the compression stroke (Figure 69), that extra work is more than gained back once combustion begins.

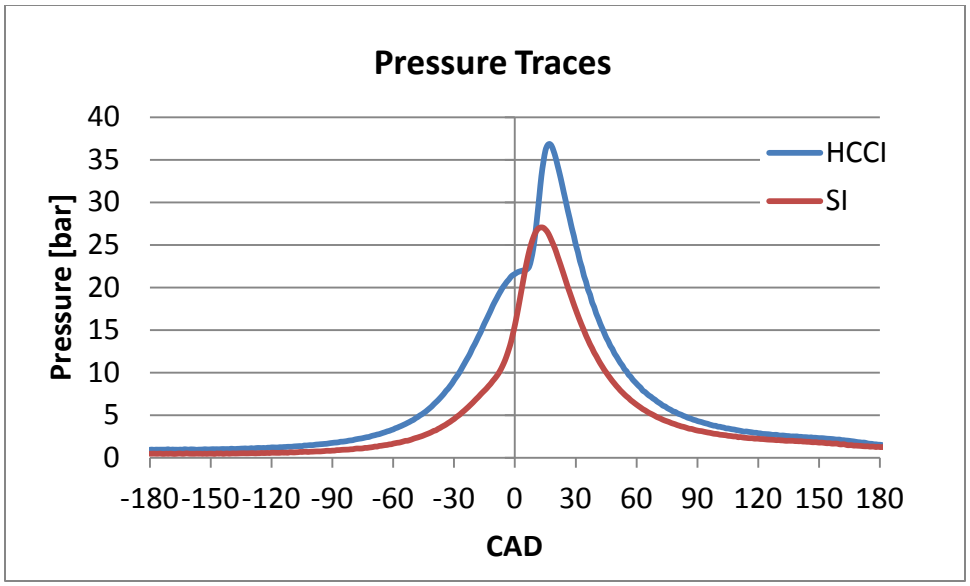

Figure 69: Compression and Expansion Stroke HCCI and SI Pressure Trace Comparison

Breaking down the IMEP calculation into single crank angle work contributions can show where the extra work output comes from in the cycle. To do this, the pressure-volume work done or required for each single CAD of piston movement is calculated as follows:

$$Work_{CAD} = P \times \Delta V$$

Using the average pressure of the beginning and ending crank position, this becomes

$$W_{i \to i+1} = \left[\frac{p_i + p_{i+1}}{2}\right] \times (V_{i+1} - V_i)$$

where W is work in Joules, p is pressure in Pascals, and V is volume in m^3, and i denotes the desired CAD for calculation. A plot of the resulting work at each CAD is shown in Figure 70. The work needed during the compression stroke in the HCCI cycle peaks at a maximum of 2.6 J/CAD compared to a maximum of only 1.3 J/CAD in the normal SI cycle. The work output in the HCCI cycle peaks at 7.0 J/CAD compared to 4.8 J/CAD in the SI cycle.

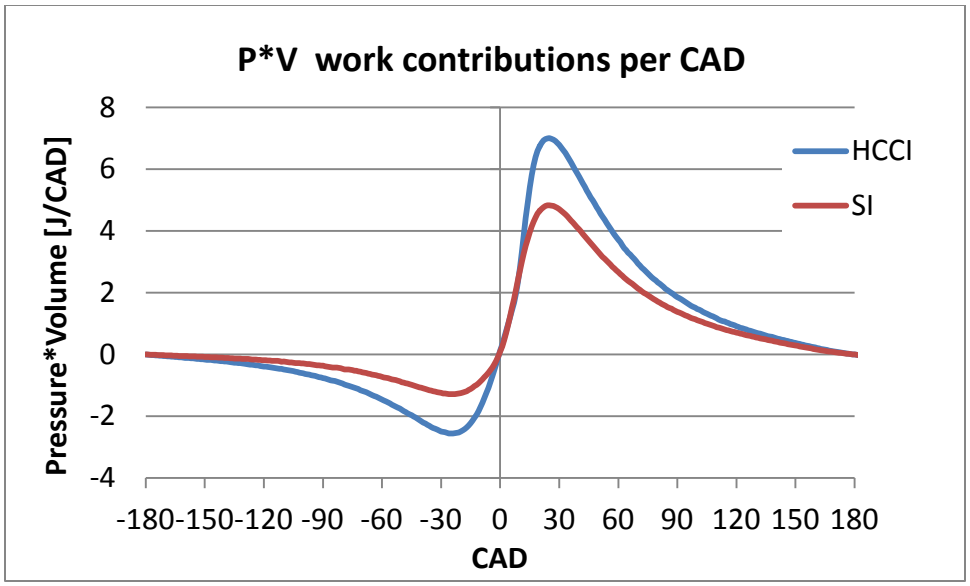

Figure 70: Work Done During Each CAD of Compression and Expansion Stroke, HCCI vs. SI Comparison

A cumulative summation of these per-crank-angle work calculations over the entire compression and expansion strokes shows just where in the cycle the extra output from the faster and later combustion allows the overall work to surpass that of the SI cycle. For example, to calculate the amount total work needed to move the piston from -180° to -170°, a summation of the work calculations from the above equations can be set up as follows:

$$W_{tot} = \sum_{i=-180}^{-170} W_i$$

More generally, the cumulative work W_j from the beginning of the cycle to any crank position j can be expressed as:

$$W_{tot\_j} = \sum_{i=-180}^{-180+j} W_i$$

where W_{tot_j} is the cumulative work from -180° to crank angle j. The plot of W_{tot_j} in Figure 71 shows that while the cumulative work of compression is larger in HCCI, the extra work from combustion allows the cumulative work of the cycle to surpass the SI by the time the crank has reached the 66° ATDC position. Through the rest of the expansion stroke, the higher pressure results in an increasingly larger amount of cumulative work. By 180° ATDC, the total work of the two strokes is 260 J for the HCCI cycle compared to 230 J for the SI cycle. Dividing this cumulative work by the cylinder displacement results in the IMEP figures found previously in Table 19.

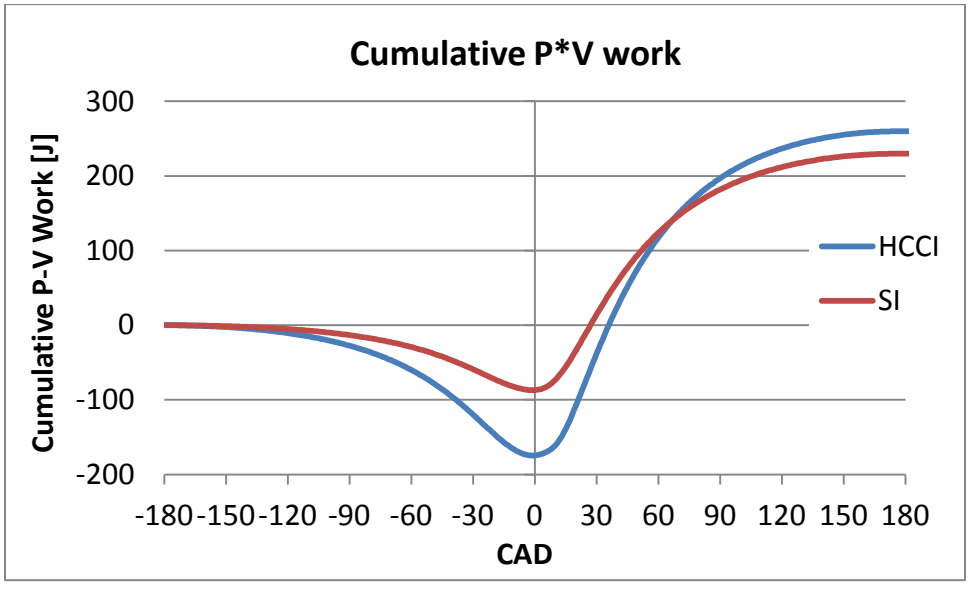

Figure 71: Cumulative Summation of P-V Work per CAD

Lower load points closer to the 4 bar NMEP point of the SI tests have been explored by altering the fueling amounts and pilot injection timings. These lower loads have shown greater variability, some of which can be improved upon with changes to the fuel split ratio between the main and pilot pulses. However, the short-pulse injector variability limitations have prevented consistent data and useful parameter sweeps from being explored.

Hybrid Mode Transition Points in Steady State Testing

In the process to manually transition into HCCI, transitional points were captured that demonstrate the hybrid mode combustion claimed by the original mode transition concept. As the cam phasing and throttle position are changed, it is predicted that a few cycles which display characteristics of both SI combustion and autoignition will be present. Combustion is initiated by a spark at normal SI timing, but after a certain amount of flame propagation, fast autoignition will take over for the rest of the combustion process.

Figure 72 shows a 200 cycle sample of exactly this hybrid process captured during the manual transition to HCCI. This condition was achieved with the intake cam in its default fully retarded 0° advance position and the exhaust cam advanced 55° from its default position. This created an asymmetrical 148° NVO period, with the longer portion of recompression actually occurring on the intake side at 80° compared to 68° on the exhaust side. Throttle position was more open than during standard SI, but not yet to WOT, resulting in a manifold pressure of 85

kPa. The air-fuel mixture was only slightly lean, with lambda equal to 1.02. Spark was still operating at the 30° BTDC timing used in the standard SI starting point.

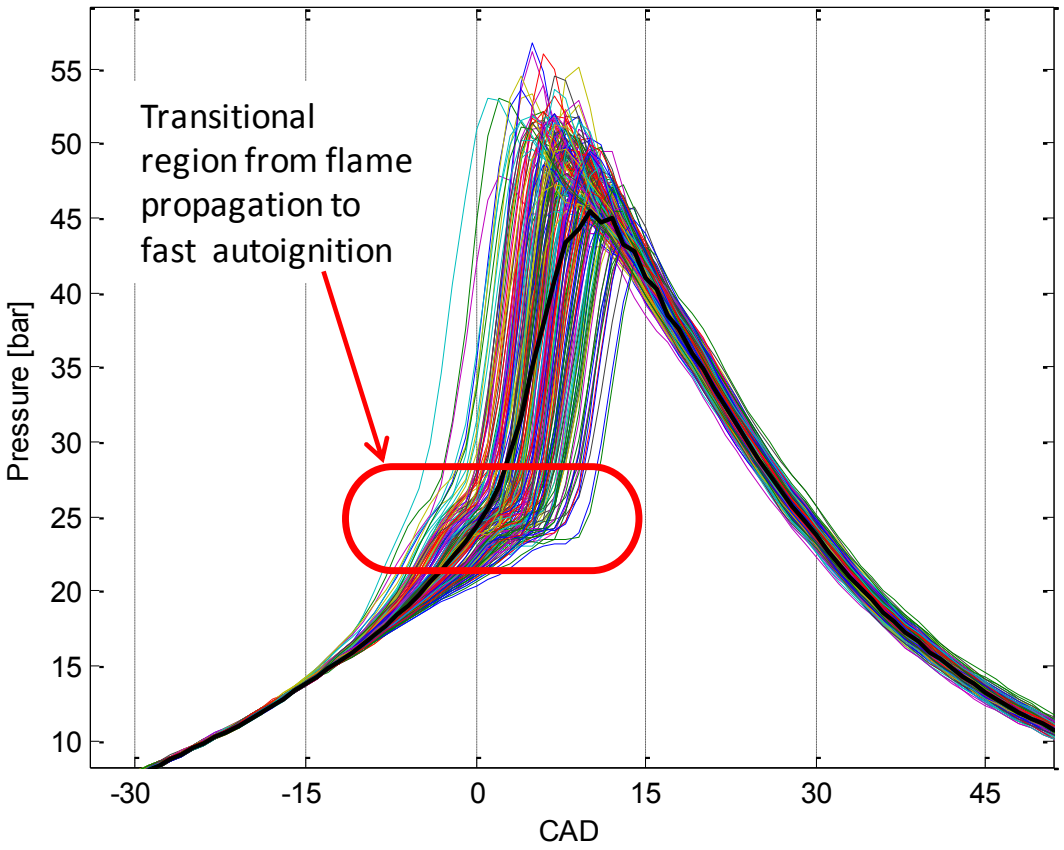

Figure 72: Overlay of 200 Hybrid Combustion Transitional Cycles

Other similar points were also discovered during the manual transition process with varying degrees of stability and ratios of propagation to autoignition depending on the cam phasing, fueling, and throttle position. Knowledge from these points was helpful when designing a fast transition strategy, particularly when dealing with how to sequence cam phasing and throttle opening together to create conditions for these hybrid cycles during the transition.

Successful SI-to-HCCI Fast Mode Transition

With the knowledge gained from the steady state tests and the manual transition tests to get to HCCI, it was possible to successfully program the mode transition strategy to successfully move the engine in and out of HCCI mode consistently with minimal misfire or knocking cycles. Unfortunately, these tests were only able to be designed for a transition with the cams already in low-lift mode due to a malfunction in the exhaust cam lift mechanism.

The first successful method involved 15 total cycles from the start to end of cam phasing. The plots in Figure 73 show the cycle-by-cycle strategy for MAP, spark timing, cam timing, and injection pulses during the transition window. Cycle-by-cycle pressure traces of these cycles are shown in Figure 74. In these figures, the process begins when cam phasing starts at cycle 50. Split injection is initiated at cycle 56 once significant recompression has built up (the initial pilot injection pulse of 0.5 ms is below the threshold pulse and does not inject any fuel). The throttle begins to open around cycles 55 and 56, and spark timing begins to retard shortly after as combustion has moved into hybrid mode, which will be shown below. By cycle 63, the spark settles at -5°, the throttle is essentially wide open, and the exhaust cam is nearly fully advanced to allow for full HCCI combustion. The entire transition took place without a significant misfire, with the lowest single-cycle IMEP still well over 4 bar (Figure 75). Lambda rose from stoichiometric in SI mode to approximately 1.12 after the transition, with a slight drop into rich combustion for a few cycles during the transition, due to cam phasing reducing incoming intake

air before the throttle began to open; this is essentially the same thing that was seen in the SI low-lift cam phasing tests summarized previously in Figure 42 .

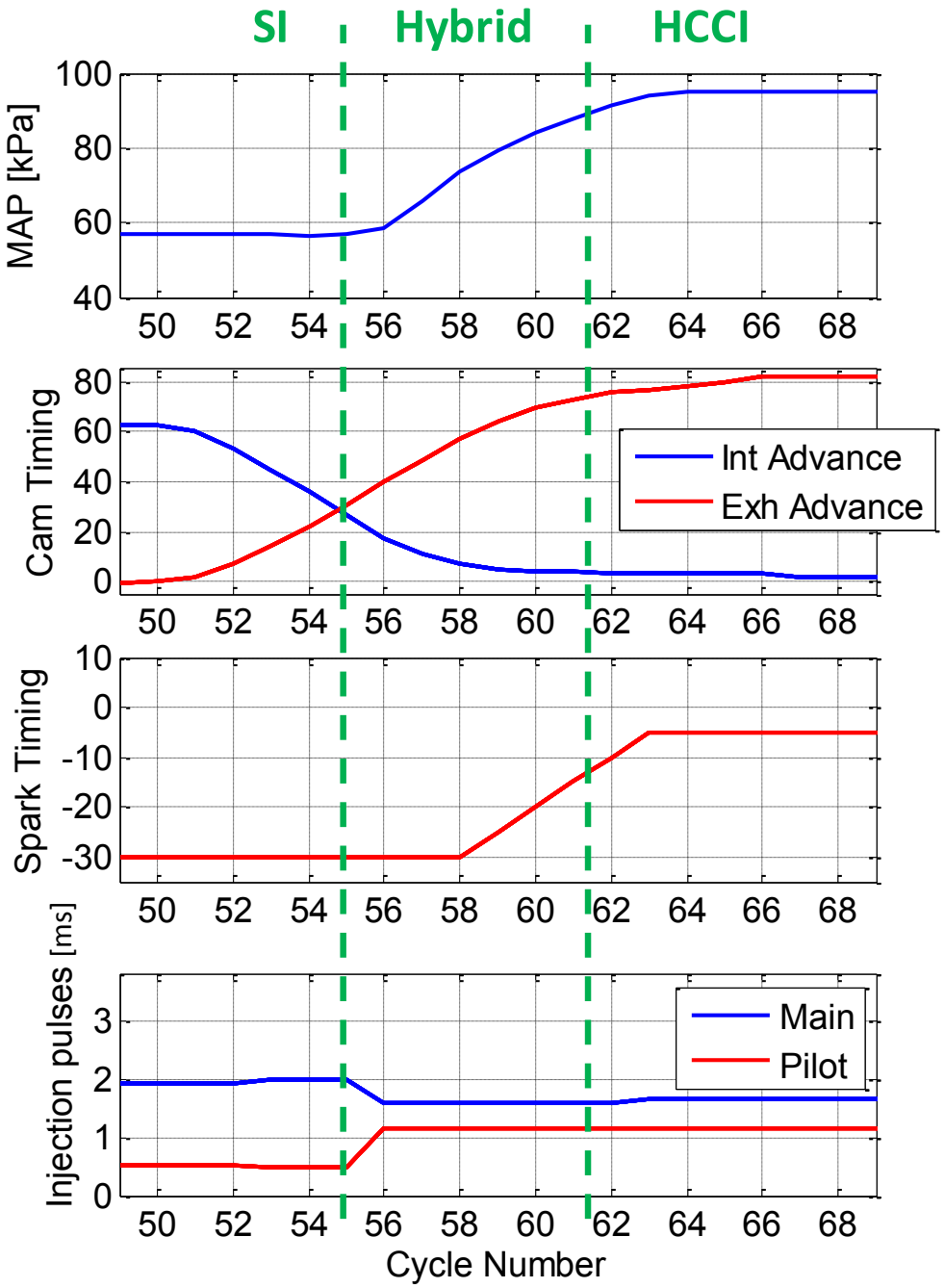

Figure 73: Control Parameter Strategy, 15-cycle Transition

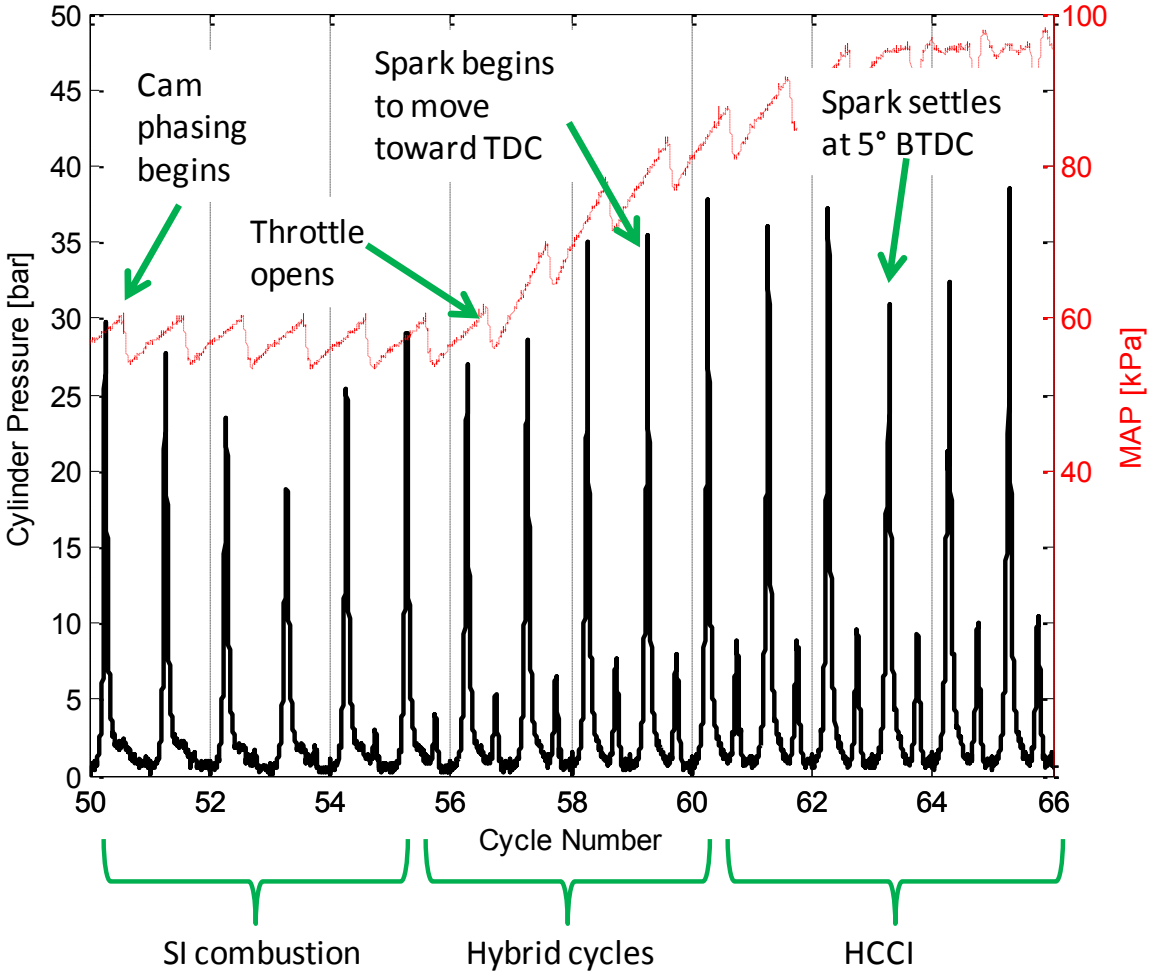

Figure 74: Cycle-By-Cycle Pressure Trace Details of 15-Cycle Transition

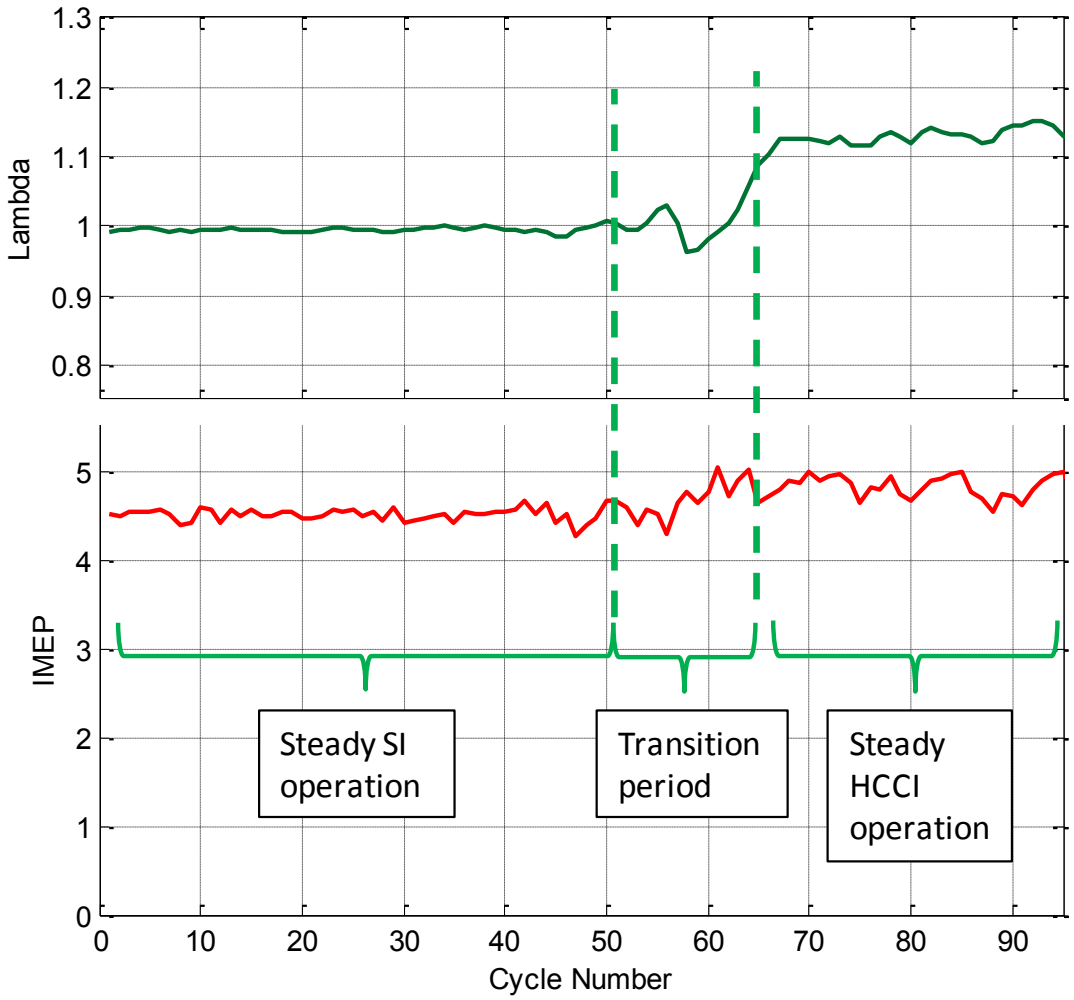

Figure 75: Lambda and IMEP Traces during 15-Cycle Transition

Examining the individual pressure traces and MFB curves through the entire transition helps show details of what happens as the parameters change. Figure 76 shows the initial 5 cycles of the transition, starting at cycle 50 just as the cams begin to move. The first cycles demonstrate typical SI characteristics with a CA50 timing of about 7° ATDC. In cycles 52-54, the increasing NVO period starts to trap more exhaust gas, and CA50 retards as peak pressure drops and variability increases.

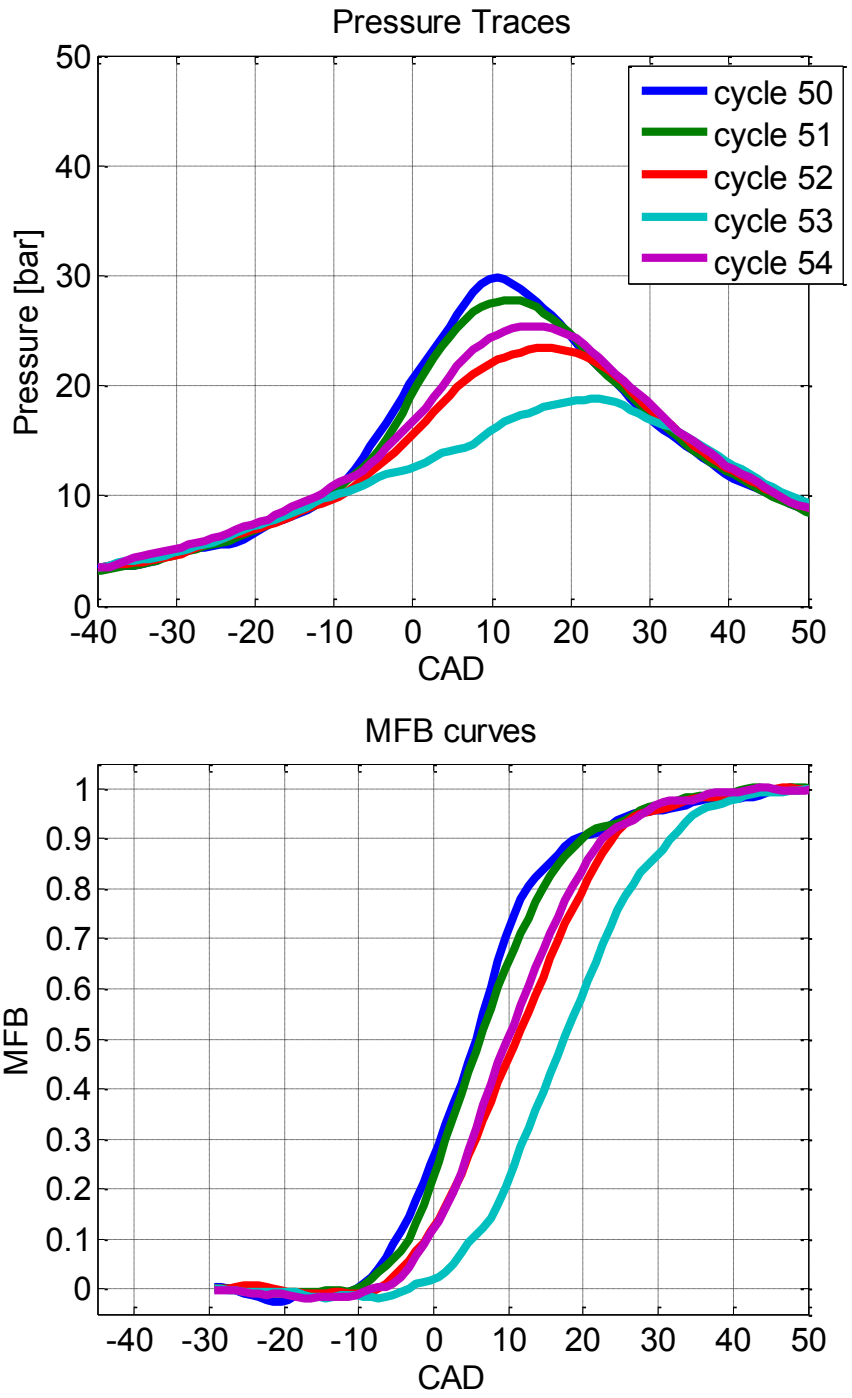

Figure 76: Pressure Trace and MFB of First Five Cycles of 15-Cycle Transition

The transition continues in Figure 77 as very clear hybrid-mode combustion begins to appear in cycle 55. Peak pressures increase from the low pressures of the preceding SI cycles as a small amount of autoignition appears at the end of the MFB curve. As the throttle opens and the

spark begins to retard, the balance between SI and autoignition shifts more towards autoignition. Over these five cycles, the percentage of burn made up of SI flame propagation decreases fairly steadily from approximately 65% in cycle 55 to around 10% by cycle 59. In each of these cycles, the transition to autoignition takes place near 10° ATDC.

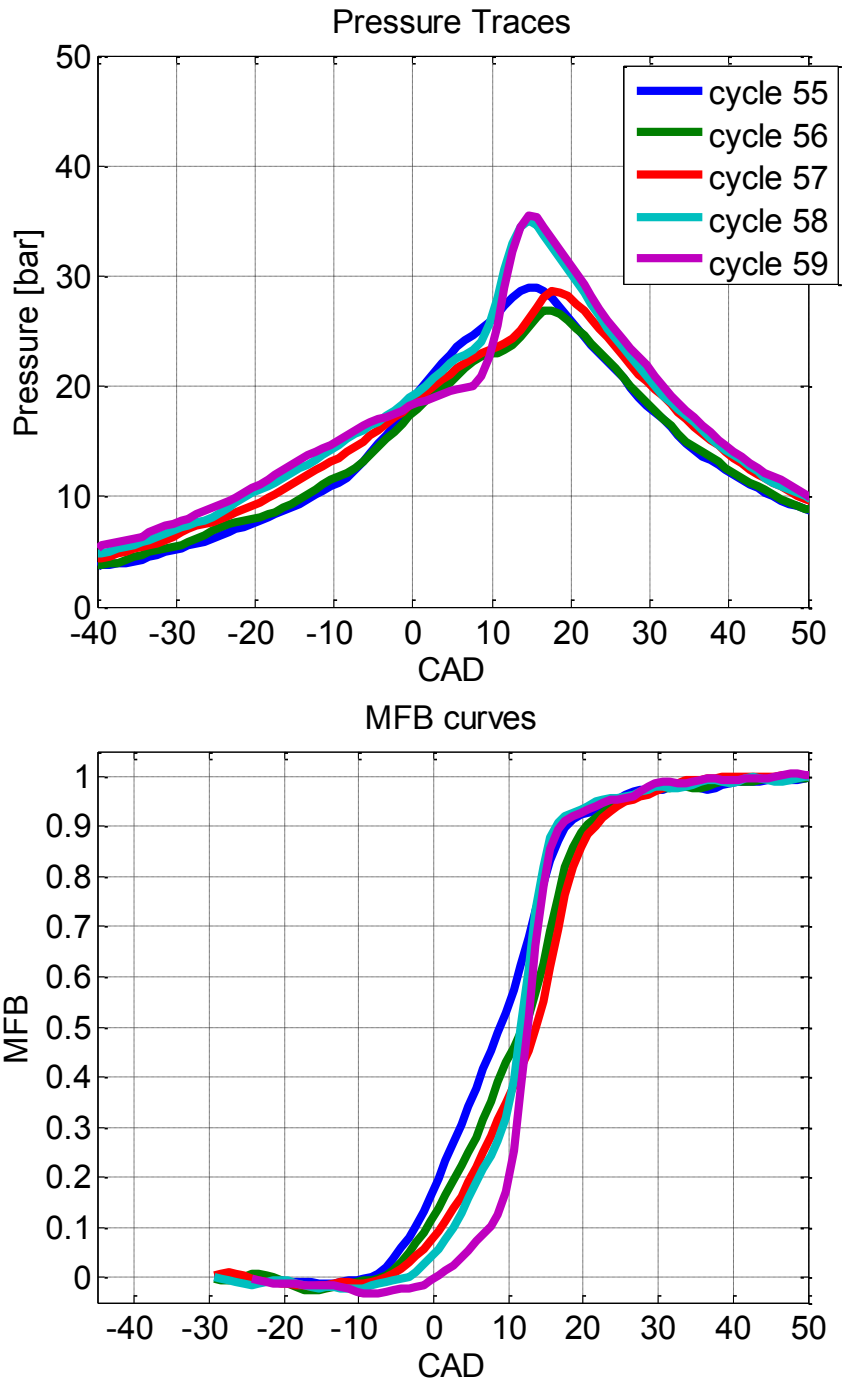

Figure 77: Pressure Trace and MFB of Middle Five Cycles of 15-Cycle Transition

By cycle 60, the cam positions and manifold pressure are such that a consistent autoignition-style trace is present. By cycle 63, spark has been retarded to 5° BTDC, cams are fully phased

for maximum NVO, and manifold pressure has reached a maximum. Following this transition, the engine settled into a 5.00 bar IMEP load with a COV of 2.9% and PMEP of -0.15 bar.

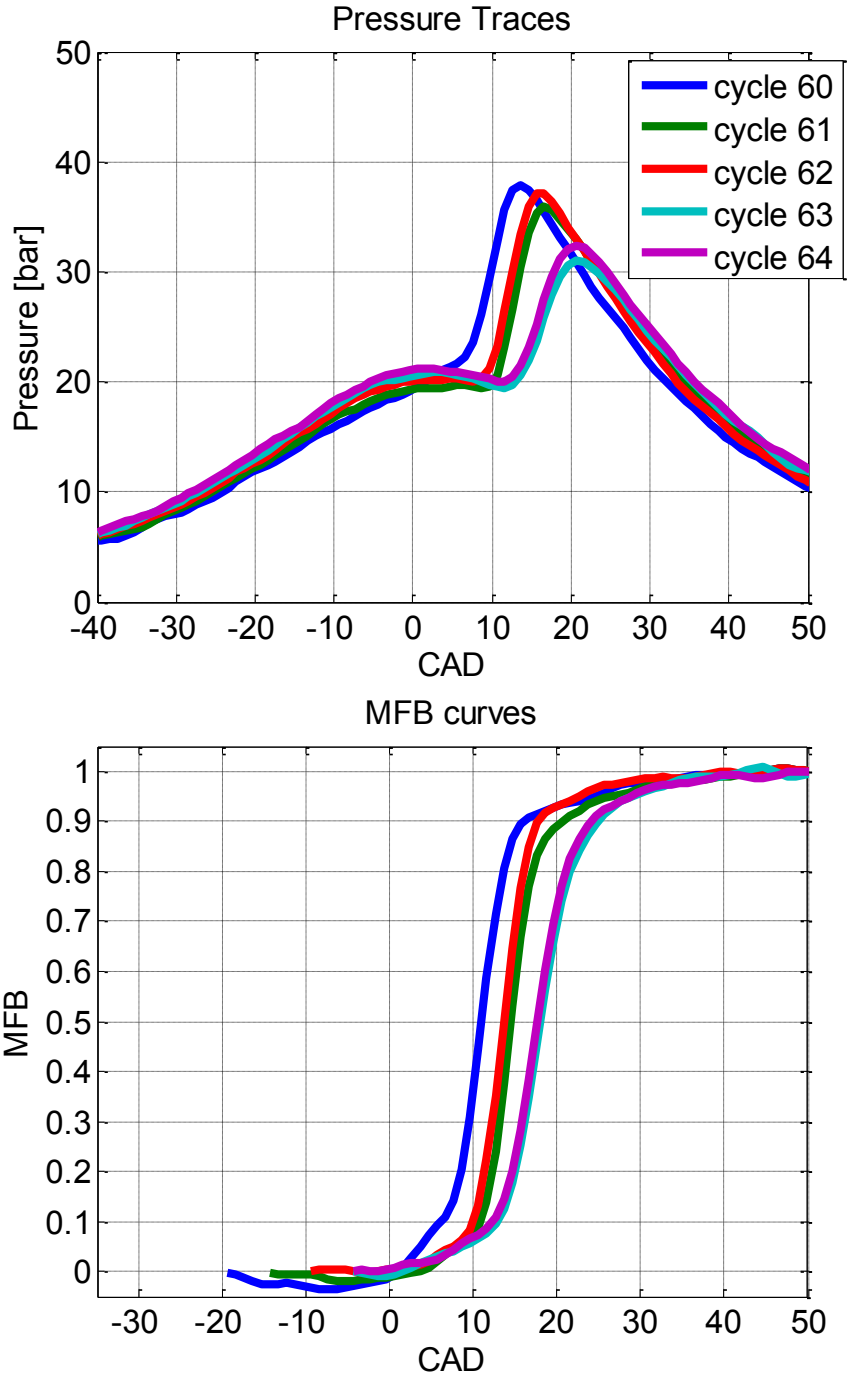

Figure 78: Pressure Trace and MFB of Last Five Cycles of 15-Cycle Transition

With the original goal of a five cycle transition, further attempts were made to shorten the transition time. Due to slow settling time of the exhaust cam phasing, total phasing time could only be reduced to 11 cycles to fully settle. However, it was possible to achieve full autoignition on the 8th cycle of the transition with the exhaust cam advanced to 75° of its total 80° total and spark settling at its final location of -5°. The transition can effectively be called an 8-cycle transition with extra cycles for cam phaser settling time. This 8-cycle setup consisted of three initial SI cycles during early cam phasing followed by four to five hybrid mode combustion cycles that led to full autoignition.

The control strategy for the 8-cycle transition is shown in Figure 81. Besides everything happening slightly faster, the only major differences in this compared to the 15-cycle transition are the timings of the throttle opening and the switch to a split injection.

The throttle was opened slightly earlier to attempt to combat the poor combustion seen just before the hybrid cycles. As the cams phase, higher levels of exhaust gas are trapped in the cylinder. These exhaust gases can slow flame propagation and inhibit the intake of fresh air slightly, which may have been causing the short rich dip in the lambda trace. By opening the throttle slightly earlier, it was believed that this dip in lambda could be eliminated, and the extra fresh intake air could combat the high levels of exhaust gas and allow better combustion.

The split injection was moved one cycle earlier relative to cam position because it helps the likelihood of a hybrid combustion cycle happening earlier in the transition before SI combustion

has become slow and weak. In the 15-cycle transition, the split injection was introduced when the intake and exhaust cams had reached their 20° and 40° positions in cycle 56 (see Figure 73). However, slight signs of hybrid combustion appeared one cycle prior to that switch. Thus, in the 8-cycle transition, the switch to split injection was made sooner as the cams reach at their 30° positions (cycle 46 in Figure 79) to take advantage of conditions that already were able to produce hybrid combustion in the longer transition. This, in combination with the earlier throttle opening, can help start hybrid combustion before a weak SI cycle has had a chance to appear.

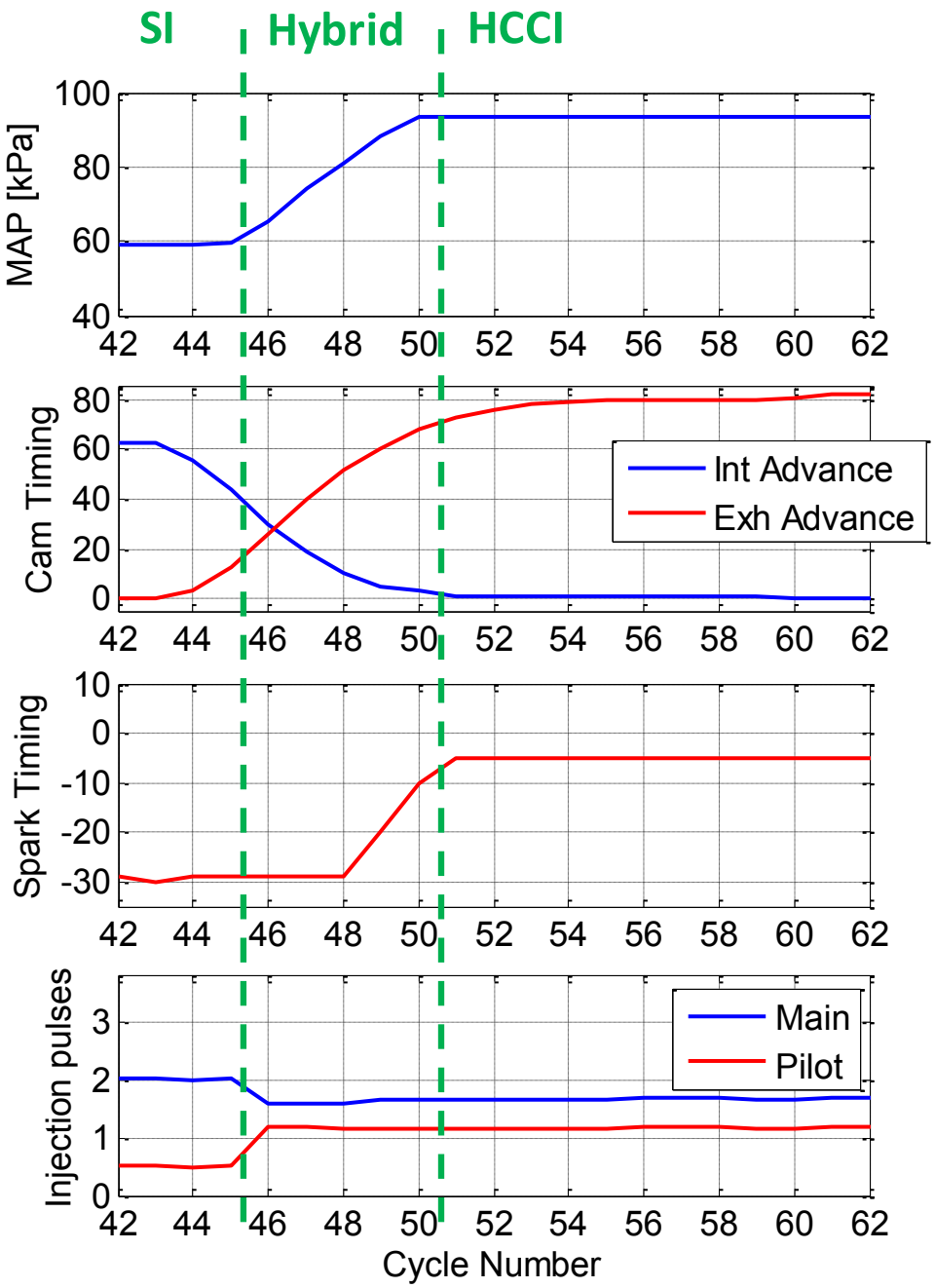

Figure 79: Control Parameter Strategy, 8-cycle Transition

The cycle-by-cycle pressure traces (Figure 80) of this transition strategy and the IMEP and Lambda traces (Figure 81) show the success of these components of the transition strategy.

The rich dip seen previously in the lambda trace was eliminated, and the IMEP trace through the transition region shows no significant peaks or dips. The strategy to induce earlier hybrid combustion was also successful, as shown in the cycle-by-cycle pressure trace and MFB curve detail of Figure 82. After cycle 43, which was the last cycle before the start of cam phasing, there were only two SI cycles before the first hybrid combustion cycle in cycle 46.

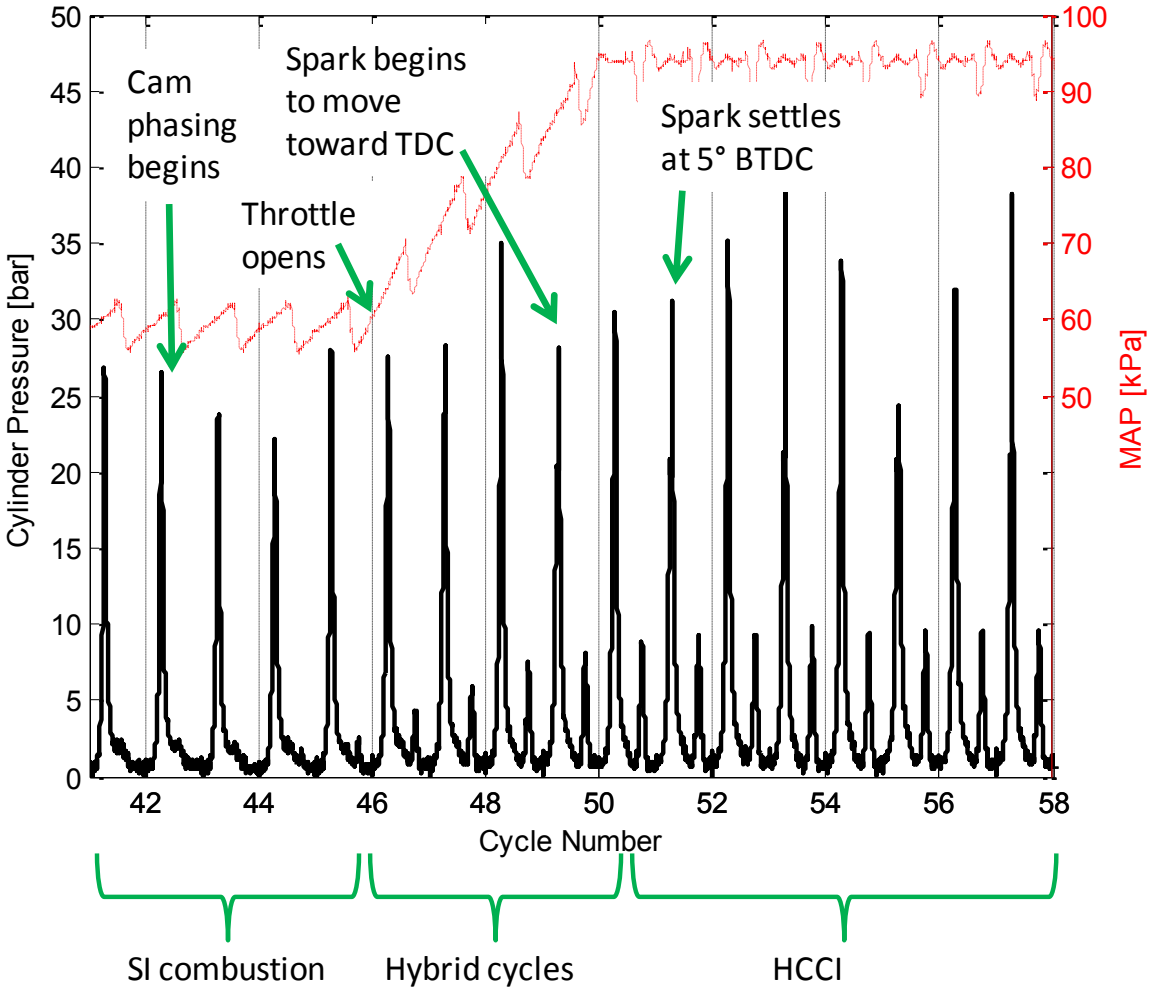

Figure 80: Cycle-By-Cycle Pressure Trace Details of 9-Cycle Transition

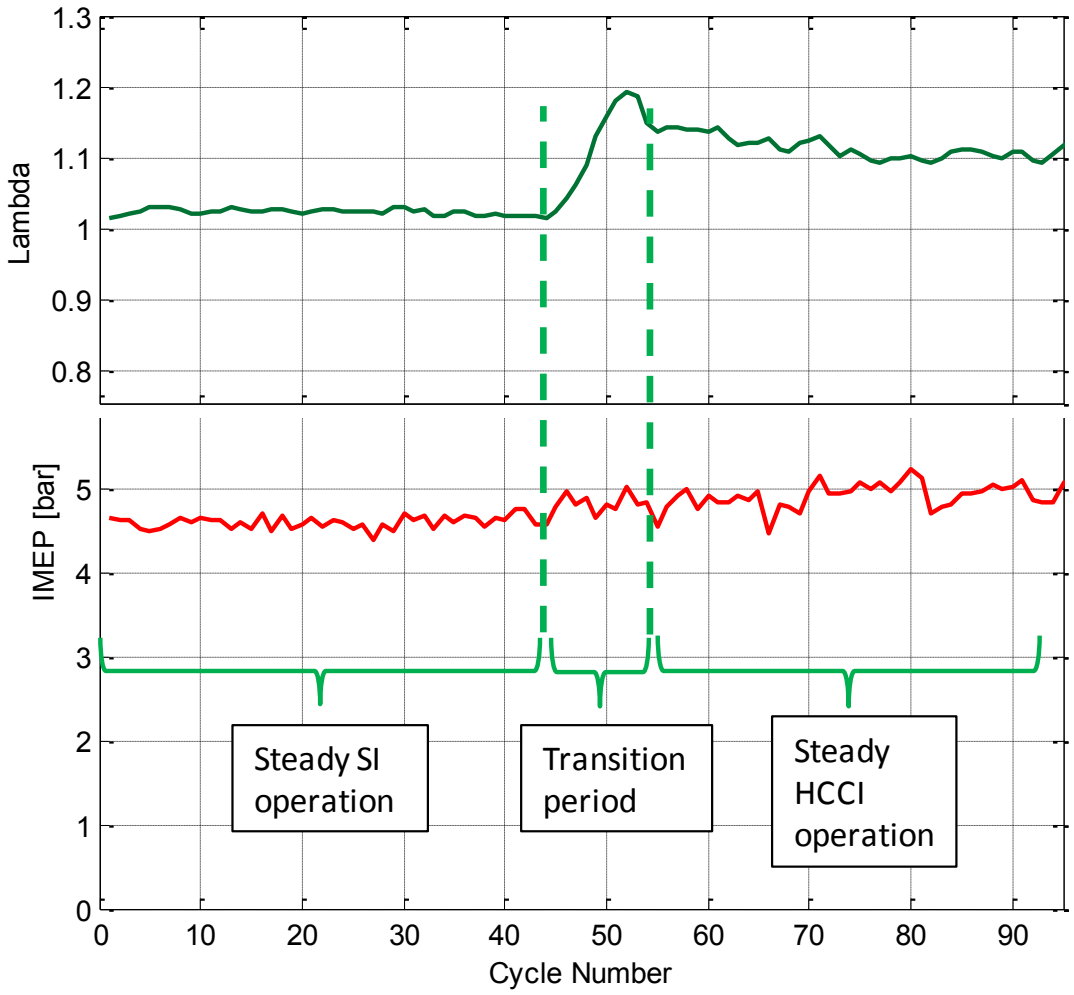

Figure 81: Lambda and IMEP Traces during 9-Cycle Transition

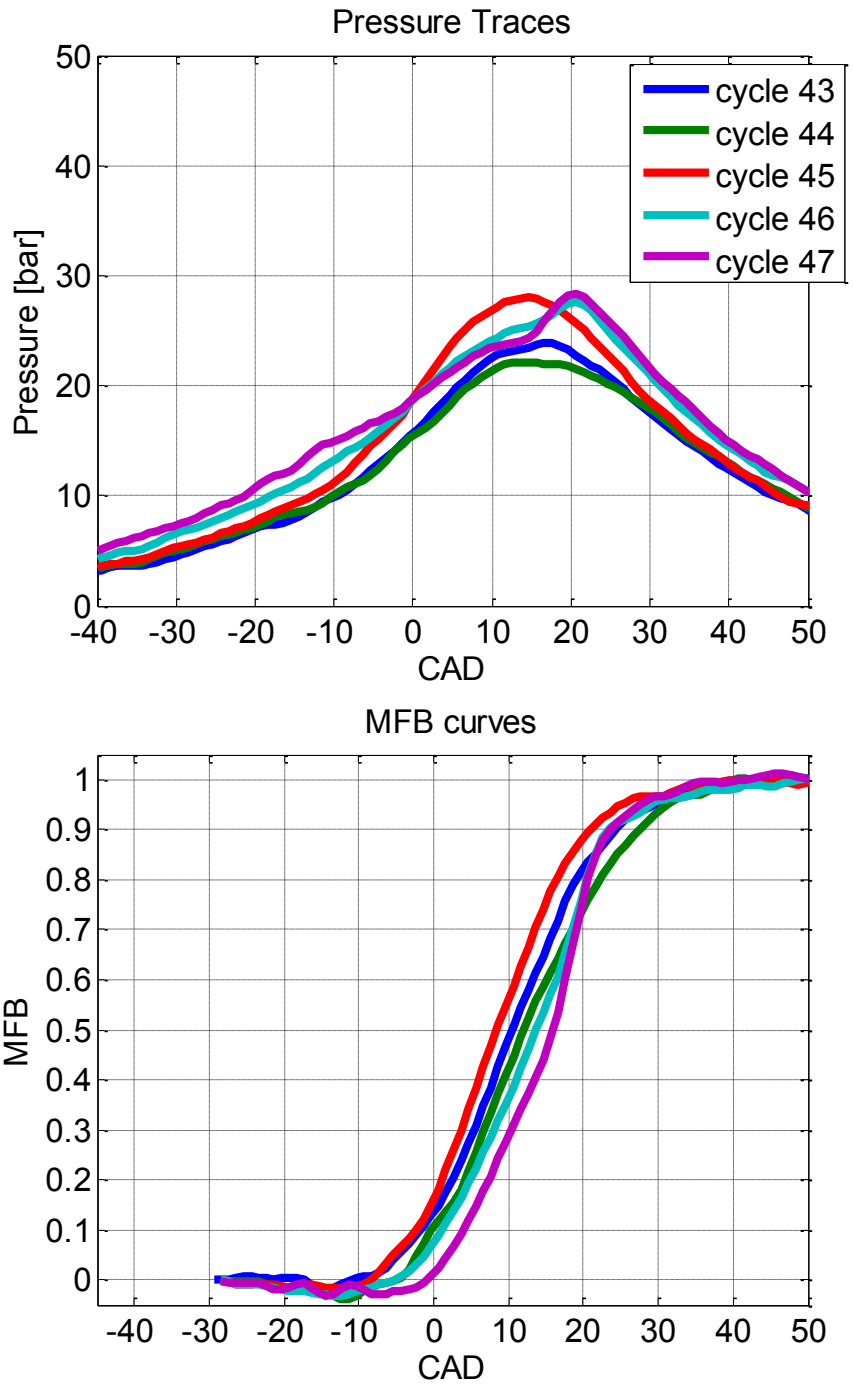

Figure 82: Pressure Trace and MFB of Initial Cycles of 8-Cycle Transition

Hybrid combustion continues in cycles 48 and 49 until the percentage of SI combustion has essentially disappeared. By cycle 50, the -10° spark timing does nothing to contribute any SI combustion, and full autoignition has been reached. From here, the engine proceeded to run

steadily at 4.90 bar IMEP with a 2.4% COV, a -0.15 bar PMEP, and a max pressure rise rate average of 3.8 bar/CAD.

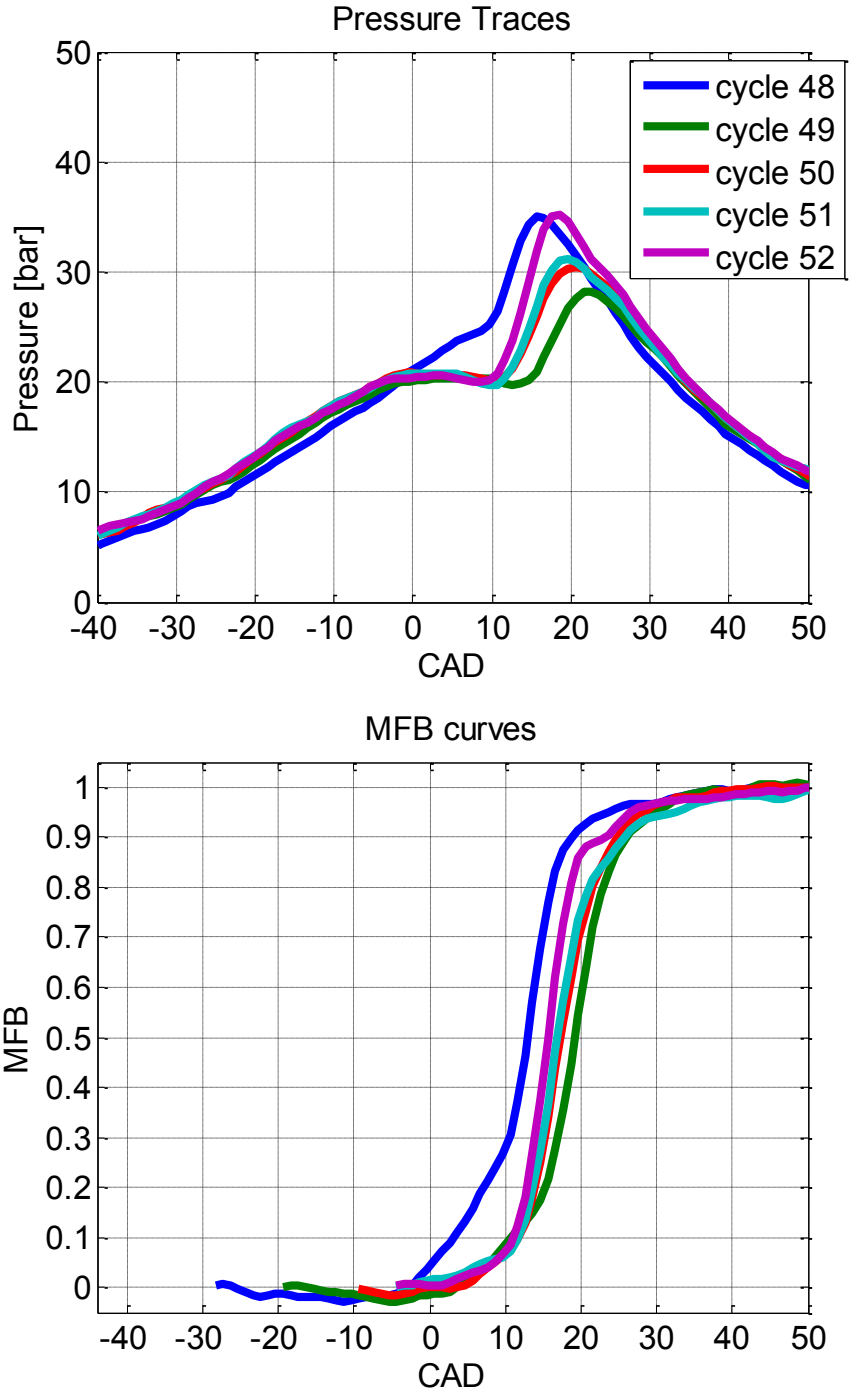

Figure 83: Pressure Trace and MFB of Final Cycles of 8-Cycle Transition

Figure 84 shows the MFB curves of the hybrid and HCCI cycles from the 8-cycle transition lined up next to each other. From this arrangement, it is very clear how the onset of autoignition advances smoothly cycle-by-cycle through the transition. The ability to traverse through this combined mode combustion quickly without a surge or loss in engine output is the ultimately successful achievement of this HCCI mode switch study.

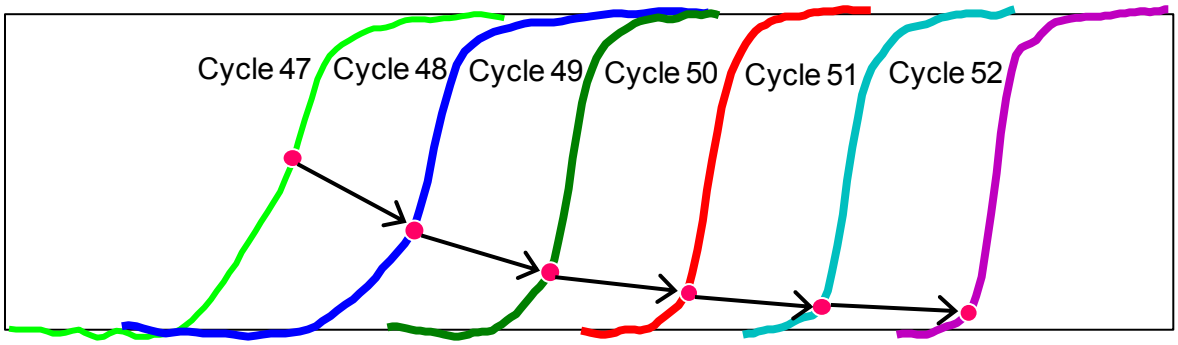

Figure 84: Progression of Hybrid Combustion Autoignition Point

Temperature Sensitivity of Mode Transition

Success of the mode transition was found to be dependent on the operating temperature of the engine and intake air. Figure 85 shows the IMEP trace of two different mode transition attempts run at slightly different engine coolant temperatures. With the coolant at 197°F and the intake air at 172°F, the transition resulted in a stable HCCI condition. However, with the coolant only slightly cooler at 190°F and the intake air at 167°F, the transition was not successful. Instead, combustion went into an unsustainable cyclic pattern similar to what was seen in previous unsuccessful steady state HCCI tests with partial and late burning cycles

appearing every 2 to 3 cycles. After some of these became too great, combustion was lost entirely.

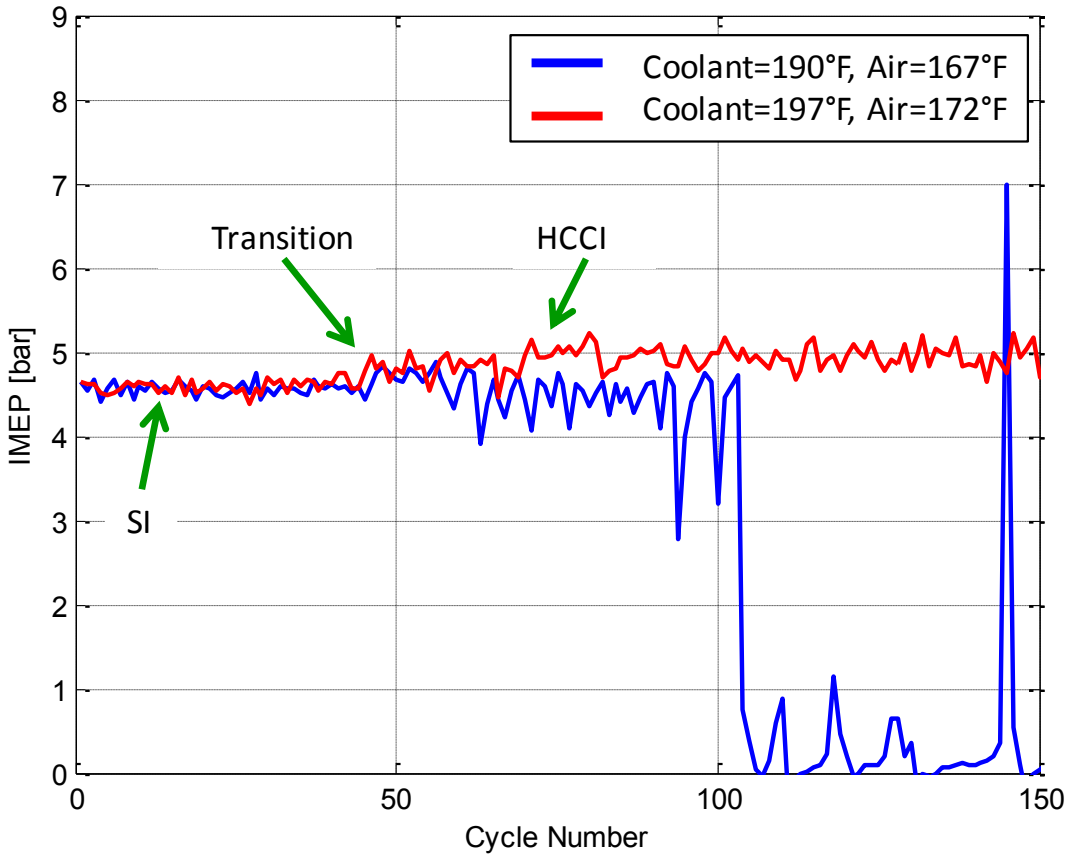

Figure 85: Engine Temperature Effects on Mode Transition Stability

Whether the coolant temperature or the intake air temperature had a greater effect on performance is left unknown, as the two were coupled in the setup used for this test. The intake air heater is fed by the engine coolant, so an increase in coolant temperature leads to an increase in intake air temperature.

CHAPTER 5: CONCLUSIONS AND RECOMMENDATIONS

As this work involved the initial fabrication of an engine test cell setup that could run in SI, HCCI, and switch between the two, many difficulties were encountered that led to further improvements to the setup that were not able to be fully implemented in this work. Despite setbacks involving the engine block and the blowby problem, injector variability, and constraints that prevented further use of the optical engine once successful HCCI operating parameter were discovered with the metal engine, this work was still able to successfully demonstrate how a mode transition can be developed with a typical cam phasing and 2-step cam lift system. Steady HCCI conditions were mapped out, the hybrid combustion mode present during transitions was demonstrated successfully, and optical images of the HCCI multiple ignition point process were taken.

Injector variability issues are currently being addressed with the use of an updated injector designed to allow better control of small fuel pulses. This injector uses a smaller flow rate, and thus is able to use longer pulses to inject smaller amounts of fuel. Continued testing with this injector is recommended in order to gain a better understanding of impact of pilot injection amounts on recompression heat release and main combustion phasing and consistency. This new injector should allow detailed parameter sweeps to provide more meaningful results that can lead to HCCI points run at lower loads with lower COV that were not possible with the previous injector.

The sensitivity of the mode transition and HCCI operation to operating temperature was mentioned, but a full exploration was not possible due to the coupling of engine temperature and intake air temperature. To solve this issue, a new coolant circuit for the intake manifold heat exchanger has been designed that allows control of the heat exchanger coolant and thus the intake air temperature independently of the engine operating temperature. This will be very useful in the future to study whether engine temperature or intake air temperature is the more dominant factor in successful mode-switching and steady HCCI operation. It also will allow wide range sweeps of intake air temperature to be possible to see what the lowest intake temperature can be that will still provide stable HCCI operation.

To further refine the mode transition process, a statistical investigation of the transition could be performed. With cycle-to-cycle variation present in all engine operation, most engine test points are analyzed through the use of an average of 200, 300, or more consecutively recorded cycles. Since the mode transition is a transient event that is finished in only a few short cycles, this typical form of average cycle analysis cannot be done with a single or even a few data sets. Running the mode transition over and over many times at tightly controlled conditions could allow for average cycles of each step along the transition to be developed. Only then could true trends appear that could point to load surges or drops on particular cycles during the transition. The demonstration of hybrid mode combustion during both the mode switch and manual transition to HCCI opens up the possibility of trying to operate the engine in a smooth hybrid-mode at steady state instead of just at an intermediate point along the path from SI to HCCI. High pressure rise rates are a limiting factor in HCCI operation at higher loads, but a successful

hybrid mode condition could alleviate this issue if some SI combustion can be initiated consistently before a small amount of autoignition completes the combustion process. This could be an alternative way to approach HCCI-style operation in the future. Rather than focusing on running with 100% autoignition, some of the beneficial aspects of autoignition could be realized while still having the simple control of a spark to set combustion timing.

A most obvious recommendation for continued research is to revisit running HCCI in the optical engine. The same alteration to the cam positions that was done on the metal engine can be performed on the optical engine head to allow for larger NVO, and the control schemes developed for the metal engine can also be transferred to use with the optical engine. This would open the door to performing an optical analysis of the hybrid cycles during a mode transition.

Finally, an improvement that could be made to future valvetrains that can be used for HCCI would involve the design of the cam profiles. In the setup used in this research, the low-lift exhaust cam was design to have the same EVC timing as the high-lift cam. This required a full 80° phasing of the exhaust cam in order to switch from SI to HCCI mode, and the time required for this became the limiting factor in how fast a mode transition could take place. If the low-lift cam could instead be designed with a profile that is already advanced (for example, match the EVO timings of the high and low profiles rather than the EVC timings), the phasing demands would reduce drastically. A similar change could also be made to the intake cam, which in its current design matches IVO timing on the high and low profiles. However, as a low-lift intake

cam can also be utilized for other types of SI operation like EIVC throttling, the placement of the low-lift intake cam profile involves more flexibility tradeoffs than are seen with the exhaust cam.

REFERENCES

REFERENCES

[1] Onishi, S., Jo, S., Shoda, K., Jo, P. et al., "Active Thermo-Atmosphere Combustion (ATAC) - A New Combustion Process for Internal Combustion Engines," SAE Technical Paper 790501, 1979, doi:10.4271/790501.

[2] Najt, P. and Foster, D., "Compression-Ignited Homogeneous Charge Combustion," SAE Technical Paper 830264, 1983, doi:10.4271/830264.

[3] Zhao, H., Li, J., Ma, T., and Ladommatos, N., "Performance and Analysis of a 4-Stroke Multi-Cylinder Gasoline Engine with CAI Combustion," SAE Technical Paper 2002-01-0420, 2002, doi:10.4271/2002-01-0420.

[4] Milovanovic, N., Dave, B., Gedge, S., and Turner, J., "Cam Profile Switching (CPS) and Phasing Strategy vs Fully Variable Valve Train (FVVT) Strategy for Transitions between Spark Ignition and Controlled Auto Ignition Modes," SAE Technical Paper 2005-01-0766, 2005, doi:10.4271/2005-01-0766.

[5] Milovanovic, N., Blundell, D., Gedge, S., and Turner, J., "SI-HCCI-SI Mode Transition at Different Engine Operating Conditions," SAE Technical Paper 2005-01-0156, 2005, doi:10.4271/2005-01-0156.

[6] Nier, T., Kulzer, A., and Karrelmeyer, R., "Analysis of the Combustion Mode Switch Between SI and Gasoline HCCI," SAE Technical Paper 2012-01-1105, 2012, doi:10.4271/2012-01-1105.

[7] Borgqvist, P., Tunestål, P., and Johansson, B., "Investigation and Comparison of Residual Gas Enhanced HCCI using Trapping (NVO HCCI) or Rebreathing of Residual Gases," SAE Technical Paper 2011-01-1772, 2011, doi:10.4271/2011-01-1772.

[8] Zhang, Y., Zhao, H., Ojapah, M., and Cairns, A., "Experiment and Analysis of a Direct Injection Gasoline Engine Operating with 2-stroke and 4-stroke Cycles of Spark Ignition and Controlled Auto-Ignition Combustion," SAE Technical Paper 2011-01-1774, 2011, doi:10.4271/2011-01-1774.

[9] Zhang, Y., Zhao, H., Peckham, M., and Campbell, B., "Direct In-cylinder CO2 Measurements of Residual Gas in a GDI Engine for Model Validation and HCCI Combustion Development," SAE Technical Paper 2013-01-1654, 2013, doi:10.4271/2013-01-1654.

[10] Koopmans, L., Ström, H., Lundgren, S., Backlund, O. et al., "Demonstrating a SI-HCCI-SI Mode Change on a Volvo 5-Cylinder Electronic Valve Control Engine," SAE Technical Paper 2003-01-0753, 2003, doi:10.4271/2003-01-0753.

[11] Zhao, H., Peng, Z., Williams, J., and Ladommatos, N., "Understanding the Effects of Recycled Burnt Gases on the Controlled Autoignition (CAI) Combustion in Four-Stroke Gasoline Engines," SAE Technical Paper 2001-01-3607, 2001, doi:10.4271/2001-01-3607.

[12] Wermuth, N., Yun, H., and Najt, P., "Enhancing Light Load HCCI Combustion in a Direct Injection Gasoline Engine by Fuel Reforming During Recompression," *SAE Int. J. Engines*2(1):823-836, 2009, doi:10.4271/2009-01-0923.

[13] Yun, H., Wermuth, N., and Najt, P., "Development of Robust Gasoline HCCI Idle Operation Using Multiple Injection and Multiple Ignition (MIMI) Strategy," SAE Technical Paper 2009-01-0499, 2009, doi:10.4271/2009-01-0499.

[14] Sellnau, M., Kunz, T., Sinnamon, J., and Burkhard, J., "2-step Variable Valve Actuation: System Optimization and Integration on an SI Engine," SAE Technical Paper 2006-01-0040, 2006, doi:10.4271/2006-01-0040.

[15] Santoso, H., Matthews, J., and Cheng, W., "Managing SI/HCCI Dual-Mode Engine Operation," SAE Technical Paper 2005-01-0162, 2005, doi:10.4271/2005-01-0162

[16] Nier, T., Kulzer, A., and Karrelmeyer, R., "Analysis of the Combustion Mode Switch Between SI and Gasoline HCCI," SAE Technical Paper 2012-01-1105, 2012, doi:10.4271/2012-01-1105.

[17] Bunting, B., "Combustion, Control, and Fuel Effects in a Spark Assisted HCCI Engine Equipped with Variable Valve Timing," SAE Technical Paper 2006-01-0872, 2006, doi:10.4271/2006-01-0872.

[18] Guo H, Neill W, Chippior W, Li H, Taylor JD. An Experimental and Modeling Study of HCCI Combustion Using n-Heptane. J. Eng. Gas Turbines Power. 2009;132(2):022801-022801-10. doi:10.1115/1.3124667.

[19] Magnus Sjöberg, John E. Dec, Comparing late-cycle autoignition stability for single- and two-stage ignition fuels in HCCI engines, Proceedings of the Combustion Institute, Volume 31, Issue 2, January 2007, Pages 2895-2902, ISSN 1540-7489, http://dx.doi.org/10.1016/j.proci.2006.08.010.

[20] Yi Yang, John E. Dec, Nicolas Dronniou, Magnus Sjöberg, Tailoring HCCI heat-release rates with partial fuel stratification: Comparison of two-stage and single-stage-ignition fuels, Proceedings of the Combustion Institute, Volume 33, Issue 2, 2011, Pages 3047-3055, ISSN 1540-7489, http://dx.doi.org/10.1016/j.proci.2010.06.114.

[21] Sellnau, M. and Rask, E., "Two-Step Variable Valve Actuation for Fuel Economy, Emissions, and Performance," SAE Technical Paper 2003-01-0029, 2003, doi:10.4271/2003-01-0029.

[22] C. Stuart Daw, Robert M. Wagner, K. Dean Edwards, Johney B. Green Jr., Understanding the transition between conventional spark-ignited combustion and HCCI in a gasoline engine, Proceedings of the Combustion Institute, Volume 31, Issue 2, January 2007, Pages 2887-2894, ISSN 1540-7489, http://dx.doi.org/10.1016/j.proci.2006.07.133.

[23] Yun, H., Kang, J., Chang, M., and Najt, P., "Improvement on Cylinder-to-Cylinder Variation Using a Cylinder Balancing Control Strategy in Gasoline HCCI Engines," SAE Technical Paper 2010-01-0848, 2010, doi:10.4271/2010-01-0848.

[24] Truedsson, I., Tuner, M., Johansson, B., and Cannella, W., "Pressure Sensitivity of HCCI Auto-Ignition Temperature for Primary Reference Fuels," SAE Int. J. Engines 5(3):1089-1108, 2012, doi:10.4271/2012-01-1128.

[25] William J. Glewen, Robert M. Wagner, K. Dean Edwards, C. Stuart Daw, Analysis of cyclic variability in spark-assisted HCCI combustion using a double Wiebe function, Proceedings of the Combustion Institute, Volume 32, Issue 2, 2009, Pages 2885-2892, ISSN 1540-7489, http://dx.doi.org/10.1016/j.proci.2008.06.029.